

Università degli Studi di Genova

Scuola Politecnica

DICCA

École Polytechnique Fédérale de Lausanne

Mechanical Engineering

LFMI



ÉCOLE POLYTECHNIQUE
FÉDÉRALE DE LAUSANNE

Non-linear adjoint-based optimisation of capillary thinning and break-up of liquid threads

Author: Giorgio Rocca

Supervisors: Prof. Alessandro Bottaro
Prof. François Gallaire

October 2013

“Gutta cavat lapidem.”

— Lucrezio, *De Rerum Natura*, IV-1281

Abstract

Jets are a topic widely covered in scientific and technical literature both for their importance in basic research - in physics and applied mathematics - and by virtue of their wide range of engineering applications, from droplet-based microfluidics to ink-jet printers and diesel engine injectors. Thanks to the progresses in research, scientists and engineers are now armed with a good understanding of the dynamic of jets. Thus, it is possible to tackle more ambitious questions of optimization and control. In this thesis a thin, axisymmetric thread of fluid with a free surface is considered. Such flow is characterized by the capillary instability named after Rayleigh and Plateau: surface tension drives the liquid thread to break into droplets. The goal is to develop an optimization tool for minimising the break-up time. After some considerations on the physics of Rayleigh-Plateau instability, a well-known one-dimensional reduced model is derived from the Navier-Stokes equations. On this basis linear stability and transient growth analysis are carried out. A comprehensive description of the numerical method developed to solve the flow is provided, and some examples of solution are shown. After a brief compendium about the adjoint method applied to non-linear constrained optimization, the adjoint equations of the model are derived. Details and issues concerning the optimization are treated: the choices about the objective function and the control are thoroughly explained, and the optimality system is derived. The results of the optimization are shown, and its effectiveness discussed. Finally, some attempts at an experimental verification are displayed, carried out exploiting high-speed cinematography.

Sommario

I getti sono un argomento largamente trattato nella letteratura scientifica e tecnica sia per l'interesse puramente euristico, data la possibilità di studiare fenomeni chiave di fisica e matematica applicata, sia per le numerose applicazioni ingegneristiche. Tra queste si possono citare la propulsione a getto, l'iniezione nei motori diesel, l'irrigazione agricola, la stampa a getto d'inchiostro, la somministrazione di farmaci. Grazie ai progressi della ricerca, gli scienziati e gli ingegneri sono armati di una buona comprensione della dinamica di questi flussi. Pertanto, è possibile affrontare problemi più ambiziosi di ottimizzazione e controllo. Questa tesi riguarda l'instabilità capillare nota come instabilità di Rayleigh-Plateau, e la conseguente rottura in gocce di flussi di forma cilindrica. Si tratta di un fenomeno fluidodinamico legato all'azione della tensione superficiale: essa infatti, sotto determinate condizioni, rende instabili le piccole perturbazioni presenti nel flusso. Queste tendono quindi a crescere in ampiezza, fino alla rottura del filo fluido. L'ottimizzazione di tali fenomeni, e in particolare la minimizzazione del tempo di rottura, è l'obiettivo finale del lavoro.

La tesi è divisa in due parti: nella prima (capitoli 1-4) vengono discusse la fisica del flusso, la sua modellazione matematica e le tecniche adottate per risolverlo numericamente. Nella seconda (capitoli 5-7) vengono introdotte ad applicate al caso specifico le tecniche di ottimizzazione basate su metodi aggiunti, e presentati i risultati. Infine, vengono mostrati alcuni esperimenti preliminari. Veniamo ora al dettaglio dei contenuti dei singoli capitoli.

Il primo capitolo è puramente introduttivo.

Il secondo capitolo è dedicato all'instabilità di Rayleigh-Plateau. Viene

presentato un breve riassunto della storia della scienza riguardante questo argomento, dalle prime pionieristiche considerazioni di Leonardo fino agli studi compiuti da Rayleigh nella seconda metà del diciannovesimo secolo. Attraverso un approccio semi-quantitativo viene poi proposta un'analisi semplificata dei processi fisici che governano i flussi cilindrici guidati dalla tensione superficiale, e vengono introdotti i numeri adimensionali caratteristici del fenomeno. Viene quindi riproposta l'analisi di stabilità lineare effettuata da Rayleigh partendo dalle equazioni di Navier-Stokes trascurando i termini viscosi.

Il terzo capitolo riguarda il modello fisico-matematico utilizzato per descrivere il filo fluido. Si tratta di un modello mono-dimensionale ben noto in letteratura, proposto da Eggers e Dupont. La sua derivazione dalle equazioni di Navier-Stokes, approssimate facendo l'ipotesi di onda lunga (ma considerando i termini viscosi), viene qui mostrata. Dopo aver adimensionalizzato le equazioni si procede nuovamente all'analisi di stabilità lineare, si confrontano i risultati con quelli ottenuti seguendo Rayleigh ponendo nulla la viscosità e si osservano gli effetti delle variazioni di quest'ultima. Infine, viene svolta un'ulteriore analisi lineare, riguardante gli effetti transitori legati alla non-normalità dell'operatore di Navier-Stokes.

Il quarto capitolo tratta la soluzione del flusso. Viene precisata la configurazione del filo fluido e vengono discusse le tecniche numeriche per la sua soluzione. I tassi di crescita ricavati dall'analisi di stabilità lineare vengono confrontati con i tempi di rottura ottenuti dalle soluzioni numeriche. Infine vengono mostrati alcuni esempi di soluzione.

Il quinto capitolo riguarda il metodo aggiunto applicato all'ottimizzazione vincolata. Dopo aver introdotto la notazione necessaria per una trattazione formale del problema si considerano il metodo del gradiente con differenze finite e il metodo aggiunto, riferito inizialmente a casi semplici. L'applicazione di quest'ultimo viene poi gradualmente estesa fino a problemi non-lineari dipendenti da spazio e tempo. Infine vengono derivate le equazioni aggiunte del caso in questione.

Il sesto capitolo è il più corposo ed è dedicato alla minimizzazione del tempo di rottura. Viene affrontato il problema della scelta della funzione obiettivo e dei parametri di ottimizzazione, con l'aiuto di alcuni test. Un'al-

tra sezione tratta il controllo: si definiscono alcuni criteri di comparabilità e si descrivono le possibili implementazioni nel processo di ottimizzazione. Infine vengono riportate le equazioni che definiscono il sistema di ottimalità e si presentano e discutono i risultati. Questi ultimi sono ordinati secondo il metodo di limitazione del controllo, e sono ottenuti inizializzando il ciclo di ottimizzazione in diversi modi, e per varie viscosità.

Il settimo capitolo presenta alcuni esperimenti preliminari aventi l'obiettivo di testare un metodo per imporre forme precise sulle interfacce di cilindri fluidi. In particolare viene osservata con una high-speed camera la rapidissima ritrazione di palloncini preventivamente riempiti di liquido.

L'ottavo capitolo, infine, è dedicato alle conclusioni e agli sviluppi futuri.

Chapter 1

Introduction

Jets are roughly cylindrical flows of matter. They occur in various situations at many scales, from microscopic distances up to the size of galaxies [1]. In this thesis the focus will be on liquid jets governed by surface tension effects, caused by cohesive properties of liquids. As we will discuss, under some circumstances cohesive forces paradoxically introduce an instability in the flow leading the jet to break up in drops. In particular, we will investigate an optimized control of the time of rupture.

Jets are a topic widely covered in scientific and technical literature both for their importance in basic research - in physics and applied mathematics - and by virtue of their wide range of engineering applications. Just to give an idea of the variety of possible applications, we can mention: diesel engine injectors (Figure 1.1a), liquid jet propulsion (Figure 1.1f), ink-jet printers (Figure 1.1c), agricultural irrigation (Figure 1.1d), water-jet manufacturing (Figure 1.1b), medical diagnostic, medicine administration, powder technology (e.g. in the food industry), droplet-based microfluidics (a field in rapid expansion in the last years). Closer to our everyday experience, jets are also present in our kitchens and bathrooms, are used during entertaining activities and for our security, e.g. in air-bag technology and for fire extinguishers (Figure 1.1e).

As far as basic sciences are concerned, jet dynamics is an excellent frame-

work to investigate liquids and their properties, such as surface tension, Newtonian and non-Newtonian rheology, interaction with the surrounding medium, etc. At micro-scales sensitivity to thermal and acoustic perturbation is an interesting characteristic, while gravity becomes important only when the length scales are large. Since the fluid can be electrically or magnetically manipulated, almost all classical physics can be included in the topic.

While studying break up of jets, time taken for the rupture and size distributions of droplets are matter of interest, and so is the sensitivity of the phenomenon to liquid properties, turbulence or the presence of an external medium. Control of jet pinch-off is often an objective pursued in applied mathematics and engineering.

In the last years the advent of high speed cameras in research laboratories has permitted to experimentally investigate in details the processes leading to rupture, rendering comparison with theory easy.

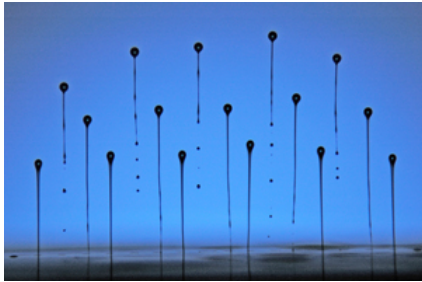
On the analytical side, linear stability analysis is a basic but precious tool. Anyway, non linear effects are important - if not dominant - in the dynamics of the process. Numerically, solving the Navier-Stokes equation (NS) for these problems remains a challenging task in term of computational effort, due to the high resolution needed near break-up. For this reason, reduced models have been developed in the past and are available in the literature. In this thesis we will employ a one-dimensional model, based on a long wavelength expansion of NS equations, to model the liquid thread, and have carried out optimization on the basis of the so-called adjoint method.



(a)



(b)



(c)



(d)



(e)



(f)

Figure 1.1: Examples of jet applications: a) Fuel injection in a diesel engine. (Property of Delphi); b) Water-jet manufacturing. (Property of American Metalcraft Industries); c) Drops emerging from a bank of ink-jet nozzles. (Cambridge Eng. Dep.); d) Agricultural irrigation. (Property of National Geographic); e) A fire extinguisher; f) Liquid jet propulsion.

Part I

Stability and solution of the flow

Chapter 2

Plateau-Rayleigh instability

Break up of a liquid jet in droplets is an ordinary event that everybody is used to experience. This common physical occurrence is driven by surface tension of the liquid, which tends to minimize the interface area between immiscible fluids. Because of this, the cylindrical shape is not a stable position of equilibrium, and under some circumstances little perturbations drive the jet to its rupture - a phenomenon known as Plateau-Rayleigh instability.

2.1 Some History

Break up of jets is a topic that fascinated scientists for centuries. We present here some history about scientific research on jets and droplets. Most of information comes from [1].

A pioneering study was conducted by Leonardo da Vinci in the Codex Leicester, a collection of scientific pieces of writing mainly regarding hydraulics (Figure 2.1). In the work Leonardo wrote his thoughts about cohesive forces in liquids, and on their role in the formation of drops. Leonardo properly noted that the detachment of drops from a faucet is driven by the fact that gravity wins over cohesive forces (surface tension). Nevertheless, he was mistaken assuming that the same mechanism governs also the forma-

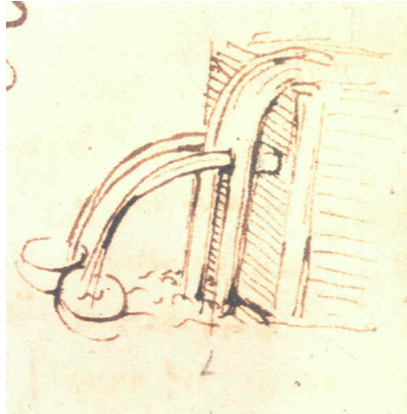


Figure 2.1: Sketch by Leonardo da Vinci [1], illustrating the impact of jets.

tion process of droplets. The physical tools necessary to the comprehension of the problem were contained in Laplace and Young's milestone [2], published at the beginning of the 19th century. In that work the fundamental role of both the axial and the radial curvature was explained for the first time, and the mean curvature introduced. In fact, surface tension acts in two opposite way: while for a hanging drop it prevents the fall, keeping the interface cohesive, for a cylindrical jet it is the engine for break up. And here we have the paradox: the more cohesive is the liquid (the larger the surface tension), the faster will be the rupture, as one can observe in Figure 2.6 which will be discussed in a short while.

The above-mentioned progresses on surface tension effects, combined with the laws of fluid motion developed by Navier and Stokes in the same years [3, 4], was what was needed to close the problem. Nonetheless, some more years had to pass before things were put together in a coherent theory. Savart [5] conducted several experiments and noted that break-up occurred spontaneously, without any dependence on the perturbations or the axial direction of the liquid jet. Therefore he correctly concluded that it had to be a feature intrinsic to the dynamics. Moreover, he noticed the presence of

smaller ‘satellite’ drops between two main ones, a fact that only non linear models can predict, as we will see later.

In 1873, Plateau [6] found experimentally that a falling jet of water breaks up into droplets if it is vertically perturbed with a disturbance of wavelength greater than about 2π times its radius. He observed that the instability was related to the capacity of the perturbation of reducing the area of the jet, eventually identifying the role of surface tension for break up. However, he found that the most destabilizing wavelength was $\lambda_{opt} = 8.76h_0$, much larger than 2π . Some decades later, Lord Rayleigh showed theoretically that a jet breaks up if it is perturbed with a wavelength that exceeds its circumference. He understood that the fact that $\lambda_{opt} > 2\pi$ was related to the dynamics [7, 8]. For inviscid jets, he found $\lambda_{opt} = 9.01h_0$, not far from Plateau’s observation. Rayleigh also applied the method of linear stability analysis to the problem, which will be the topic of Section 2.3.

2.2 A semi-quantitative approach

Drop formation is easy to experimentally observe and analyze, nevertheless its mathematical description is anything but simple. The theory based on the NS equations, which will be introduced later, is not the easiest way to get to the physical meaning of the problem. In this section, inspired by Grubelnik & Marhl [9], we will provide a simple description of what happens in a jet during a droplet formation. The quantitative part concerns only the key processes which determine the formation of drops. As we want to make things simple to understand and easy to imagine, we set a quite familiar frame: a water jet falling from a faucet, breaking up in droplets at its lower end, as in Figure 2.2. However, since the physical mechanism is general, the following considerations hold for any cylindrical liquid jet, may that be a squirt, a liquid bridge or a simple falling thread, as in our case.



Figure 2.2: Water jet falling from a faucet [9].

2.2.1 Drop formation

When the water leaves the faucet some wave-like perturbations emerge in the flow, so little that it is almost impossible to see them. During the fall these perturbations grow in amplitude, eventually leading to break up. As we stated before, this is due to surface tension, which tends to reduce the area of the liquid surface. If it was not for inertia, which works against transfer of large amount of liquid, the flow would gather in a unique large spherical volume.

To understand why the flow is unstable we have to write down the expression of the pressure inside the fluid thread. We approximate the shape of the flow with a cylinder and neglect gravity contribution: because of surface tension the pressure inside is greater than that of the environment. The pressure difference $\Delta p = p - p_0$ between inside and outside, times the lateral surface of the cylinder S , is in relation with the force F due to surface tension. With reference to Figure 2.3, we can write a force balance in the radial direction:

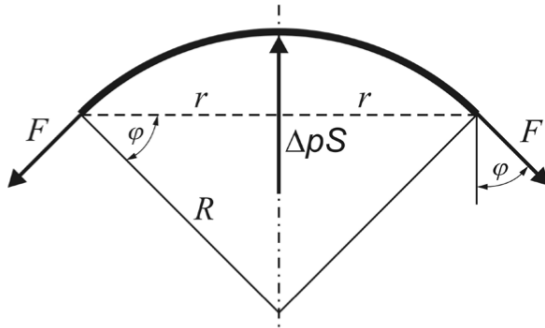


Figure 2.3: Cross section of the cylindrical flow [9].

$$\Delta p S - 2F \cos \varphi = 0. \quad (2.1)$$

If we approximate the chord with the arc, then $S = 2rl$, where l is the length of the cylinder, while $F = \gamma l$, where γ is the surface tension. Then:

$$\Delta p = \frac{\gamma \cos \varphi}{r}. \quad (2.2)$$

Since $r = R \cos \varphi$, we can write:

$$\Delta p = \frac{\gamma}{R}. \quad (2.3)$$

As clear from Figure 2.4 the instability is caused by the fact that the pressure increases in constricted regions driving out the fluid and thus reducing the radius even more. Any swelling is then a source of instability in the flow that potentially can lead to its rupture.

There are also a few stabilizing and/or retarding factors that must be taken into account.

- **Radius of curvature of the perturbation.** Looking at Figure 2.4 it is evident that the cylindrical shape is only an approximation. In order to evaluate correctly the pressure inside the jet, also the radius of curvature in the plane parallel to the axis should be considered, as it is evident from Figure 2.5. In a similar way to the one just seen, it

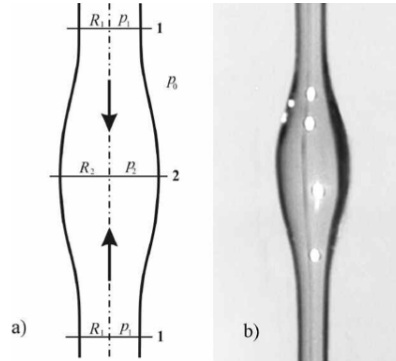


Figure 2.4: Initial stage of drop formation: (a) scheme and (b) photo [9].

can be shown that the pressure that arises inside the jet in virtue of this radius is stabilizing. In fact this contribution can be expressed again as $\Delta p_2 = \frac{\gamma}{R_2}$, and the total pressure difference result:

$$\Delta p = \gamma \left(\frac{1}{R_1} + \frac{1}{R_2} \right). \quad (2.4)$$

This curvature of the perturbation is alternatively positive and negative along the jet. Due to surface tension, it induces in the flow an over-pressure in correspondence of the swellings, and an under-pressure in correspondence of the valleys. Therefore, also the reason for which a jet is unstable and breaks up only if the perturbation wavelength is large enough becomes clear. If the perturbation has a short wavelength, also the corresponding radius of curvature will be small, inducing a strong stabilizing pressure that annihilates the unstable contribution of the other radius and ‘kills’ the perturbation itself. On the other hand for long wavelengths this contribution is over-ruled by the one arising by virtue of the first radius of curvature, and rupture becomes unavoidable.

- **Inertia.** Anything that has a mass exhibits a resistance to any change in its motion. Inertia affects the dynamics of the rupture process and

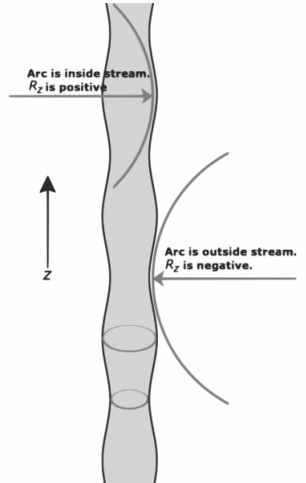


Figure 2.5: Scheme of radii of curvature (from Wikipedia).

the resultant diameter of the drops. We introduce a dimensionless parameter which measures the ratio between the kinetic energy of a drop issuing from the jet relative to its surface energy, the *Weber* number:

$$We = \frac{\rho h_0 v_0^2}{\gamma} = \frac{\textit{inertial forces}}{\textit{surface forces}}, \quad (2.5)$$

where h_0 is the radius of the jet and v_0 the velocity at the outlet.

- **Viscosity.** Any fluid exhibits a resistance to deformation, connected to the idea of friction. In this case this property tends to slow processes. Its relative importance with respect to surface energy and inertia is represented by the ‘Ohnesorge’ number:

$$Oh = \frac{\mu}{\sqrt{\rho\gamma h_0}} = \frac{\textit{viscosity forces}}{\sqrt{\textit{inertial forces} \cdot \textit{surface forces}}}. \quad (2.6)$$

The time of detachment of the first drop can be estimated from a dimensional analysis of the physical problem, neglecting viscosity. The parameters that come into play are density ρ , surface tension γ and radius of

the jet h_0 . The characteristic time τ_c is then given by:

$$\tau_c = \sqrt{\frac{\rho h_0^3}{\gamma}}, \quad (2.7)$$

and this provides with a characteristic time at which the cylinder will break in droplets. It predicts that massive flows have slower pinch-off processes (inertia slows down the evolution of perturbations), while fluids with large surface tension exhibit earlier breakups.

It is possible to define also a viscous timescale:

$$\tau_v = \frac{\eta h_0}{\gamma}. \quad (2.8)$$

The ratio of the viscous timescale τ_v to the inertial one τ_c is precisely the Ohnesorge number Oh , illustrating the slowing down of the instability by viscosity when Oh is large.

To conclude this section we show how surface tension (Figure 2.6), the presence of forced mechanical perturbations (Figure 2.7) and acoustic perturbations (Figure 2.8) can influence the rupture of jets.

2.3 Rayleigh linear stability analysis

In this section we perform a linear stability analysis of the problem, a technique pioneered by Rayleigh. We will show theoretically that any perturbation of long ‘enough’ wavelength will result in the growth of the perturbation itself. Rayleigh was the first to evidence the importance of the most unstable wavelength, which can be found only by studying the dynamics.

Before we begin the analysis of the jet, it is worth to outline the basic procedure involved in a linear stability analysis:

1. specify the governing (full, non linear) equations and boundary conditions;
2. find the base state;

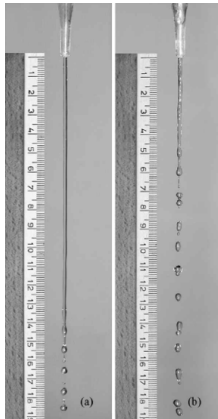


Figure 2.6: Effect of γ on drop formation: (a) water and soap ($\gamma = 0,03$ N/m), (b) pure water ($\gamma = 0,073$ N/m) [9].

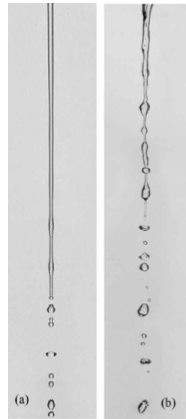


Figure 2.7: Effect of flow irregularity on drop formation: (a) without and (b) with forced perturbations [9].

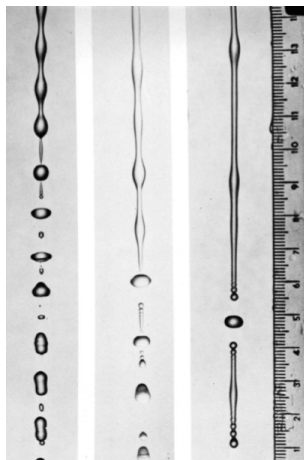


Figure 2.8: A thin jet of water is perturbed at various frequencies by a loudspeaker. Photograph by Rutland and Jameson (1971), taken from van Dyke (1982).

3. subject the base state to a small perturbation;
4. linearise the equations (substitute the perturbed forms (3) into the governing equations (1) and expand these equations about the base state (2) in increasing powers of the perturbation's amplitude δ ; neglect terms $O(\delta^2)$ and higher);
5. solve the linearised equations and get the dispersion relation using normal modes (reduce to the form of an eigenvalue problem) ;
6. analyze the dispersion relation and find stable and unstable modes.

Rayleigh considered as *base flow* an infinite, incompressible, inviscid and axisymmetric cylinder of radius h_0 , with axial velocity U_{z0} and zero radial velocity. With these assumptions we can write for the jet the following Euler equations:

$$\begin{cases} \frac{\partial U_r}{\partial r} + \frac{\partial U_z}{\partial z} + \frac{U_r}{r} = 0, \\ \frac{\partial U_r}{\partial t} + U_r \frac{\partial U_r}{\partial r} + U_z \frac{\partial U_r}{\partial z} = -\frac{1}{\rho} \frac{\partial P}{\partial r}, \\ \frac{\partial U_z}{\partial t} + U_r \frac{\partial U_z}{\partial r} + U_z \frac{\partial U_z}{\partial z} = -\frac{1}{\rho} \frac{\partial P}{\partial z} - g. \end{cases} \quad (2.9)$$

In order to close the problem these equations have to be coupled with a kinematic condition at the interface,

$$\frac{\partial h}{\partial t} = U_r - U_z \frac{\partial h}{\partial z} \quad (2.10)$$

and the equilibrium of the forces at the interface,

$$P - P_{atm} = \gamma \left(\frac{1}{h [1 + (\frac{\partial h}{\partial z})^2]^{0.5}} - \frac{(\frac{\partial^2 h}{\partial z^2})}{[1 + (\frac{\partial h}{\partial z})^2]^{1.5}} \right). \quad (2.11)$$

The details of the derivation of Equations (2.10) and (2.11) are given in Section 3.1. From Equations (2.9) it is clear that for the base flow the

pressure is constant along the jet, and Equation (2.11) implies that at the interface this pressure is $p_{bf} = p_{atm} + \frac{\gamma}{h_0}$.

Before proceeding further it is convenient to write a non-dimensional formulation of the problem. The fundamental units present in the variables are distance L , time T and mass M , non-dimensionalized respectively with the radius of the jet h_0 , the characteristic time $\tau_c = \sqrt{\frac{\rho h_0^3}{\gamma}}$ and the density of the fluid ρ . Thus, the non-dimensional fluid thread has radius $h_0^* = 1$, velocity $u_{z0}^* = \frac{\tau_c}{h_0} U_{z0} = \sqrt{We}$ and pressure $p^* = \frac{h_0}{\gamma}$. The non-dimensional system of equations results:

$$\begin{cases} \frac{\partial U_r^*}{\partial r^*} + \frac{\partial U_z^*}{\partial z^*} + \frac{U_r^*}{r^*} = 0, \\ \frac{\partial U_r^*}{\partial t^*} + U_r^* \frac{\partial U_r^*}{\partial r^*} + U_z^* \frac{\partial U_r^*}{\partial z^*} = -\frac{\partial P^*}{\partial r^*}, \\ \frac{\partial U_z^*}{\partial t^*} + U_r^* \frac{\partial U_z^*}{\partial r^*} + U_z^* \frac{\partial U_z^*}{\partial z^*} = -\frac{\partial P^*}{\partial z^*} - Bo \cdot g, \end{cases} \quad (2.12)$$

where the *Bond* number, $Bo = \frac{\rho h^2 g}{\gamma}$, is a measure of the ratio between gravitational and surface forces. In this dissertation Bo will always be neglected, an approximation acceptable if h is small enough or if the liquid jet is immersed in another liquid with the same density. The conditions at the boundaries become:

$$\frac{\partial h^*}{\partial t^*} = U_r^* - U_z^* \frac{\partial h^*}{\partial z^*}, \quad (2.13)$$

$$P^* - \frac{h_0}{\gamma} P_{atm} = \left(\frac{1}{h^* [1 + (\frac{\partial h^*}{\partial z^*})^2]^{0.5}} - \frac{(\frac{\partial^2 h^*}{\partial z^{*2}})}{[1 + (\frac{\partial h^*}{\partial z^*})^2]^{1.5}} \right). \quad (2.14)$$

Since we will always deal with non-dimensional equations, for convenience hereafter the asterisks will be dismissed.

If we now superpose an infinitesimal little perturbation to the base flow, the variables become:

$$\begin{aligned} U_r &= 0 + \epsilon u_r(z, r, t), \\ U_z &= U_{z0} + \epsilon u_z(z, r, t), \\ P &= P_0 + \epsilon p(z, r, t), \\ h &= h_0 + \epsilon \eta(z, t). \end{aligned}$$

Substituting in (2.12) and linearizing (keeping only the leading order terms), one gets:

$$\begin{cases} \frac{\partial u_r}{\partial r} + \frac{\partial u_z}{\partial z} + \frac{u_r}{r} = 0, \\ \frac{\partial u_r}{\partial t} + U_{z0} \frac{\partial u_r}{\partial z} = -\frac{\partial p}{\partial r}, \\ \frac{\partial u_z}{\partial t} + U_{z0} \frac{\partial u_z}{\partial z} = -\frac{\partial p}{\partial z}. \end{cases} \quad (2.15)$$

Doing the same for boundary conditions (2.13) and (2.14):

$$\frac{\partial \eta}{\partial t} + U_{z0} \frac{\partial \eta}{\partial z} = u_r \quad (2.16)$$

$$p = -\left(\eta + \frac{\partial^2 \eta}{\partial z^2}\right) \quad (2.17)$$

Combining Equations (2.12) it can be shown that the laplacian of the pressure has to vanish [10], so that:

$$\frac{\partial^2 p}{\partial r^2} + \frac{1}{r} \frac{\partial p}{\partial r} + \frac{\partial^2 p}{\partial z^2} = 0. \quad (2.18)$$

In order to perform a normal mode analysis we Fourier-transform the perturbation along z and t , obtaining:

$$\begin{aligned} u_r &= \hat{u}_r(r) e^{i(kz - \omega t)} \\ u_z &= \hat{u}_z(r) e^{i(kz - \omega t)} \\ p &= \hat{p}(r) e^{i(kz - \omega t)} \\ \eta &= B e^{i(kz - \omega t)} \end{aligned} \quad (2.19)$$

where k is the wavenumber and ω the frequency. Then, the Equation (2.18) can be written as:

$$\frac{\partial^2 \hat{p}}{\partial r^2} + \frac{1}{r} \frac{\partial \hat{p}}{\partial r} - k^2 \hat{p} = 0. \quad (2.20)$$

The solution of this equation is a Bessel function, in particular it results:

$$\hat{p} = AI_0(kr) + CK_0(kr), \quad (2.21)$$

where $I_0 = \frac{1}{\pi} \int_0^\pi e^{kr \cos(\theta)} d\theta$ and $K_0 = \int_0^\infty e^{-kr \cosh(t)} dt$, while A and C are constants that depend on the boundary conditions. From the condition $\frac{\partial \hat{p}}{\partial r} \Big|_{r=0} = 0$ it follows that $C = 0$, hence:

$$\hat{p}(r) = AI_0(kr). \quad (2.22)$$

Substituting (2.19) in the first of (2.15), one gets:

$$-i\omega \hat{u}_r + ikU_{z0} \hat{u}_r = -AkI_0'(kr), \quad (2.23)$$

where primes denote $\frac{d}{d(kr)}$. This gives an expression for \hat{u}_r :

$$\hat{u}_r = -\frac{i}{(\omega - kU_{z0})} AkI_0'(kr), \quad (2.24)$$

which, substituted in (2.16), leads to:

$$-i\omega B + ikU_{z0} B = -\frac{i}{(\omega - kU_{z0})} AkI_0'(kr). \quad (2.25)$$

Finally, from 2.17, one gets:

$$AI_0(k) = -B(1 - k^2). \quad (2.26)$$

Gathering all the results in a system, we can write the *dispersion relation*, that will tell us which perturbations are destabilizing:

$$\begin{pmatrix} I_0(k) & (1 - k^2) \\ \frac{kI_0'(k)}{(\omega - U_{z0}k)} & -(\omega - U_{z0}k) \end{pmatrix} \begin{pmatrix} A \\ B \end{pmatrix} = 0.$$

A non-trivial solution exists if and only if the determinant of the matrix is equal to zero. Imposing this condition we can eventually write an expression for ω :

$$\omega = Uk \pm \sqrt{k(k^2 - 1) \frac{I_0'(k)}{I_0(k)}} \quad (2.27)$$

Following from its definition, the perturbation will be unstable if and only if $\text{Im}(\omega) > 0$. As shown in Figure 2.9, this means that there is an exponential

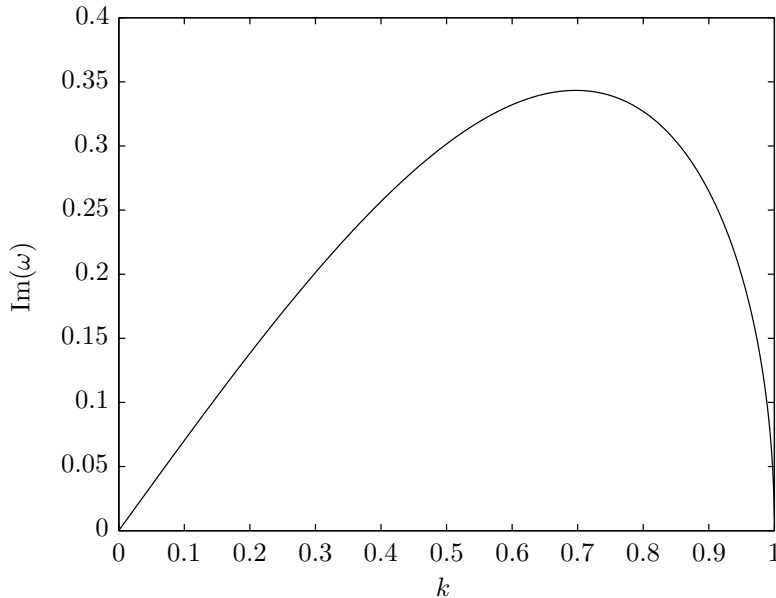


Figure 2.9: Dimensionless growth rate $\text{Im}(\omega)$ of perturbations as a function of the dimensionless wave number k . The flow is unstable only if $k < 1$.

growth of the initial disturbance, i.e. the flow is unstable, if $k < 1$. This result has been successfully tested experimentally, even if highly accurate measurements of linear jet stability are not simple [11]. It turns out that, for approximately inviscid flows, the most unstable among the non-dimensional wavenumbers is $k_{opt} \approx 0.7$, which means $\lambda_{opt} \approx 9$, as anticipated at the beginning of the chapter. The fact that there is a cut-off wavenumber $k_{cut-off} = 1$, beyond which the flow is stable, is not surprising and is consistent with what discussed in Subsection 2.2.1

Thanks to linear stability analysis we have theoretically described and explained some non-trivial behaviors of slender jets, extrapolating precious information with relatively modest effort. Of course, as soon as the pertur-

bations are no longer small, non-linear effects become important, and eventually dominate close to breakup. The growth of sinusoidal modes cannot explain the presence of satellite drops and cannot predict the evolution of the shape of the jet. Thus, it appears reasonable that including non-linear effects in an optimization loop will lead to finding pinch-off times shorter than the shortest one identified by Rayleigh. The first step will consist in finding a simplified set of equations for the physical problem, in order to keep the computational costs low.

Chapter 3

Equations of motion

In this Chapter we discuss the physical model of the jet and derive the equations that describe it. We consider a liquid having a columnar shape, with a free surface. The flow is viscous and is supposed to be axisymmetric. As we know from the previous Chapter, this situation is unstable under certain circumstances and, after some time, surface tension leads the cylindrical configuration to collapse and break into droplets. Droplets detach when the radius becomes locally zero. When this happens equations develop a singularity and the model will not be able to describe the flow anymore.

Linear stability analysis performed in Section 2.3 predicted the existence of two zones (stability and instability) if the cylinder is perturbed with modal disturbances. For the unstable range of perturbations, it gave an estimate of the diameter of the drops formed. However, it does not give information on the evolution of the shape of the jet in time. For example, it does not explain the fact that main drops of regular size in many cases induce tiny ‘satellite’ drops. Higher order perturbation theory gives a qualitative prediction of the differences in size of the drops, but fails to give a description of the evolution of the flow [12, 13]. In fact, the non linearity of the flow has to be taken into account in order to study the problem at this level of analysis, especially if we want to control the break-up, which is the goal of this thesis.

A model with the full Navier-Stokes equations would be extremely complicated to employ, for both analytical and numerical studies. Since the zone neighboring to pinch off requires very high resolution, simulations would result extremely onerous. This becomes even more unacceptable for optimization purposes, because, as we will see, the flow will have to be solved a large number of times in the course of the optimization procedure. Thus, a reduction of the physical problem to a simpler one is sought, in order to get savings in computation time up to four order of magnitude, making the optimization loops feasible. We will therefore use a set of one-dimensional equations, developed by Eggers and Dupont [14]. In the following section we will derive them expanding the radial variable in a Taylor series and neglecting terms of the Navier-Stokes equations larger than leading order.

3.1 Eggers and Dupont (1D) model

The continuity and Navier-Stokes equations in cylindrical coordinates for an axisymmetric column of fluid with kinematic viscosity ν and density ρ read:

$$\frac{\partial V_r}{\partial t} + V_r \frac{\partial V_r}{\partial r} + V_z \frac{\partial V_r}{\partial z} = -\frac{1}{\rho} \frac{\partial p}{\partial r} + \nu \left(\frac{\partial^2 V_r}{\partial r^2} + \frac{\partial^2 V_r}{\partial z^2} + \frac{1}{r} \frac{\partial V_r}{\partial r} - \frac{V_r}{r^2} \right), \quad (3.1)$$

$$\frac{\partial V_z}{\partial t} + V_r \frac{\partial V_z}{\partial r} + V_z \frac{\partial V_z}{\partial z} = -\frac{1}{\rho} \frac{\partial p}{\partial z} + \nu \left(\frac{\partial^2 V_z}{\partial r^2} + \frac{\partial^2 V_z}{\partial z^2} + \frac{1}{r} \frac{\partial V_z}{\partial r} \right), \quad (3.2)$$

$$\frac{\partial V_r}{\partial r} + \frac{\partial V_z}{\partial z} + \frac{V_r}{r} = 0, \quad (3.3)$$

where V_z is the axial velocity, V_r the radial velocity and p the pressure. Equations (3.2) and (3.3) hold for $0 \leq r < h(z, t)$, where $h(z, t)$ is the radial coordinate of the interface. A scheme of the configuration is displayed in Figure 3.1. Recalling Equation (2.4), we write the balance of normal forces at the interface as:

$$(\mathbf{n}^T \sigma) \cdot \mathbf{n} = -\gamma \left(\frac{1}{R_1} + \frac{1}{R_2} \right), \quad (3.4)$$

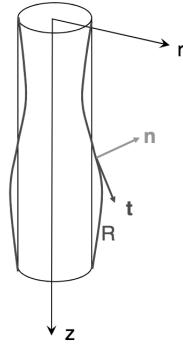


Figure 3.1: Cylindrical configuration.

where γ is the surface tension acting at the interface of the two fluids, \mathbf{n} is the unit vector in the normal direction to the interface, σ is the stress tensor and R_1 and R_2 are the principal radii of curvature. Forces linked to surface tension only act in the direction normal to the interface. In the tangential balance of forces the interaction between the jet and the outer fluid is neglected. This approximation is reasonable because of the relative low velocity of the jet, its tiny surface and, if the external fluid is air, the small viscosity of the latter. Therefore:

$$(\mathbf{n}^T \sigma) \cdot \mathbf{t} = 0, \quad (3.5)$$

where \mathbf{t} is the unit vector in the direction tangential to the interface. From geometrical considerations \mathbf{n} and \mathbf{t} are explicitly given as functions of h by:

$$\mathbf{n}(r, z) = \left(\frac{1}{\sqrt{1 + \left(\frac{\partial h}{\partial z}\right)^2}}, -\frac{\frac{\partial h}{\partial z}}{\sqrt{1 + \left(\frac{\partial h}{\partial z}\right)^2}} \right), \quad (3.6)$$

$$\mathbf{t}(r, z) = \left(\frac{\frac{\partial h}{\partial z}}{\sqrt{1 + \left(\frac{\partial h}{\partial z}\right)^2}}, \frac{1}{\sqrt{1 + \left(\frac{\partial h}{\partial z}\right)^2}} \right). \quad (3.7)$$

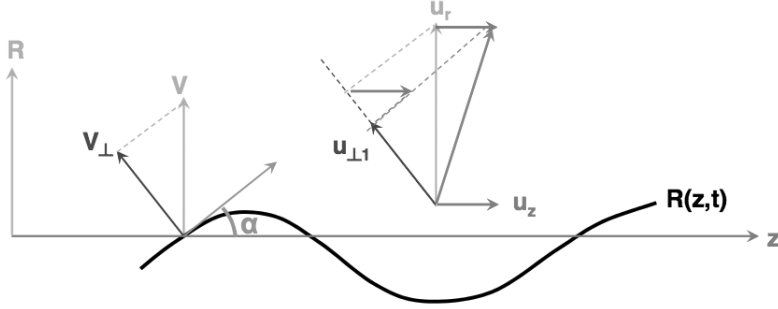


Figure 3.2: Velocity field at the boundary.

Hence, the boundary conditions (3.4) and (3.5) become:

$$\frac{p}{\rho} - \frac{2\nu}{1 + \left(\frac{\partial h}{\partial z}\right)^2} \left[\frac{\partial V_r}{\partial r} + \frac{\partial V_z}{\partial z} \left(\frac{\partial h}{\partial z}\right)^2 - \left(\frac{\partial V_z}{\partial r} + \frac{\partial V_r}{\partial z}\right) \frac{\partial h}{\partial z} \right] = -\gamma \left(\frac{1}{R_1} + \frac{1}{R_2} \right) \quad (3.8)$$

$$\frac{\nu}{1 + \left(\frac{\partial h}{\partial z}\right)^2} \left[2 \frac{\partial V_r}{\partial r} \frac{\partial h}{\partial z} + \left(\frac{\partial V_z}{\partial r} + \frac{\partial V_r}{\partial z}\right) \left(1 - \left(\frac{\partial h}{\partial z}\right)^2\right) - 2 \frac{\partial V_z}{\partial z} \frac{\partial h}{\partial z} \right] = 0 \quad (3.9)$$

In addition, the surface has to move with the velocity field at the boundary (impermeability condition). We refer to Figure 3.2:

$$V_{\perp} = u_{\perp 1},$$

$$V_{\perp} = \frac{\partial h}{\partial t} \cos(\alpha),$$

$$u_{\perp 1} = u_r \cos(\alpha) - u_z \sin(\alpha),$$

so that we can write, as in Equation (2.10):

$$\frac{\partial h}{\partial t} + V_z \frac{\partial h}{\partial z} = V_r|_{r=h}. \quad (3.10)$$

Finally, because of symmetry, in $r = 0$ we have:

$$\frac{\partial V_z}{\partial r} = 0, \quad V_r = 0. \quad (3.11)$$

Solving directly Equations (3.1), (3.2), (3.3), (3.8), (3.9), (3.10) would be a challenging task, especially close to pinch off, where $h \rightarrow 0$. As already pointed out, high resolution needed to capture the singularity would result in an exaggerated computational cost. Hence, we now want to reduce the problem to one dimension. The idea is that the column of fluid is thin relative to its length ($r \ll L$, where L is the elongation of the jet), so that in a Taylor expansion with respect to r one is allowed to neglect terms of order $\mathcal{O}(r^2)$ and larger.

The flow exhibits a varicose symmetry, therefore we can expand V_z and p in r in the following way:

$$V_z(r, z, t) = V_0(z, t) + V_2(z, t)r^2 + \dots \quad (3.12)$$

$$p(r, z, t) = p_0(z, t) + p_2(z, t)r^2 + \dots \quad (3.13)$$

From continuity (3.3), V_r has to be:

$$V_r(r, z, t) = -\frac{\partial V_0(z, t)}{\partial z} \frac{r}{2} - \frac{\partial V_2(z, t)}{\partial z} \frac{r^3}{4} + \dots \quad (3.14)$$

We now insert Equations (3.12)-(3.14) into (3.1), (3.2) and (3.8), (3.9) and solve the equations to leading order in r . Equation (3.1) is identically satisfied, while in the case of (3.2) we have:

$$\frac{\partial V_0}{\partial t} + V_0 \frac{\partial V_0}{\partial z} = -\frac{1}{\rho} \frac{\partial p_0}{\partial z} + \nu \left(4V_2 + \frac{\partial^2 V_0}{\partial z^2} \right) \quad (3.15)$$

Long wave-length description implies that $\frac{\partial h}{\partial z}$ is also of order r , so from (3.8) we get an expression for p_0 :

$$\frac{p_0}{\rho} + \nu \frac{\partial V_0}{\partial z} = \frac{\gamma}{\rho} \left(\frac{1}{R_1} + \frac{1}{R_2} \right). \quad (3.16)$$

Equation (3.9) gives an expression involving V_2 :

$$-3 \frac{\partial V_0}{\partial z} \frac{\partial h}{\partial z} + 2V_2 h - \frac{1}{2} \frac{\partial^2 V_0}{\partial z^2} = 0. \quad (3.17)$$

We eliminate V_2 and p_0 from (3.15) using (3.16) and (3.17):

$$\frac{\partial V_0}{\partial t} = -V_0 \frac{\partial V_0}{\partial z} - \frac{\gamma}{\rho} \frac{\partial}{\partial z} \left(\frac{1}{R_1} + \frac{1}{R_2} \right) + 3\nu \frac{\frac{\partial}{\partial z} \left(h^2 \frac{\partial V_0}{\partial z} \right)}{h^2}. \quad (3.18)$$

From impermeability (3.10) it follows:

$$\frac{\partial h}{\partial t} = -V_0 \frac{\partial h}{\partial z} - \frac{1}{2} \frac{\partial V_0}{\partial z} = \frac{1}{2h} \frac{\partial}{\partial z} (h^2 V_0); \quad (3.19)$$

the expression for the mean curvature $\frac{1}{2} \left(\frac{1}{R_1} + \frac{1}{R_2} \right)$ can be found in differential geometry literature [15]. Hence, dropping the subscript ‘0’ on V_0 and denoting the surface tension contribution of the pressure by p , we eventually get:

$$\begin{cases} \frac{\partial h}{\partial t} = \frac{1}{2h} \frac{\partial}{\partial z} (h^2 V), \\ \frac{\partial V}{\partial t} = -V \frac{\partial V}{\partial z} - \frac{1}{\rho} \frac{\partial p}{\partial z} + 3\nu \left(\frac{2 \frac{\partial h}{\partial z} \frac{\partial V}{\partial z}}{h} + \frac{\partial^2 V}{\partial z^2} \right), \\ p = \gamma \left(\frac{1}{h [1 + (\frac{\partial h}{\partial z})^2]^{0.5}} - \frac{(\frac{\partial^2 h}{\partial z^2})}{[1 + (\frac{\partial h}{\partial z})^2]^{1.5}} \right). \end{cases} \quad (3.20)$$

This system of equations, that will concern us for the rest of the thesis, has to be solved for $z \in [-L, L]$ imposing boundary and initial conditions:

$$h(\pm L, t) = h_0 f_{1,2}(t) \quad (3.21)$$

$$V(\pm L, t) = V_0 f_{3,4}(t) \quad (3.22)$$

$$h(z, 0) = g_1(z) \quad (3.23)$$

$$V(z, 0) = g_2(z) \quad (3.24)$$

Where $f_{1,2}$ and $g_{1,2}$ depend on the configuration considered. We reiterate that the physical velocity field (3.12),(3.14) has both radial and longitudinal components which are r -dependent. The physical pressure (3.13) also has contributions from the shear stress. When referring to V and p in (3.20) as ‘velocity’ and ‘pressure’, these considerations have to be kept in mind.

3.2 Non-dimensional equations

Similarly to what we have already seen in Section 2.3, the fundamental units present in the variables are distance L , time T and mass M , respectively non-dimensionalized with the radius of the unperturbed jet h_0 , the characteristic time $\tau_c = \sqrt{\frac{\rho h_0^3}{\gamma}}$, and the density of the fluid, ρ . We can write:

$$\begin{aligned} z &= h_0 z^*, \\ h &= h_0 h^*, \\ L &= h_0 L^*, \\ V &= \frac{h_0}{\tau_c} V^*, \\ t &= \tau_c t^*, \end{aligned}$$

which implies $V^* = \sqrt{We}$ and $h_0^* = 1$. Hence, the non-dimensional equations are:

$$\begin{cases} \frac{\partial h^*}{\partial t^*} = \frac{1}{2h^*} \frac{\partial}{\partial z^*} (h^2 V_0^*), \\ \frac{\partial V^*}{\partial t^*} = -V^* \frac{\partial V^*}{\partial z^*} - \frac{\partial p^*}{\partial z^*} + 3Oh \left(\frac{2 \frac{\partial h^*}{\partial z^*} \frac{\partial V^*}{\partial z^*}}{h^*} + \frac{\partial^2 V^*}{\partial z^{*2}} \right), \\ p^* = \gamma \left(\frac{1}{h^* [1 + (\frac{\partial h^*}{\partial z^*})^2]^{0.5}} - \frac{(\frac{\partial^2 h^*}{\partial z^{*2}})}{[1 + (\frac{\partial h^*}{\partial z^*})^2]^{1.5}} \right). \end{cases} \quad (3.25)$$

The boundary and initial conditions result:

$$h^*(\pm L^*, t^*) = f_{1,2}(t^*), \quad (3.26)$$

$$V^*(\pm L^*, t^*) = \sqrt{We} f_{3,4}(t^*), \quad (3.27)$$

$$h^*(z^*, 0) = g_1(z^*), \quad (3.28)$$

$$V^*(z^*, 0) = g_2(z^*). \quad (3.29)$$

The meaning of non-dimensional numbers Oh and We has already been discussed in Section 2.2.1. From now on we will deal only with non-dimensional variables, so the asterisks will be left out.

In conclusion, we will have to solve a pair of coupled nonlinear partial differential equations (PDEs) in time and space (only one dimension).

3.2.1 Equations in $F = h^2$

For numerical reasons, in many cases solving equations containing h^2 instead of h results more convenient. We report here the system in F , obtained applying the change of variable $F = h^2$ to (3.25). The system is already non-dimensionalized and without asterisks. The velocity V remains unchanged.

$$\left\{ \begin{array}{l} \frac{\partial F}{\partial t} = -\frac{\partial}{\partial z}(FV), \\ \frac{\partial V}{\partial t} = -V\frac{\partial V}{\partial z} - \frac{\partial p}{\partial z} + 3Oh\frac{\partial}{\partial z}\left(\frac{F\frac{\partial V}{\partial z}}{F}\right), \\ p = \frac{\left(2 - \frac{\partial^2 F}{\partial z^2}\right)F + \left(\frac{\partial F}{\partial z}\right)^2}{2\left(0.25\left(\frac{\partial F}{\partial z}\right)^2 + F\right)^{1.5}}. \end{array} \right. \quad (3.30)$$

Inserting p in the second equation, more explicitly the system reads:

$$\left\{ \begin{array}{l} \frac{\partial F}{\partial t} = -F \frac{\partial V}{\partial z} - V \frac{\partial F}{\partial z}, \\ \frac{\partial V}{\partial t} = -V \frac{\partial V}{\partial z} + \frac{1}{2} \frac{\left(\frac{\partial^3 F}{\partial z^3} F - \frac{\partial^2 F}{\partial z^2} \frac{\partial F}{\partial z} - 2 \frac{\partial F}{\partial z} \right)}{\left(0.25 \left(\frac{\partial F}{\partial z} \right)^2 + F \right)^{1.5}} + \dots \\ \dots + \frac{3}{4} \frac{\left(\frac{1}{2} \left(\frac{\partial F}{\partial z} \right)^3 \frac{\partial^2 F}{\partial z^2} + \left(\frac{\partial F}{\partial z} \right)^3 - \frac{1}{2} \left(\frac{\partial^2 F}{\partial z^2} \right)^2 \frac{\partial F}{\partial z} F + 2 \frac{\partial F}{\partial z} F \right)}{\left(0.25 \left(\frac{\partial F}{\partial z} \right)^2 + F \right)^{2.5}} + \dots \\ \dots + 3Oh \frac{1}{F} \frac{\partial F}{\partial z} \frac{\partial V}{\partial z} + 3Oh \frac{\partial^2 V}{\partial z^2}. \end{array} \right. \quad (3.31)$$

It is obviously always allowed to solve (3.31) - or (3.30) - instead of (3.25). After having applied $h = \sqrt{F}$ the results will be exactly the same.

3.3 Linear stability analysis

Following the same procedure of Section 2.3 we now perform a linear stability analysis on the one-dimensional equations that have just been derived. We refer again to an infinite cylinder initially at rest and we apply a little sinusoidal perturbation with wavelength $\lambda = \frac{2\pi}{k}$ and frequency $f = \frac{\omega}{2\pi}$:

$$h(z, t) = 1 + \epsilon e^{i(kz - \omega t)}, \quad (3.32)$$

where $\omega \in \mathbb{C}$ and $k \in \mathbb{R}$. Inserting (3.32) in (3.25) one gets:

$$V = V_0 \epsilon e^{i(kz - \omega t)},$$

$$V_0 \omega = -k + k^3 - 6Oh \cdot \omega i k,$$

where $V_0 = \frac{2\omega}{k}$. Solving with respect to ω leads to:

$$2\omega^2 + (6Oh \cdot h k^2 i) \omega + k^2 - k^4 = 0; \quad (3.33)$$

the perturbation is destabilizing if and only if $\text{Im}(\omega) > 0$, which is verified for $0 < k < 1$, independently of Oh . Therefore, this analysis suggests that there is a cut off wavenumber, or limit of stability, $k_{cut-off} = 1 \rightarrow \lambda = 2\pi$, which is the same we found in Section 2.3. The most unstable mode or fastest growing rate is reached when:

$$k = k_{opt} = \sqrt{\frac{1}{2 + 3\sqrt{2}Oh}}. \quad (3.34)$$

We now compare the instability curves obtained with Rayleigh theory (2 dimensions, inviscid flow) with Eggers and Dupont model (1 dimension), setting $Oh = 0$ in the latter. As it is evident from Figure 3.3, there is a good agreement between the two analysis. In Figure 3.4 are plotted instability curves for different values of Oh (i.e. viscosity) based on the equations by Eggers and Dupont (E-D). Referring to this picture some considerations can be made:

- $k_{cut-off} = 1$ for every Oh . The limit of stability is univocally determined by geometry considerations involving the ratio between the two radii of curvature (one stabilizing and the other destabilizing, see Section 2.3), i.e. by the relative dimension of the wavelength of the perturbation compared to the radius of the jet. On the other hand viscous stresses, which are proportional to rates of deformation, affect the dynamics of jet instabilities, and the dynamics only.
- A greater Oh number means a smaller growth rate. This is not very surprising: we already pointed out (see Section 2.3) that viscosity slows down the process.
- The fastest growth rate for every iso- Oh curve shifts toward lower k as Oh decreases. This is evident from (3.34), which implies also that in the limit of infinite viscosity the infinite-wavelength perturbation becomes the most unstable one. The fact that the instability selects longer wavelengths at larger Oh can be qualitatively explained with the fact that viscosity slows down shorter wavelengths more efficiently.

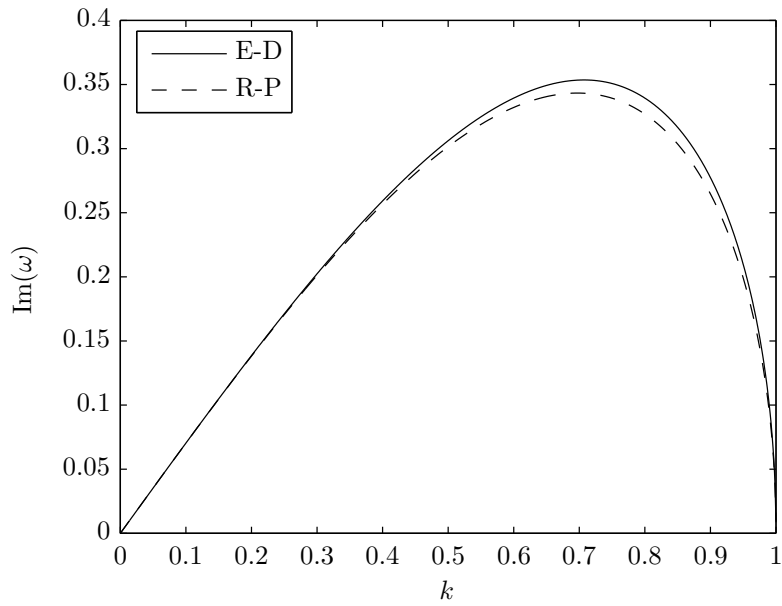


Figure 3.3: Comparison between Rayleigh's theory (dotted line) and Eggers and Dupont's (continuous line).

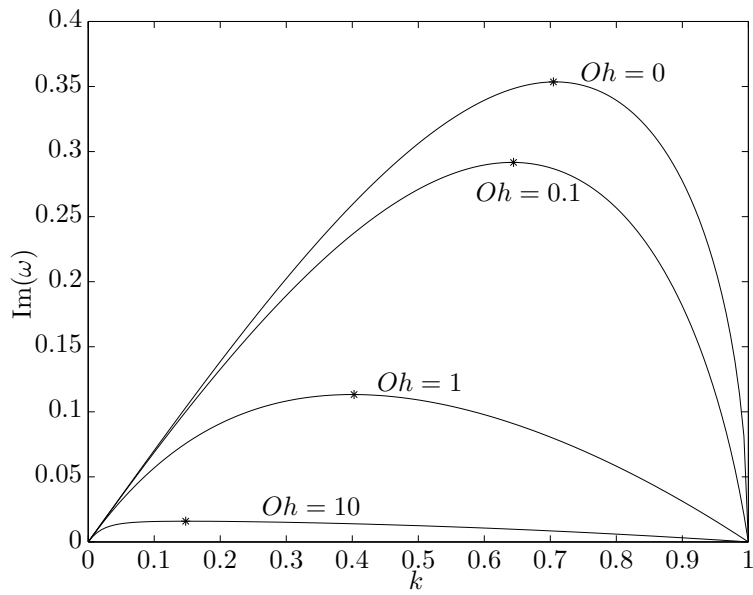


Figure 3.4: E-D instability curves for different values of Oh . The asterisks represent the fastest growth rate for every iso- Oh curve.

3.4 Transient growth analysis

Linear stability analysis does not explore the short time behavior of an arbitrary disturbance of a flow. The idea behind classical eigenmode analysis is testing the asymptotic evolution of a system under the effect of a perturbation \mathcal{X} , small enough to assume that non-linear terms $\mathcal{X}^2, \mathcal{X}^3$, etc. are negligible. It is obvious that if the perturbation is no longer small these terms cannot be discarded anymore and non linearity has to be included in order to get physical reliable answers. Non linear systems can be highly unpredictable and normally the full equations have to be solved to know their behavior. Nevertheless, another linear instability exists, it is non-modal and is termed *transient growth*. In effect, small perturbations may under some circumstances grow for a period of time before decaying, even if they are eigenmode stable. This effect is completely overlooked by classical analysis, which is not capable of predicting initial transients. Even if such a growth is only a transient phenomenon, it may drive the perturbation to an amplitude at which non linear terms prevail and drive the evolution of the system, as sketched in Figure 3.6. Thus, linearly stable flows can in some cases become unstable even if the perturbation is effectively small enough to justify linearity assumptions.

Transient growth is caused by the non-normality of the linearized Navier-Stokes operator. A normal operator has normal eigenvectors. If their eigenvalues are negative, they will decay and the response in time of the system will be monotonically decreasing. On the other hand, a non-normal operator is characterized by non-normal eigenvectors. In this case, even if all the eigenvalues are negative, the decay of eigenvectors can lead to a temporary growth in time of the system under the action of the operator, as sketched in Figure 3.5. In particular, this can happen if the eigenvectors are non-normal ‘enough’, i.e. the angle between them is large enough, and the respective decay rates are sufficiently different [17]. Figure 3.6 shows how non-normality may give rise to transient growth and thus drive a system toward a (non linear) instability, despite the system being nominally linearly stable.

Thus, transient growth is a linear temporary effect that flows gov-

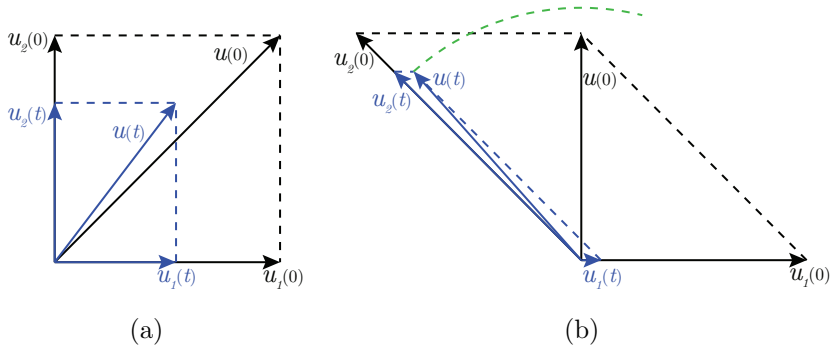


Figure 3.5: a) Vector sum of two orthogonal decaying vectors cannot do anything but decay. b) Vector sum of two non-orthogonal decaying vectors can grow in time before eventually decay.

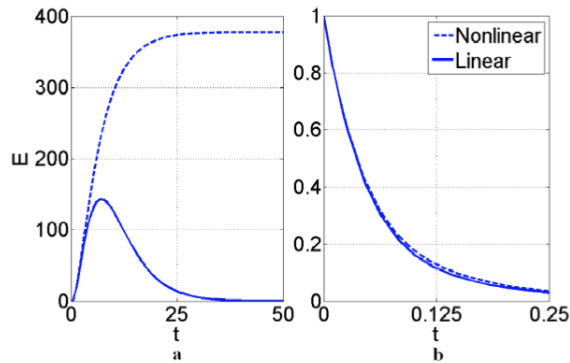


Figure 3.6: a) Evolution of a dynamic system characterized by a non-normal operator. The linear solution exhibits a transient growth, which ‘activates’ non linear effects even if the initial perturbation is small. The system reaches a steady state completely different from the one predicted by linear stability analysis. b) Linear and non linear response of a system governed by a normal operator are superposable if the initial disturbance is small [16].

erned by the Navier-Stokes equations can exhibit under some circumstances. Since the goal of this thesis is to control the rupture of jets, minimizing the time necessary to attain it, we are interested to know if transient growth is possible in our case, and how important it is. Break up is caused by the growth of instabilities, and transient growth analysis is an extra tool we can use to understand the origin of them. The question is if there are any causes of growth which could be important for break up overcome by classical analysis (but still linear). Since we will perform a non linear optimization, we would not be able to discern linear and non-linear effects without having analyzed well the problem before.

3.4.1 Mathematical description

Given a dynamical system, transient growth can be mathematically described in terms of change in a given norm of the variables of the system. For example, a two-norm will be a measure of its energy. Thus, indicating the initial condition of the state with \mathbf{q}_0 and its linear evolution at time t as $\mathbf{q}(t)$, it is possible to define a suitable gain parameter, as:

$$G(t) = \max_{\mathbf{q}_0} \frac{\|\mathbf{q}(t)\|}{\|\mathbf{q}_0\|}, \quad (3.35)$$

which gives the largest attainable linear growth at time t over all possible initial conditions \mathbf{q}_0 .

Formally, the linearization of the system reads:

$$\frac{d\mathbf{q}}{dt} = L\mathbf{q}, \quad (3.36)$$

where L is the linearized operator in matrix form, e.g. once the system has been suitably discretized. The linear evolution of \mathbf{q} in time can be computed as:

$$\mathbf{q} = e^{Lt}\mathbf{q}_0, \quad (3.37)$$

where the matrix exponential is defined as follows: let A be an $n \times n$ matrix, then its exponential, denoted by e^A , is the $n \times n$ matrix given by the always

convergent power series:

$$e^A = \sum_{k=0}^{\infty} \frac{1}{k!} A^k. \quad (3.38)$$

Since, by definition [19]:

$$\|A\| = \max_{\mathbf{u}} \frac{\|A\mathbf{u}\|}{\|\mathbf{u}\|}, \quad (3.39)$$

it results:

$$G(t) = \max_{\mathbf{q}_0} \frac{\|e^{Lt}\mathbf{q}_0\|}{\|\mathbf{q}_0\|} = \|e^{Lt}\|. \quad (3.40)$$

Thus, to get $G(t)$ it is sufficient to compute the matrix exponential of Lt .

We refer to the case of an infinite cylinder, as already done for the linear stability analysis. We need the linearization of Equations 3.31 around a base flow F, V . The linear variables are $\mathbf{q} = [\tilde{f}, \tilde{v}]$. Linear equations will be derived further and are displayed in Subsection 5.3.2, Equations (5.28). We consider a steady base flow, with a plain interface and at rest, $F(z, t) \equiv 1$ and $V(z, t) \equiv 0$. Equations (5.28) reduce to:

$$\begin{cases} \frac{\partial \tilde{f}}{\partial t} = -F \frac{\partial \tilde{v}}{\partial z}, \\ \frac{\partial \tilde{v}}{\partial t} = 3Oh \frac{\partial^2 \tilde{v}}{\partial z^2} + \frac{1}{2} \frac{1}{F^{\frac{3}{2}}} \frac{\partial \tilde{f}}{\partial z} + \frac{1}{2} \frac{1}{F^{\frac{1}{2}}} \frac{\partial^3 \tilde{f}}{\partial z^3}. \end{cases} \quad (3.41)$$

Assuming \mathbf{q} of the form $\mathbf{q} = \hat{\mathbf{q}}e^{ikz}$, system (3.41) can be rewritten as:

$$\frac{\partial \mathbf{q}}{\partial t} = \begin{pmatrix} 0 & -ik \\ \frac{1}{2}(ik - ik^3) & -3Ohk^2 \end{pmatrix} \mathbf{q} = L\mathbf{q}$$

Which is now of the same form of (3.36), so that we can easily compute $G(t)$ as $G(t) = \|e^{Lt}\|$.

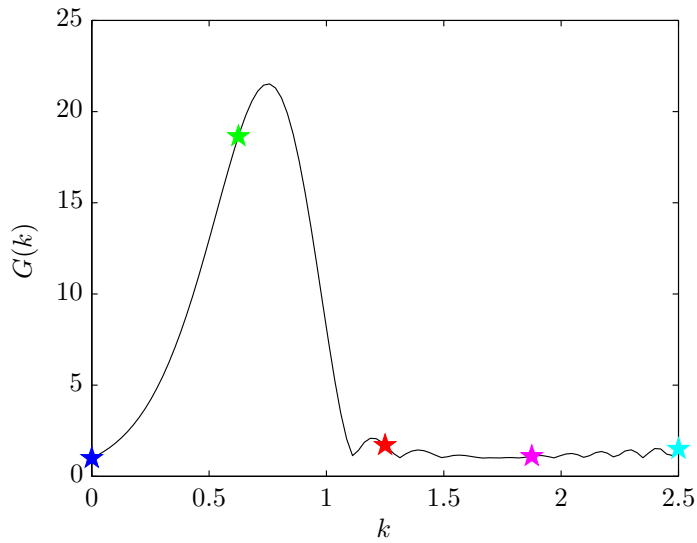
3.4.2 Results

In this part we carry out a preliminary transient growth analysis in order to understand if these effects are relevant in our model. Given the results we are about to show, a deeper analysis does not seem necessary. We let Oh span from 0 to 10. For every Oh we report two graphs (see Figures 3.7, 3.8, 3.9, 3.10):

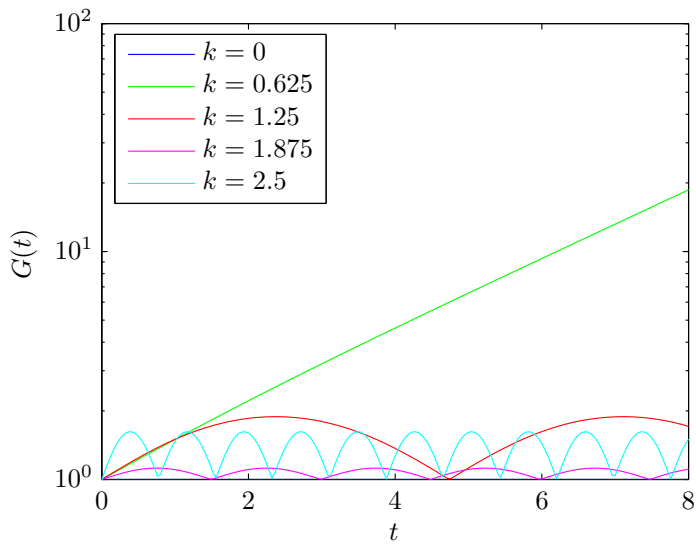
1. $G(t = T)$ versus k . Here we compute the maximum growth in the energy of the system at a given time T , and we plot it as a function of k . T is different for every Oh , but it is always $T < 0.5t_{break\ up}$. This graph is a sort of check test of the results obtained via linear stability analysis, displaying how the growth is affected by the wavenumber of the perturbation. The colored stars correspond to the values of k displayed in the second graph. Plots start from $G(T) = 1$ for $k = 0$ for every Oh , since the system starting from an initial condition with $k = 0$ is always steady. For large k the system is damped in the presence of viscosity, so in any case $G \rightarrow 0$ as k exceeds k_{cutoff} . Since T is finite, $G(T)$ can be non-zero even if $k > 1$, especially if k is not very large. When $Oh = 0$ the system is not damped, and so it keeps oscillating around $G = 1$ if $k > 1$. For $0 < k < 1$ we do not observe substantial differences from what we would have expected from the classical linear stability analysis, for any Oh . Also the peaks tend to correspond.
2. $G(t)$ versus t for different k . Here we compute G for a given k and we plot it on a log-scale as a function of time. This graph really checks the presence of transient growth effects, showing how linear growth evolves in time. If the operator is normal or slightly non-normal, we expect to see straight lines for every k , whose slope is the growth rate of the system predicted by linear stability analysis; instead if the operator is ‘sufficiently’ non-normal, we will see G growing differently than what predicted by linear stability analysis. For any Oh , $k = 0$ is an horizontal straight line and $k = 0.625$ (linearly unstable wavenumber) is always a positive-sloped straight line (the slope decreases as

Oh increases, as expected). So, as far as unstable wavenumbers are concerned, no transient growth effect is appreciable. For large viscosity ($Oh = 10$) also in case of higher k we have straight lines with negative slope, and no interesting behavior is found. Something different happens for linearly stable wavenumbers and lower viscosity. In the case of $Oh = 0$, which is not damped, we can notice for G a ‘bouncing’ behavior: stable wavenumbers lead to an oscillation of the system, which however remains bounded. In particular, for wavenumber $k = 2.5$ the growth of the system in the first half unit of time is more than the growth of the system with the unstable wavenumber $k = 0.625$. A similar effect can be seen for $Oh = 0.1$, where we have this temporary ‘overtaking’ in growth of stable wavenumbers on unstable ones, in this case for an even smaller window of time. The system is damped, thus G keeps bouncing, but it goes toward zero.

In conclusion, some slight transient growth effects are present for stable wavenumbers and low viscosity. Still, given their amplitude and their behavior they do not appear to be very important in the flow, especially if we consider that our horizon is the breakup, which requires large displacements. Thus, non linear effects will be reasonably the key in the enhancements in break up time to be achieved through the optimization.

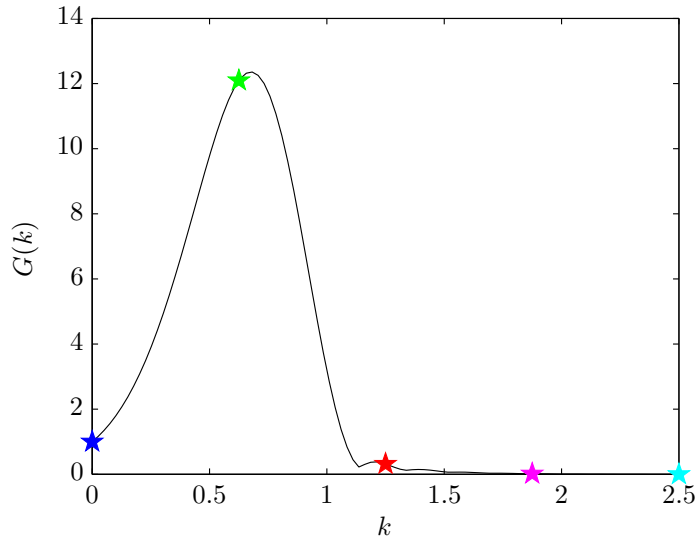
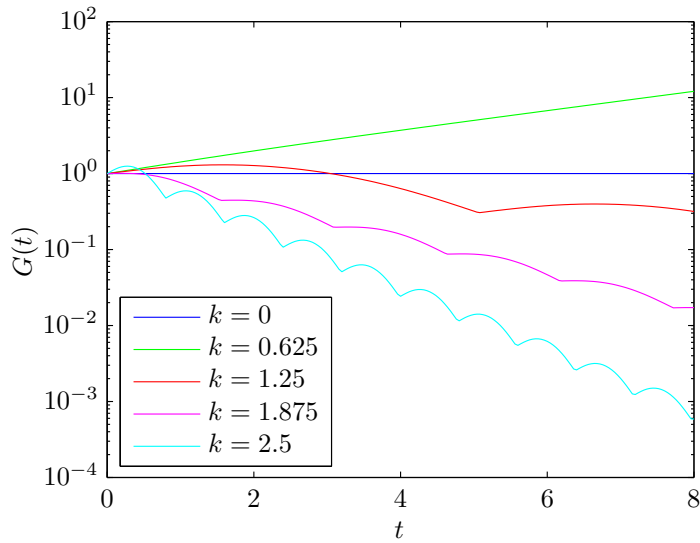


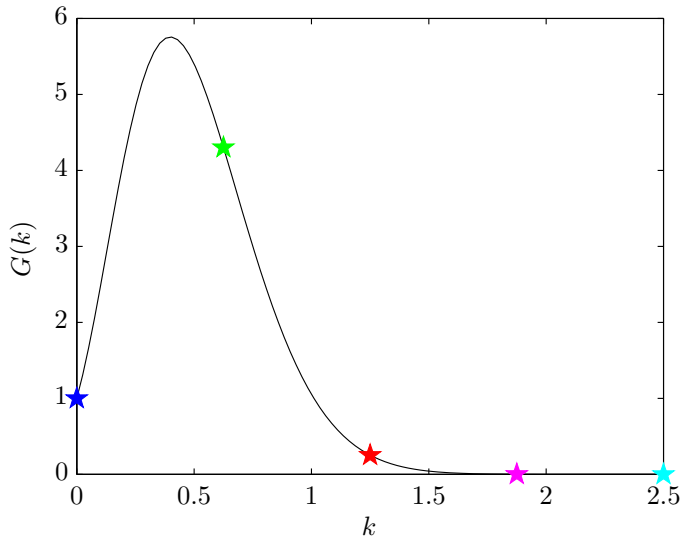
(a) $G(k)$, $T = 8$



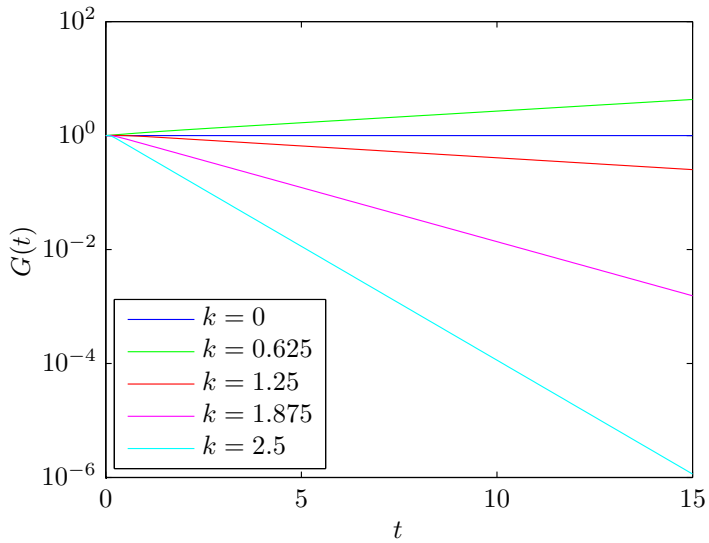
(b) $G(t)$ for different wavenumbers

Figure 3.7: Transient growth graphs, $Oh = 0$.

(a) $G(k)$, $T = 8$ (b) $G(t)$ for different wavenumbersFigure 3.8: Transient growth graphs, $Oh = 0.1$.

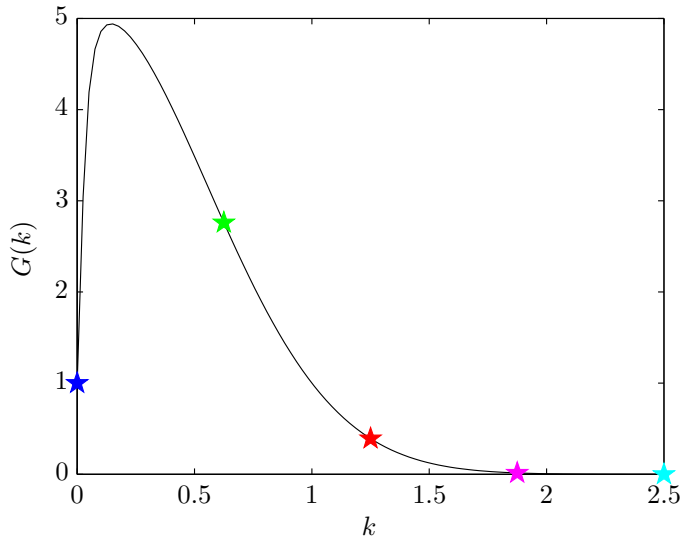
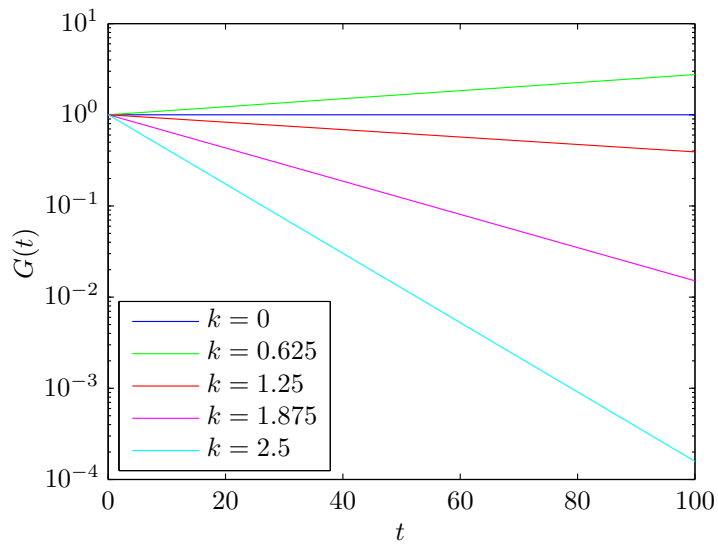


(a) $G(k)$, $T = 15$



(b) $G(t)$ for different wavenumbers

Figure 3.9: Transient growth graphs, $Oh = 1$.

(a) $G(k)$, $T = 100$ (b) $G(t)$ for different wavenumbersFigure 3.10: Transient growth graphs, $Oh = 10$.

Chapter 4

Flow configuration and numerical solution

In this Chapter we will present the physical configuration of the flow that further will be object of optimization. We will also discuss numerical methods used to solve the flow from the initial condition until pinch-off.

4.1 Physical configuration

We will deal with the same configuration which has already been object of a linear stability analysis, both in Section 2.3 with Rayleigh theory and in Section 3.3 using Eggers and Dupont model. We refer to an infinite cylinder of radius h_0 , initially at rest ($V = 0$). When imposing the initial condition a little perturbation can be superposed to the unperturbed flow (see Figure 4.1), the radius becoming a function of z , e.g. $h = h_0 + \epsilon f(z)$, respecting the varicose symmetry (the axis always remains in $r = 0$). The viscosity can be controlled acting on Oh , with effects on the dynamics of the flow. The stability depends entirely on the initial condition. Having chosen Oh and the initial conditions, it remains to discretize the equations and choose the ODE solver in order to let the flow evolve in time.

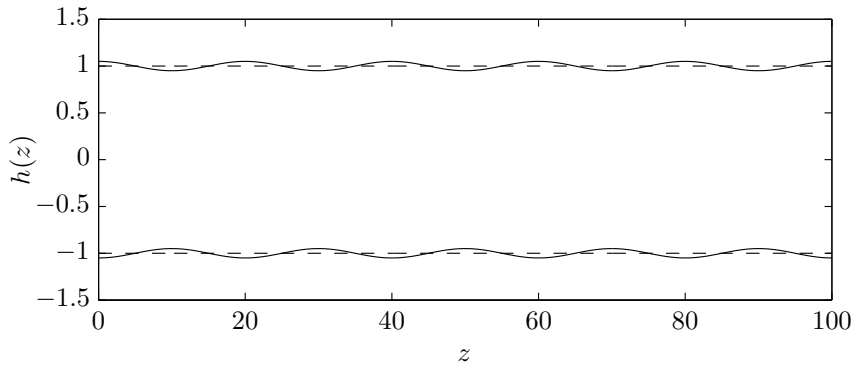


Figure 4.1: Portion of an infinite cylinder. The dashed line represents an unperturbed interface $h(z) \equiv h_0 = 1$, the continuous line represents a perturbed situation. In particular in the latter case $h(z) = h_0 + \epsilon \cos(5\frac{2\pi}{L}z)$, $\epsilon = 0.05$, $L = 100$

4.2 Numerical method

For the numerical techniques we took advantage of the work done in Ansaldi's thesis [20], from which our code is derived. A reliable validation of the code itself is already presented in [20], so we will not deal with this matter. For the solution of the system of PDEs we used a numerical technique called 'method of lines' (MOL), in which all but one dimension is discretized [21]. In Figure 4.2 an example of application of MOL to a diffusion equation is shown. It also illustrates the origin of its name. The key aspect of the MOL is that it allows standard, general-purpose methods and software, developed for the numerical integration of ordinary differential equations (ODEs) to be used. We proceed by first discretizing the spatial derivatives only and leaving the time variable continuous. We use a regular, equally spaced grid, discretized with the finite difference method (FDM). This leads to a system of ODEs to which a numerical method for initial value ordinary differential equations can be applied. In fact, in this way, partial derivatives of V and h become in every node ordinary derivatives.

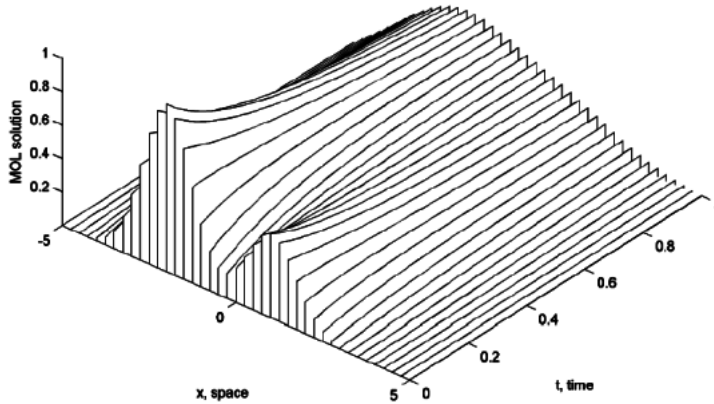


Figure 4.2: An example of solution of a PDE using the method of lines. Diffusion equation: $\frac{\partial u}{\partial t} = D \frac{\partial^2 u}{\partial x^2}$; initial condition: $u(x, t = 0) = \frac{1}{2}e^{-(x-1)^2} + e^{-(x+1)^2}$.

The two PDEs reduce to a system of $2N$ ODEs, where N is the number of nodes of the spatial grid. Diffusive terms are always treated with finite centered differences while convective terms can need upwind schemes depending on the complexity of the configuration. As far as the ODE solver is concerned, we used solvers from MATLAB libraries. The selection of the solver depends, case by case, on the stiffness of the problem, on accuracy considerations and on computation time. Further considerations on numerical methods will be made in the next paragraphs. Before proceeding, it is worth to remember that while solving our one dimensional model we will have, for every node and for a given time, a value of h and a value of V . The first represents the radial position of the interface of the thread in that node. The second is the first term of the radial Taylor expansion in r of the axial velocity (see Section 3.1), i.e. the value of the axial velocity in that node, and the approximation of the velocity in all the z -section located by the node (including $r = h$). It has been decided to define pinch off occurrence as the reaching of a certain lower limit value (close to zero) of the interface radius, at any instant of time and in any node.

4.2.1 Discretization

The infinite length of the thread is rendered imposing periodic conditions at the boundaries when discretising. We consider a finite set of nodes representing a finite portion of space (more precisely of length), imagining that it reiterates itself endlessly along the z axis in both the positive and the negative directions. In fact, an infinite cylinder could be retrieved juxtaposing infinite sets of points. Thus, the domain sets a sort of ‘box’ of periodicity. Given a certain domain length L , the maximum wavelength allowed in the flow will be $\lambda_{max} = L$. More than that, only periodic initial conditions consistent with that wavelength make sense; otherwise continuity of the interface would not be verified when juxtaposing more boxes. This means that the wavenumber of allowed initial conditions has to be a multiple of $\frac{2\pi}{L}$. In Figure 4.1, for example, the perturbation has a wavelength $\lambda = \frac{L}{5}$. Having chosen the length of the domain L , the lowest number of nodes N which guarantees a converged solution has to be identified, in order to minimize computational time and maximize accuracy. This can be done carrying out a grid dependency study: solving the flow using an increasing number of nodes it is possible to identify the number N for which the solution converges.

Finite differences

Periodicity can be easily implemented in a finite difference method using precisely the idea of juxtaposition. For example, given a grid made up of N nodes, the discretization of the first derivative of V in the generic interior node i ($2 \leq i \leq N - 1$) using a second-order central difference scheme, will be:

$$\left(\frac{\partial V}{\partial z}\right)_i = \frac{V_{i+1} - V_{i-1}}{2\Delta z}.$$

For the boundary nodes 1 and N , one can write:

$$\left(\frac{\partial V}{\partial z}\right)_1 = \frac{V_2 - V_N}{2\Delta z}, \quad \left(\frac{\partial V}{\partial z}\right)_N = \frac{V_1 - V_{N-1}}{2\Delta z},$$

and similarly for higher derivatives.

Fourier spectral method

Another option is represented by spectral methods. They are spatial discretization methods used to numerically solve differential equations. The idea is to write the solution of the differential equation as a sum of certain ‘basis function’ (for example, as a Fourier series which is a sum of sinusoids) and then to choose the coefficients in the sum in order to satisfy the differential equation as well as possible. These functions usually have global support on the flow domain, and spatial derivatives are defined in terms of derivatives of them. The coefficients pertaining to the basis functions can be considered as a spectrum of the solution, which explains the name for the method. Due to the global (or at least extended) nature of these functions, spectral methods are usually global methods, i.e. the value of a derivative at a certain point in space depends on the solution at all the other points in space, and not just the neighboring grid points. Due to this fact, spectral methods usually have a very high order of approximation [22]. Using a Fourier series method periodicity is automatically satisfied. We do not enter in the details of the implementation of this method, that was not present in Ansaldi’s code. It is sufficient to say that the solution of the flow obtained with it were superposable to the ones obtained with finite differences. Better accuracy did not change the results, confirming the good quality of the code.

4.3 Stability analysis and pinch-off time

Now that we have a tool for the numerical solution of the flow, we want to compare it with the results obtained via linear stability analysis. In particular we want to check if and how the growth rates found via linear analysis are related with the break up times found numerically. We let the system (3.31) evolve starting from initial conditions like $h(z, 0) = h_0 + \epsilon \cos(kz)$ until break up, maintaining ϵ constant and letting k vary from 0 to 1. In Figure 4.3 normalized growth rates found via E-D linear stability analysis (dashed line) and inverses of break up times (solid line) are plotted versus k , for different Oh . We remark that the stability analysis is linear, while

E-D equations, although simplified, are not. Thus, we are not surprised to find differences among the results. The two lines are actually very similar for $Oh = 0$ and detach more and more for larger Oh . In particular, $k_{opt,po}$ for pinch off time is larger than $k_{opt,\omega}$ for the growth rate found via linear stability analysis, and the shift becomes stronger as Oh increases. Also, the shape of the lines, very similar for small values of Oh , changes for larger Oh : when $Oh = 10$ the minimum t_{po} is located in a plateau-like zone (the neighboring values are very similar), while the maximum of the growth rate is a quite sharp peak. Thus, from this comparison it seems that non linear effects become more important for large Oh , at least for this type of initial conditions. Despite these differences, growth rates predicted by linear stability analysis and pinch-off times appear to be somehow related: earlier break up correspond to larger growth rates, especially when $Oh \leq 1$. However, from this comparison a good potential for non linear optimization appears, especially if we consider that we tested only sinusoidal initial conditions of varying wavelength. What would happen allowing general initial conditions?

4.4 Examples

We show now some significative examples of solution, varying Oh and the initial condition. Further comments can be found in the captions of the related pictures (4.4-4.7).

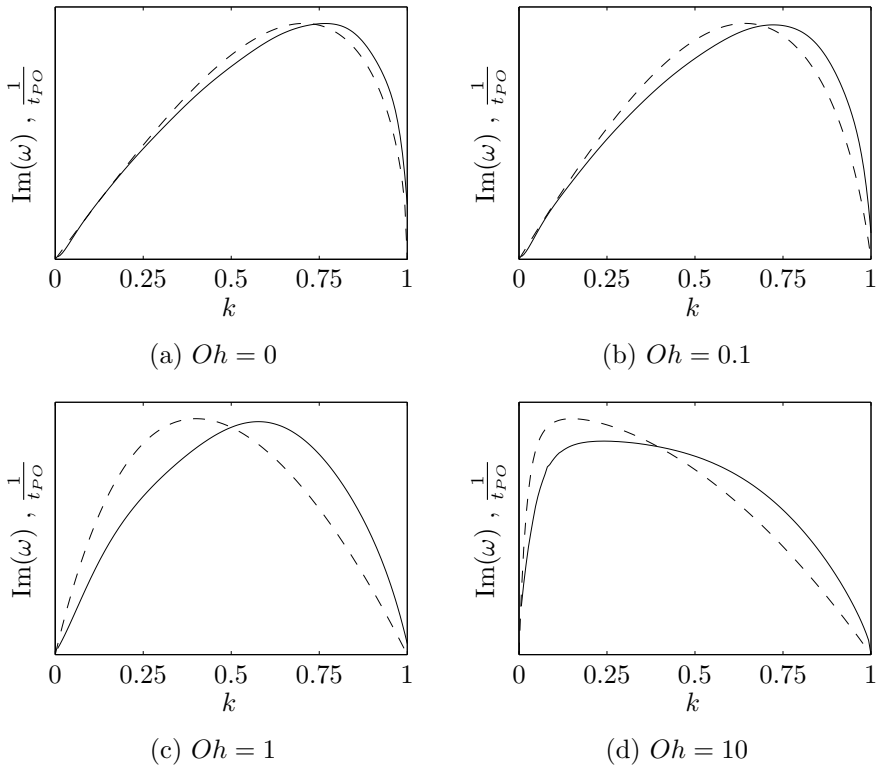


Figure 4.3: Comparison between normalized growth rates from E-D linear stability analysis (dashed line) and $\frac{1}{t_{po}}$ (solid line) versus k for different Oh .

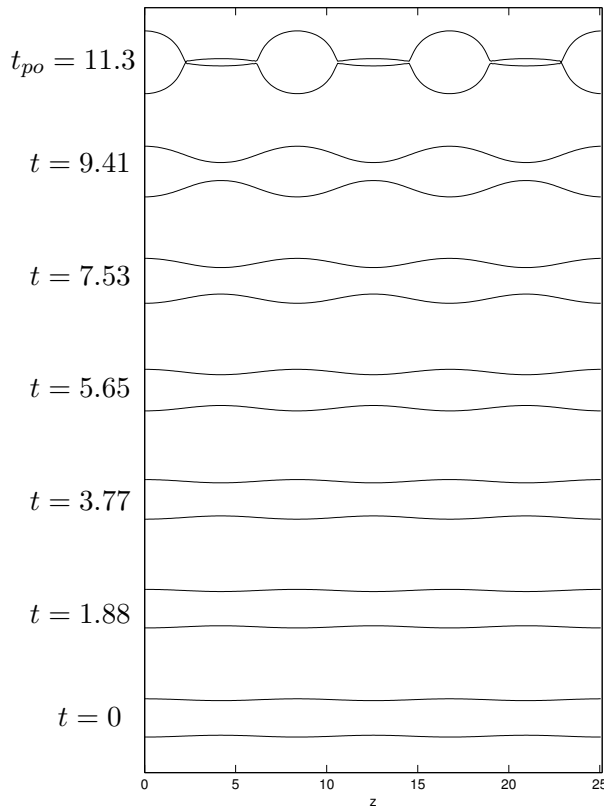


Figure 4.4: $Oh = 0.1$, $h(z, 0) = h_0 + 0.05\cos(0.75z)$. Viscosity is small compared to surface tension, the wavenumber of the perturbation (0.75) is one of the most unstable according to Figure 4.3b. The formation of relatively big satellite drops is of interest. Pinch off occurs clearly between a drop and its ‘satellites’. The interface moves initially quite slowly and accelerates in the course of time, especially in the very end of the process, insomuch that in the last two steps the interface cover more or less the same distance of the first five. In Figure 4.5 the last part of the process is shown in more detail.

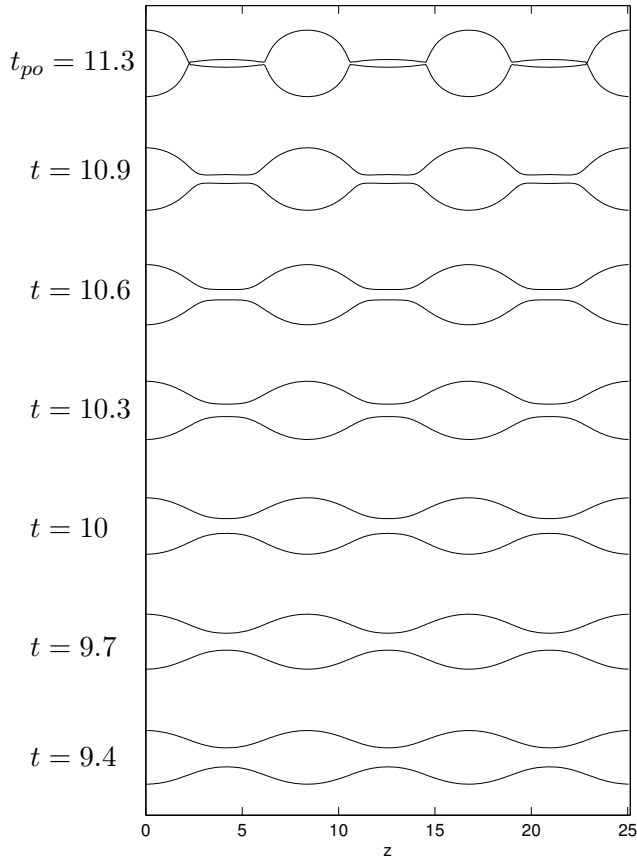


Figure 4.5: $Oh = 0.1$, $h(z, 0) = h_0 + 0.05\cos(0.75z)$. Temporal ‘zoom’ of the previous Figure, $9.4 \leq t \leq 11.3 = t_{po}$. The acceleration of the process in the last instants and the formation of satellite drops are clearly visible.

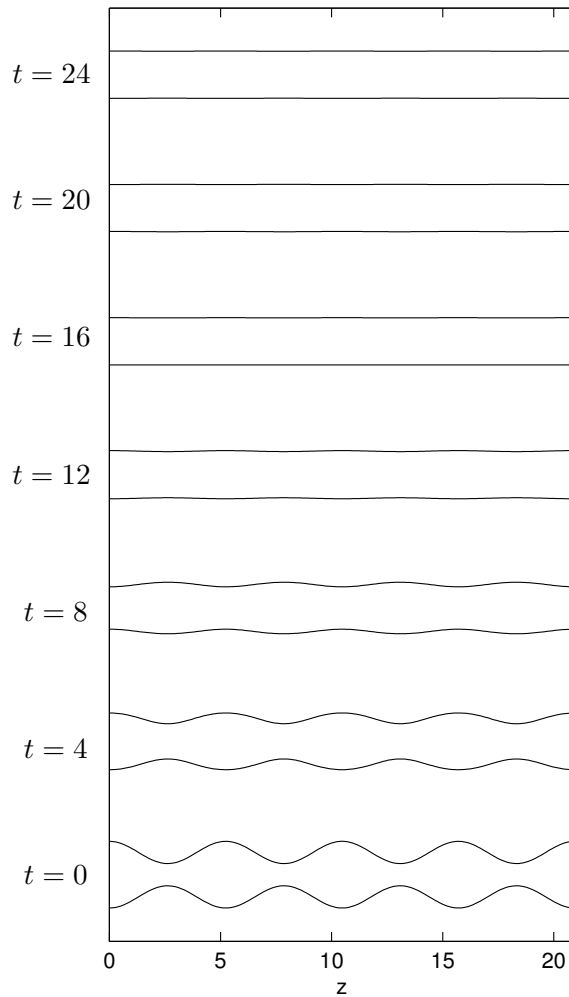


Figure 4.6: $Oh = 0.1$, $h(z, 0) = h_0 + 0.5\cos(1.2z)$. Here the wavenumber of the perturbation (1.2) is out of the limits of instability. Even with a large initial perturbation ($\epsilon = 0.5h_0$) the interface oscillates for a period of time until viscosity dissipates all the energy and a position of equilibrium is reached.

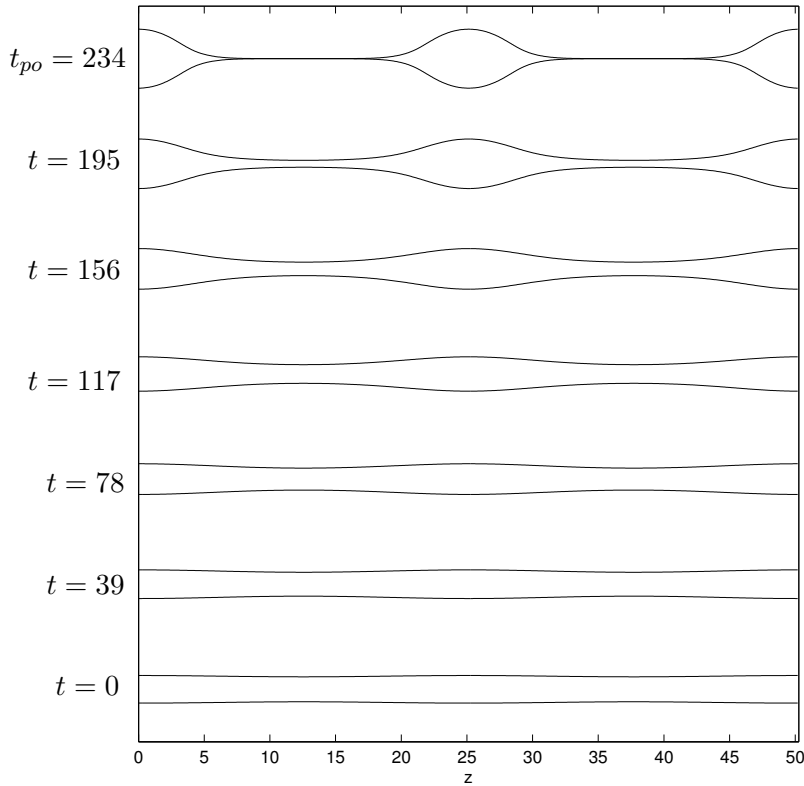


Figure 4.7: $Oh = 10$, $h(z, 0) = h_0 + 0.05\cos(0.25z)$. Viscosity is large compared to surface tension, and slows down the break up more than 20 times with respect to the case of $Oh = 0.1$; the wavenumber of the perturbation (0.25) is again one of the most unstable referring to Figure 4.3d. In this case we cannot see the formation of satellites drops: in fact thanks to viscosity the fluid has all the time to flow toward the main drops and only a very thin thread connects two drops at the moment of break up. After pinch off this threads can be either rapidly ‘sucked’ by the drops or form tiny satellite drops, depending on the relative importance of viscosity, inertia, surface tension and external disturbances.

Part II

Optimization and control of droplet formation time

Chapter 5

Method and equations

Flow control concerns the alteration of flows with the aim to satisfy required performances and features. Examples include drag reduction, noise attenuation, improved mixing, stabilization, among many other industrial applications. The goal normally has to be reached considering physical, technical and economic limits, often minimizing the ‘costs’ associated to the control, e.g. the control energy. Therefore, flow control falls very naturally within the field of constrained optimization. Adjoint methods in particular provide a very efficient way to determine the sensitivity of an objective with respect to control variables. Moreover, the adjoint approach can deal with nonlinear and time-dependent problems.

In this Chapter we provide a brief introduction to constrained optimization, with particular focus on adjoint methods. Notations and some of the concepts of these Sections are taken from [23] and [24]. Finally we will apply the adjoint method to our case deriving the equations adjoint of (3.31).

5.1 Preliminaries and some notation

In a constrained optimization problem normally we have:

- \mathbf{q} , a state vector, e.g. a field of pressure and velocity,

- \mathbf{g} , a control vector, e.g. BCs, ICs, a flap on a wing, etc,
- $J(\mathbf{q}, \mathbf{g})$, the objective function (scalar), e.g. drag, noise, etc,
- $S(\mathbf{q}, \mathbf{g}) = 0$, the state equation (constraint), e.g. Navier-Stokes equations.

In the simpler case of unconstrained optimization there are only \mathbf{q} and $J(\mathbf{q})$. In this case the goal is to find \mathbf{q} that minimizes $J(\mathbf{q})$. It is assumed that the state \mathbf{q} can be directly changed in order to attain the optimal solution. If the minimum of J lies in internal points of the domain of definition of \mathbf{q} , assuming J continuous with continuous derivatives, then the gradient $\frac{\partial J}{\partial \mathbf{q}}$ has to become zero in correspondence of the optimal point. An intuitive way to find the minimum is the steepest descent method, based on the gradient of the objective. Given an initial guess $\mathbf{q}^{(0)}$, we update it step by step following the direction of steepest descent: $\mathbf{q}^{(k+1)} = \mathbf{q}^{(k)} - \rho^{(k)} \left(\frac{\partial J}{\partial \mathbf{q}} \right)^k$. The idea is that following the path of maximum slope indicated by the gradient of J a minimum will be eventually reached.

In most situations, such as flow optimization, acting directly on \mathbf{q} is not possible and one can only act on a set of control variables \mathbf{g} . The state and the control satisfy the state equation $S(\mathbf{q}, \mathbf{g}) = 0$, which represent the constraint of the problem. The goal of constrained optimization is to minimize the objective function $J(\mathbf{q}, \mathbf{g})$ by acting on \mathbf{g} under the constraint $S(\mathbf{q}, \mathbf{g}) = 0$. The strategy of optimization can be again descending on J level curves, but this time we have to stay on the path indicated by $S = 0$.

5.2 Optimization methods

The basic ideas and methods of constrained optimization methods will be initially introduced in a time and space independent framework. Then, they will be extended to time and space dependent cases. For the moment $\mathbf{q} \in \mathbb{R}^P$ and $\mathbf{g} \in \mathbb{R}^N$.

5.2.1 Gradient method with finite difference approximation

Constrained optimization problems can be solved using iterative gradient methods, in a similar way as for unconstrained problems. In fact at the k -th iteration, known $g^{(k)}$ one can get a guess for $g^{(k+1)}$ computing the total derivative $\frac{DJ}{D\mathbf{g}}$. One way to do that is to use a finite difference approximation:

$$\frac{DJ}{Dg_N} = \frac{J[\mathbf{q}(\mathbf{g} + \Delta g_N \mathbf{e}_N), \mathbf{g} + \Delta g_N \mathbf{e}_N] - J[\mathbf{q}(\mathbf{g}), \mathbf{g}]}{\Delta g_N}. \quad (5.1)$$

Evaluating (5.1) requires $N + 1$ computations of the state equation (one for every Δg_N to have $\mathbf{q}(\mathbf{g} + \Delta g_N \mathbf{e}_N)$). Considering that solving the state equation in flow control means dealing with NS equations, this can become computationally very challenging.

5.2.2 The adjoint method

Consider a simple case where \mathbf{q} and \mathbf{g} are one dimensional. It can be shown that in correspondence of the optimum of $J(q, g)$ the path given by the constraint $S(q, g) = 0$ is tangent to the iso- J_{opt} curve. This means that the gradient of J and the gradient of S are parallel in that point of the $q - g$ plane, hence:

$$\left[\frac{\partial J}{\partial g}, \frac{\partial J}{\partial q} \right] = a \left[\frac{\partial S}{\partial g}, \frac{\partial S}{\partial q} \right]. \quad (5.2)$$

It is possible to define an augmented function $\mathcal{L} = J - aS$, called Lagrangian, that encapsulates in itself all the information and conditions of the constrained optimization problem, transforming it in an unconstrained one. The scalar a is called ‘Lagrange multiplier’.

This approach can be generalized to the multidimensional case:

$$\mathcal{L}(\mathbf{q}, \mathbf{g}, \mathbf{a}) = J(\mathbf{q}, \mathbf{g}) - \mathbf{a} \cdot S(\mathbf{q}, \mathbf{g}), \quad (5.3)$$

where the Lagrange multiplier \mathbf{a} has the same dimension of \mathbf{q} . The problem can be treated as an unconstrained one, retrieving the optimality conditions

setting the derivative of \mathcal{L} with respect to its independent variables $\mathbf{q}, \mathbf{g}, \mathbf{a}$ equal to zero:

$$\frac{\partial \mathcal{L}}{\partial \mathbf{a}} = 0, \quad \frac{\partial \mathcal{L}}{\partial \mathbf{q}} = 0, \quad \frac{\partial \mathcal{L}}{\partial \mathbf{g}} = 0, \quad (5.4)$$

leading to, respectively, the state equation, the adjoint equation (further we will understand the origin of its name) and the optimality condition:

$$\left\{ \begin{array}{l} S = 0, \\ \left(\frac{\partial S}{\partial \mathbf{q}} \right)^T = \mathbf{a} \frac{\partial J}{\partial \mathbf{q}}, \\ \left(\frac{\partial S}{\partial \mathbf{g}} \right)^T = \mathbf{a} \frac{\partial J}{\partial \mathbf{g}}. \end{array} \right. \quad (5.5)$$

Derivatives in (5.4) are rarely directly accessible, because $\mathbf{q}, \mathbf{g}, \mathbf{a}$ are usually functions. In this case optimality conditions can be retrieved using a variational approach: one can substitute derivatives of \mathcal{L} with the variation of the Lagrangian $\delta \mathcal{L}$ provoked by small variations of the variables (e.g. $\delta \mathbf{a} = \epsilon \tilde{\mathbf{a}}$). Setting them equal to zero for any $\tilde{\mathbf{q}}, \tilde{\mathbf{g}}, \tilde{\mathbf{a}}$ is equivalent to 5.4. It reads:

$$\frac{\delta \mathcal{L}}{\delta \mathbf{a}} = 0, \quad \frac{\delta \mathcal{L}}{\delta \mathbf{q}} = 0, \quad \frac{\delta \mathcal{L}}{\delta \mathbf{g}} = 0, \quad (5.6)$$

where the first term can be expressed as:

$$\frac{\delta \mathcal{L}}{\delta \mathbf{a}} = \lim_{\epsilon \rightarrow 0} \frac{\mathcal{L}(\mathbf{q}, \mathbf{g}, \mathbf{a} + \epsilon \tilde{\mathbf{a}}) - \mathcal{L}(\mathbf{q}, \mathbf{g}, \mathbf{a})}{\epsilon \tilde{\mathbf{a}}}, \quad (5.7)$$

and similarly for the other two. This leads again to find respectively the state equation, the adjoint equation and the optimality condition. Because of what we have explained, a solution of system of equations (5.5) necessarily identifies a local minimum. In order to solve the system, an iteration loop is normally required, as we will show. Since adjoint equations give the sensitivity of the state to a variation of its variables, another way to reach the optimum is to use adjoint fields to compute the gradient, and then proceed with a steepest descent method, as explained in [23]. What

is important to remark is that, in both cases, for every iteration only one solution of the state equation is required. The computational cost is 1, compared to the cost $N + 1$ of the gradient method with the finite differences approximation (N is the dimension of the control \mathbf{g}). For example in a discrete flow control problem, if \mathbf{g} depends on the spatial grid, in the case of gradient method with finite differences approximation one iteration of the optimization loop requires solving the flow many times as the number of nodes of the grid, versus the single computation of an adjoint method. The order of magnitude of the saving in terms of computational time and effort can make the difference in the feasibility of an optimization.

Inner product and adjoint operators

Before proceeding further, we introduce some more concepts and notation that will help to extend the adjoint method to the general case of flow control.

An *inner product* (or scalar product) maps two elements of a vector space \mathcal{V} in a field of scalars \mathcal{F} (which can be either \mathbb{R} or \mathbb{C}):

$$\langle u, v \rangle : \mathcal{V} \times \mathcal{V} \rightarrow \mathcal{F} \quad (5.8)$$

It has to satisfy the following properties:

- $\langle u, v \rangle = \langle v, u \rangle$,
- $\langle u, \alpha v \rangle = \alpha \langle v, u \rangle$,
- $\langle u, v + w \rangle = \langle u, v \rangle + \langle u, w \rangle$,
- $\langle u, u \rangle \geq 0$,
- $\langle u, u \rangle = 0 \leftrightarrow u = 0$,

where $u, v, w \in \mathcal{V}$ and $\alpha \in \mathcal{F}$. Given a linear operator L , that maps \mathcal{V} in itself, its adjoint operator L^\dagger is defined by:

$$\langle u, Lv \rangle = \langle L^\dagger u, v \rangle, \quad \forall u, v \in \mathcal{V}. \quad (5.9)$$

The Lagrangian function can be redefined in light of these definitions. Equation (5.3) can be rewritten as:

$$\mathcal{L} = J - \langle \mathbf{a}, S \rangle. \quad (5.10)$$

In general in flow control one deals with differential equations, so equality relation (5.9) has to be completed with terms that appear at the boundaries of the domain of integration:

$$\langle u, Lv \rangle = \langle L^\dagger u, v \rangle + B.T., \quad (5.11)$$

where the right hand side can be calculated integrating by parts (B.T.= boundary terms), as it will be clear soon.

Time dependent problems (ODE)

The variational approach discussed in the previous pages can be quite easily extended to time-dependent problems. We consider a model initial value problem:

$$\begin{cases} \frac{d\mathbf{q}}{dt} = L(\mathbf{q}, \mathbf{g}, t)\mathbf{q}, & t \in [0, T], \\ \mathbf{q}(0) = \mathbf{q}_0, \end{cases} \quad (5.12)$$

with L a linear operator. In this case we have two constraints: $S(\mathbf{q}, \mathbf{g}, t) = \frac{d\mathbf{q}}{dt} - L(\mathbf{q}, \mathbf{g}, t) = 0$ and $S_0 = \mathbf{q}(0) - \mathbf{q}_0 = 0$. When writing the Lagrangian function we will have to take into account the second constraint, assigning to it its own Lagrange multiplier:

$$\mathcal{L} = J - \int_0^T \langle \mathbf{a}(t), S \rangle dt - \langle \mathbf{b}, S_0 \rangle. \quad (5.13)$$

Since in this case the inner product can be defined as the classical scalar product between vectors, more explicitly the Lagrangian functional reads:

$$\mathcal{L}(\mathbf{q}, \mathbf{g}, \mathbf{a}, \mathbf{b}) = J - \int_0^T \mathbf{a}(t) \cdot \left(\frac{d\mathbf{q}}{dt} - L(\mathbf{q}, \mathbf{g}, t) \right) dt - \mathbf{b} \cdot (\mathbf{q}(0) - \mathbf{q}_0), \quad (5.14)$$

where $\mathbf{a}(t)$ ensures that the state equation is respected $\forall t \in [0, T]$ and \mathbf{b} (which does not depend on time) enforces the initial condition at $t = 0$. The optimality system can be retrieved setting to zero the variation of \mathcal{L} with respect to all its independent variables, $(\mathbf{q}, \mathbf{g}, \mathbf{a}, \mathbf{b})$.

The conditions $\frac{\delta \mathcal{L}}{\delta \mathbf{a}} = 0$ and $\frac{\delta \mathcal{L}}{\delta \mathbf{b}} = 0$ lead simply to the original system, along with its initial condition in $t = 0$. Enforcing $\frac{\delta \mathcal{L}}{\delta \mathbf{q}} = 0$ implies integrating by parts and will give the adjoint equation and a boundary condition on the adjoint temporal domain in $t = T$, through a relation between $\mathbf{q}(T)$ and $\mathbf{a}(T)$.

It can be shown that the adjoint equation reads:

$$-\frac{d\mathbf{a}}{dt} = L^\dagger \mathbf{a}, \quad (5.15)$$

where $L^\dagger = L^T$ if L is a real matrix. Hence, we will solve the adjoint equation as an initial value problem to be integrated backward in time. Finally, $\frac{\delta \mathcal{L}}{\delta \mathbf{g}} = 0$ leads to the optimality condition, giving a relation used to update the control \mathbf{g} .

In a time-dependent problem an iteration of the optimization loop will consist of the following (very general) steps:

1. integrate the state equation from $t = 0$ to $t = T$ using previous guess of \mathbf{g} ;
2. check the variation of J with respect to the previous iteration: if convergence has not been reached yet, proceed, otherwise stop;
3. retrieve the initial condition $\mathbf{a}(T)$ for the adjoint equation from the final state $\mathbf{q}(T)$;
4. integrate the adjoint equation backward in time from $t = T$ to $t = 0$;
5. find a new guess for \mathbf{g} using the sensitivity information given by the adjoint solution while applying the optimality condition.

Step 4 can be substituted with the computation of the gradient, as discussed before. In this case, a new guess for \mathbf{g} is given by the gradient itself.

Time and space dependent problems (PDE)

In flow control the state (velocity, pressure, etc.) is function of real variables such as space coordinates. Thus, in order to extend the adjoint method to this kind of problems, we just need to define coherently the inner product. For example, given the space \mathcal{V} of functions $f(x)$, $x \in [a, b]$, the scalar product can be defined as:

$$\langle u, v \rangle = \int_a^b u(x)v(x)dx, \quad (5.16)$$

where it is assumed that u and v are integrable with continuous and integrable derivatives. Thus, in the general case, where $\mathbf{q} = \mathbf{q}(x, t)$, the Lagrangian function will be defined as $\mathcal{L} = J - \int_0^T \langle \mathbf{a}(x, t), \mathbf{q}(x, t) \rangle dt$. The inner product is therefore a spatial integration. Using this definition it is easy to compute adjoints and boundary conditions of derivative operators. For the first derivative operator $L = \frac{\partial}{\partial x}$, for example we have:

$$\begin{aligned} \langle u, \frac{\partial v}{\partial x} \rangle &= \int_a^b u \frac{\partial v}{\partial x} dx = \dots \\ &\dots = [uv]_a^b - \int_a^b \frac{\partial u}{\partial x} v dx = \langle -\frac{\partial u}{\partial x}, v \rangle + [uv]_a^b, \end{aligned} \quad (5.17)$$

where integrating by parts boundary terms arise, that will have to be related to appropriate adjoint boundary conditions in order to satisfy the equality. Thus, in this case $L^\dagger = -\frac{\partial}{\partial x}$. It similarly happens for second and third derivatives:

$$\langle u, \frac{\partial^2 v}{\partial x^2} \rangle = \dots = \langle \frac{\partial^2 u}{\partial x^2}, v \rangle + \left[u \frac{\partial v}{\partial x} \right]_a^b - \left[\frac{\partial u}{\partial x} v \right]_a^b, \quad (5.18)$$

$$\langle u, \frac{\partial^3 v}{\partial x^3} \rangle = \dots = \langle -\frac{\partial^3 u}{\partial x^3}, v \rangle + \left[u \frac{\partial^2 v}{\partial x^2} \right]_a^b - \left[\frac{\partial u}{\partial x} \frac{\partial v}{\partial x} \right]_a^b + \left[\frac{\partial^2 u}{\partial x^2} v \right]_a^b, \quad (5.19)$$

In fact, even derivative operators have adjoint operators of their same sign, odd derivative operators have adjoints of opposite sign.

The Lagrangian function can be defined in the same way as in (5.13), adding in it proper terms in order to account for boundary conditions in the space domain. Every boundary condition is a constraint that has to be enforced with an associated Lagrange multiplier, similarly to the initial condition. As far as the derivation of the optimality system and the iterative loop to solve it are concerned, there are no substantial differences with respect to only-time dependent problems.

Non-linear problems

In flow control most of problems are non-linear, and so is ours, while so far we have treated adjoints only for linear operators. Although it is not straight forward to define the adjoint of a nonlinear operator, it is possible to introduce it, on the basis of the theory of linear operators. Basically, the procedure is to linearise the non-linear system and then to define its adjoint. Thus, during the iteration loop, direct non-linear equations have to be integrated from $t = 0$ to $t = T$, and then adjoint equations (which are linear) can be solved backward in time.

5.3 Adjoint equations of E-D model

In this section we will derive and display the adjoint of system (3.31). We remark that, in order to get to the complete optimality system from the Lagrangian function, the complete physical framework of the optimization problem has to be defined. Thus, initial conditions (coordinates of the interface, velocity), boundary conditions (periodicity, presence of inlets and outlets), entity of disturbances must be specified. Moreover, it has to be decided which objective function one wants to optimize, and which type of control will do the job. All these topics will be discussed in detail in the next Chapters. Here we limit ourselves to the derivation of the adjoint equations without boundary and initial conditions, which directly derive from the original equations and will remain the same in any possible configuration.

5.3.1 A formal synopsis

Making use of the notation introduced in Section 5.2.2, the system of equations (3.31) can be formally rewritten as:

$$\frac{d\mathbf{q}(t)}{dt} = \left[A(\mathbf{q}(t)) \right] \mathbf{q}(t), \quad (5.20)$$

where $\mathbf{q}(t) = [F(t); V(t)]$ is the vector of the state, containing values of the interface position and velocity (for every node in case of discretization) and $A(\mathbf{q}(t))$ is the non-linear operator (in matrix form) which contains also the spatial derivatives. In order to derive the adjoint of this equation it is convenient to linearize it around a base flow $\mathbf{Q}(t)$. The dependence of \mathbf{Q} and $\tilde{\mathbf{q}}$ on time will not be anymore indicated from now on. The linearized operator can be found as:

$$L(\mathbf{Q}) = \frac{\left[A(\mathbf{Q} + \tilde{\mathbf{q}}) \right] (\mathbf{Q} + \tilde{\mathbf{q}}) - \left[A(\mathbf{Q}) \right] \mathbf{Q}}{\tilde{\mathbf{q}}}, \quad (5.21)$$

and the linearized system for the perturbation $\tilde{\mathbf{q}}(t)$ reads:

$$\frac{d\tilde{\mathbf{q}}}{dt} = \left[L(\mathbf{Q}) \right] \tilde{\mathbf{q}}. \quad (5.22)$$

The Lagrangian function can be written as:

$$\mathcal{L} = \dots - \int_0^T \left\langle \mathbf{a}, \frac{d\mathbf{Q}}{dt} - \left[A(\mathbf{Q}) \right] \mathbf{Q} \right\rangle dt + \dots, \quad (5.23)$$

where dots represent the objective function and other constraints. The inner product with this formalization is just a scalar product between vectors. The adjoint equations can be found setting to zero $\frac{\partial \mathcal{L}}{\partial \mathbf{Q}}$, for any $\tilde{\mathbf{q}}$. It can be shown that the variation of \mathcal{L} can be expressed directly through an inner product containing the linearization of the original system. It results:

$$\frac{\partial \mathcal{L}}{\partial \mathbf{Q}} \tilde{\mathbf{q}} = - \int_0^T \left\langle \mathbf{a}, \frac{d\tilde{\mathbf{q}}}{dt} - \left[L(\mathbf{Q}) \right] \tilde{\mathbf{q}} \right\rangle dt + \dots, \quad (5.24)$$

where the presence of terms linked to the objective function and other constraints is indicated by dots. Now it is sufficient to integrate by parts and collecting around $\tilde{\mathbf{q}}$:

$$\frac{\delta \mathcal{L}}{\delta \mathbf{Q}} \tilde{\mathbf{q}} = -[\mathbf{a}\tilde{\mathbf{q}}]_0^T - \int_0^T \left\langle -\frac{d\mathbf{a}}{dt} - [L^\dagger(\mathbf{Q})]\mathbf{a}, \tilde{\mathbf{q}} \right\rangle dt + \dots; \quad (5.25)$$

the integral vanishes for arbitrary variations $\tilde{\mathbf{q}}$ only if the adjoint equation

$$-\frac{d\mathbf{a}}{dt} - [L^\dagger(\mathbf{Q})]\mathbf{a} = 0 \quad (5.26)$$

is satisfied, $\forall t \in [0, T]$, and the conditions at the boundaries are verified. Note that other boundary terms normally arise when considering the Lagrangian altogether. It is to be stressed that the (linear) adjoint operator is $L^\dagger = L^\dagger(\mathbf{Q}(\mathbf{t}))$. This means that while solving the adjoint equations backward in time, the solution $\mathbf{Q}(\mathbf{t})$ of the non-linear problem is needed throughout the integration.

5.3.2 Linearized equations

We display here the linearization of the system of equations (3.31) around the base state $F(z, t), V(z, t)$. The linearized variables are $\tilde{f}(z, t), \tilde{v}(z, t)$. Dependence on space and time is omitted. The first equation reads:

$$\frac{\partial \tilde{f}}{\partial t} = -\frac{\partial F}{\partial z} \tilde{v} - F \frac{\partial \tilde{v}}{\partial z} - \frac{\partial V}{\partial z} \tilde{f} - V \frac{\partial \tilde{f}}{\partial z}; \quad (5.27)$$

the second equation reads:

$$\begin{aligned} \frac{\partial \tilde{v}}{\partial t} &= -\frac{\partial V}{\partial z} \tilde{v} - V \frac{\partial \tilde{v}}{\partial z} + \dots \\ &\dots + \frac{1}{2} \left[-\frac{3}{2} \frac{\frac{1}{2} \frac{\partial F}{\partial z} \frac{\partial \tilde{f}}{\partial z} + \tilde{f}}{\left(\frac{1}{4} \left(\frac{\partial F}{\partial z}\right)^2 + F\right)^{\frac{5}{2}}} \left(\frac{\partial^3 F}{\partial z^3} F - \frac{\partial^2 F}{\partial z^2} \frac{\partial F}{\partial z} - 2 \frac{\partial F}{\partial z} \right) + \dots \right. \end{aligned}$$

$$\begin{aligned}
& \dots + \frac{\frac{\partial^3 F}{\partial z^3} \tilde{f} + F \frac{\partial^3 \tilde{f}}{\partial z^3} - \frac{\partial^2 F}{\partial z^2} \frac{\partial \tilde{f}}{\partial z} - \frac{\partial F}{\partial z} \frac{\partial^2 \tilde{f}}{\partial z^2} - 2 \frac{\partial \tilde{f}}{\partial z}}{\left(\frac{1}{4} \left(\frac{\partial F}{\partial z}\right)^2 + F\right)^{\frac{3}{2}}} + \dots \\
& \dots + \frac{3}{4} \left[-\frac{5}{2} \frac{\frac{1}{2} \frac{\partial F}{\partial z} \frac{\partial \tilde{f}}{\partial z} + \tilde{f}}{\left(\frac{1}{4} \left(\frac{\partial F}{\partial z}\right)^2 + F\right)^{\frac{7}{2}}} \times \dots \right. \\
& \dots \times \left(\frac{1}{2} \left(\frac{\partial F}{\partial z}\right)^3 \frac{\partial^2 F}{\partial z^2} + \left(\frac{\partial F}{\partial z}\right)^3 - \frac{1}{2} \left(\frac{\partial^2 F}{\partial z^2}\right)^2 \frac{\partial F}{\partial z} F + 2 \frac{\partial F}{\partial z} F \right) + \dots \\
& \dots + \frac{\frac{3}{2} \frac{\partial^2 F}{\partial z^2} \left(\frac{\partial F}{\partial z}\right)^2 \frac{\partial^2 \tilde{f}}{\partial z^2} + \frac{1}{2} \left(\frac{\partial F}{\partial z}\right)^3 \frac{\partial^2 \tilde{f}}{\partial z^2} + 3 \left(\frac{\partial F}{\partial z}\right)^2 \frac{\partial \tilde{f}}{\partial z} - \frac{1}{2} \left(\frac{\partial^2 F}{\partial z^2}\right)^2 F \frac{\partial \tilde{f}}{\partial z}}{\left(\frac{1}{4} \left(\frac{\partial F}{\partial z}\right)^2 + F\right)^{\frac{5}{2}}} + \dots \\
& \dots + \frac{-\frac{\partial^2 F}{\partial z^2} \frac{\partial F}{\partial z} F \frac{\partial^2 \tilde{f}}{\partial z^2} - \frac{1}{2} \left(\frac{\partial^2 F}{\partial z^2}\right)^2 \frac{\partial F}{\partial z} \tilde{f} + 2 \frac{\partial F}{\partial z} \tilde{f} + 2F \frac{\partial \tilde{f}}{\partial z}}{\left(\frac{1}{4} \left(\frac{\partial F}{\partial z}\right)^2 + F\right)^{\frac{5}{2}}} + \dots \\
& \left. \dots + 3Oh \left(\frac{\frac{\partial V}{\partial z} \frac{\partial \tilde{f}}{\partial z}}{F} + \frac{\frac{\partial F}{\partial z} \frac{\partial \tilde{v}}{\partial z}}{F} - \frac{\frac{\partial F}{\partial z} \frac{\partial V}{\partial z} \tilde{f}}{F^2} + \frac{\partial^2 \tilde{v}}{\partial v^2} \right) \right]. \quad (5.28)
\end{aligned}$$

Collecting terms we can write these equations in a more compact way. Finally the linearized system can be written as:

$$\begin{cases} \frac{\partial \tilde{f}}{\partial t} = -A_1 \tilde{v} - A_2 \frac{\partial \tilde{v}}{\partial z} - A_3 \tilde{f} - A_4 \frac{\partial \tilde{f}}{\partial z}, \\ \frac{\partial \tilde{v}}{\partial t} = -B_1 \tilde{v} - B_2 \frac{\partial \tilde{v}}{\partial z} - B_3 \frac{\partial^2 \tilde{v}}{\partial v^2} - B_4 \tilde{f} + \dots \\ \dots - B_5 \frac{\partial \tilde{f}}{\partial z} - B_6 \frac{\partial^2 \tilde{f}}{\partial z^2} - B_7 \frac{\partial^3 \tilde{f}}{\partial z^3}, \end{cases} \quad (5.29)$$

where A_i and B_i depend in general on $F, \frac{\partial F}{\partial z}, \frac{\partial^2 F}{\partial z^2}, \frac{\partial^3 F}{\partial z^3}, V, \frac{\partial V}{\partial z}, \frac{\partial^2 V}{\partial z^2}$, i.e. base flow quantities which are functions of time and space. The complete expression of the terms A_i and B_i is given in the appendix.

5.3.3 Adjoint equations

Now that we have the linearized system, adjoint equations are at our fingertips. Since the state is described by two equations, we will need a Lagrange multiplier (an adjoint variable) associated to each of them: $a_1(z, t)$ for the first and $a_2(z, t)$ for the second:

$$\mathcal{L} = - \int_0^T \langle a_1, \frac{\partial F}{\partial t} - \dots \rangle dt - \int_0^T \langle a_2, \frac{\partial V}{\partial t} - \dots \rangle dt + \dots, \quad (5.30)$$

where this time the inner product is defined as in (5.16). Following the same approach of Subsection 5.3.1, we can retrieve the adjoint equations setting to zero the variation of the Lagrangian with respect to the state variables. The variation can be expressed through the inner product between the Lagrange multipliers and the linearized state equations.

$$\frac{\delta \mathcal{L}}{\delta F} \tilde{f} + \frac{\delta \mathcal{L}}{\delta V} \tilde{v} = - \int_0^T \langle a_1, \frac{\partial \tilde{f}}{\partial t} - \dots \rangle dt - \int_0^T \langle a_2, \frac{\partial \tilde{v}}{\partial t} - \dots \rangle dt + \dots \quad (5.31)$$

Integrating by parts, collecting around \tilde{f} and \tilde{v} and setting to zero the terms for arbitrary variations, without taking into account boundary terms, we eventually find the adjoint system:

$$\left\{ \begin{array}{l} -\frac{\partial a_1}{\partial t} = \left(-A_3 + \frac{\partial A_4}{\partial z} \right) a_1 + A_4 \frac{\partial a_1}{\partial z} + \dots \\ \quad \dots + \left(-B_4 + \frac{\partial B_5}{\partial z} - \frac{\partial^2 B_6}{\partial z^2} + \frac{\partial^3 B_7}{\partial z^3} \right) a_2 + \dots \\ \quad \dots + \left(B_5 - 2 \frac{\partial B_6}{\partial z} + 3 \frac{\partial^2 B_7}{\partial z^2} \right) \frac{\partial a_2}{\partial z} + \dots \\ \quad \dots + \left(-B_6 + 3 \frac{\partial B_7}{\partial z} \right) \frac{\partial^2 a_2}{\partial z^2} + B_7 \frac{\partial^3 a_2}{\partial z^3}, \\ -\frac{\partial a_2}{\partial t} = \left(-B_1 + \frac{\partial B_2}{\partial z} - \frac{\partial^2 B_3}{\partial z^2} \right) a_2 + \left(B_2 - 2 \frac{\partial B_3}{\partial z} \right) \frac{\partial a_2}{\partial z} + \dots \\ \quad \dots - B_3 \frac{\partial^2 a_2}{\partial z^2} + \left(-A_1 + \frac{\partial A_2}{\partial z} \right) a_1 + A_2 \frac{\partial a_1}{\partial z}, \end{array} \right. \quad (5.32)$$

where, given the definition of inner product and the dependence of A_i, B_i on z , some more terms have arisen coming from integration by parts. We remark that the system (5.32) is the adjoint of system (3.31) on the whole, that is to say that it is impossible to associate a single equation of (5.32) to a single equation of (3.31).

Chapter 6

Break-up time minimisation

This Chapter is entirely dedicated to the minimization of the break-up time of an infinite thread of liquid, in the configuration described in Section 4.1. Therefore, we refer to a cylinder of fluid, approximately of radius h_0 , initially at rest. Surface tension acts amplifying small disturbances present in the flow - if they are destabilizing - eventually driving the thread to break up into droplets. In this configuration disturbances can be present in the flow as perturbations of the interface, that we introduce enforcing the initial condition: $F(z, 0) = [h(z, 0)]^2 = [h_0 + h'(z)]^2$. This initial perturbation therefore constitutes the control, because it is acting on it that we can obtain faster ruptures. Since we are interested only in small perturbations and we want the available control laws to be comparable, we will also have to define some conditions on the control, to be enforced in the optimization loop. This can be done imposing more constraints in the Lagrangian or introducing a suitable penalization term in the objective function. Indeed, the optimal initial condition in order to get the earlier break up is found optimizing an objective function which is related to the pinch-off time and may contain some terms regarding the control itself. The initial condition on the velocity will always be set to zero: $V(z, 0) \equiv 0$. The objective function (in its part related to the pinch-off time) and the control will be the topics of the next two Sections. In Section 6.3 the complete optimization

system is displayed in some of its possible configurations and the results are shown, discussing the effectiveness of the optimization depending on different choices that can be made.

6.1 Objective function

An optimization process aims at finding a local optimum for a given objective function, acting on a control. In this Chapter our goal is to enhance the break-up of an infinite thread, acting on its initial shape. The latter, as already anticipated, is the control. Let t_{po} be the time at which the first drop detaches, considering $t = 0$ the instant at which initial conditions are enforced and the integration of equations (3.31) begins. We recall that the detachment of the first drop happens when the radial coordinate of the interface reaches a certain value close to zero (e.g. 10^{-5} non-dimensional units of length). Thus, our purpose is to minimize t_{po} selecting the ‘best’ control within a set defined by certain conditions, that we will discuss in the next Section and may enter the final structure of the objective function. For the moment, we refer to the objective function just as the function related to pinch-off time, J_{po} .

6.1.1 A problem of definition

The first question that raises is: can we use directly $J_{po} = t_{po}$ as the objective function to be minimized? For the reasons we will now explain, the answer is that unfortunately we cannot. Indeed t_{po} is just the time at which an event - the first break-up of the interface - happens. Thus, it is just a numerical parameter of the integration, and not an analytic function of the state variables F and V . The objective function has to be $J = J(\mathbf{q})$ (or, eventually, $J = J(\mathbf{q}, \mathbf{g})$, since it will be setting the variation of the Lagrangian (which contains J) with respects to its variables (\mathbf{q} , \mathbf{g} and the Lagrange multipliers) to zero that we will be able to get the information about the sensitivity of J to the control. If J were not even dependent on the state $\mathbf{q} = [F; V]$, how could we relate it with the control and the physical system that effectively governs the process?

Therefore, the objective function has to be an analytic function containing the state variables, in a certain sense ‘connectable’ to the control through the optimality system. The first idea that comes into mind is to look for a function which analytically defines t_{po} and respects the above-mentioned characteristics. This task should not be impossible to accomplish. However, again this approach collides with the limits of the adjoint method applied to our specific case. Indeed, as we have already pointed out, when the interface reaches the z -axis and the thread breaks (i.e. $t = t_{po}$) the equations develop a singularity and the model is not able to describe the flow anymore. Thus, the integration has to stop in correspondence of the break-up. Besides, in order to use the adjoint tool described in the previous chapter, the time span $[0, T]$ has to be fixed during the iterative loop. Since we are minimizing t_{po} , it will be $t_{po}^{k+1} < t_{po}^k$, where k is the number of the generic iteration. In order to be able to perform the $(k + 1)$ th iteration, though, we have to avoid that $t_{po}^{k+1} < T$, or the integration will stop before T is reached. It follows that it has to be $T < t_{po,opt}$. So, in this framework, it is impossible to directly capture the moment of break up, and some surrogate function has to be used, ‘significantly related’ to the rupture even if the integration stops before it happens. In fact, as far as computational time is concerned, we have the interest to choose the lowest possible T , also considering that solving the adjoint equations is more costly than solving the original system. Moreover, since the procedure is iterative, any gain from this point of view has to be multiplied for the number of iterations needed to reach convergence. The choice of the surrogate function and of time T will be discussed in the next paragraphs.

6.1.2 Choice of surrogate function

We have to find one or more functions which depend on the state variables and are significantly related to break-up. That is to say that optimizing them will result in the minimization of the pinch off time. Since the ‘engine’ of the process is the instability due to surface tension, the idea is to use functions connected to the growth of the instability itself. If we consider the evolution of different comparable flows (same size, same Oh ,

‘similar’ initial condition, etc.) at a given time T , we expect that the one which exhibits the largest growth will be the first to break. We have to keep in mind that we will optimize these functions in a domain $[0, T]$, with $T < t_{po}$. Since the process consists basically in the amplification of physical disturbances, monitoring the evolution of the growth, even if only in the first stages, seems a good way to predict (and optimize) the rupture, which is the final consequence of the growth itself. We identified two functions that have the above-mentioned characteristics. In both cases we used the integral over the spatial domain of a function of the interface which becomes larger when the unstable flow evolves in time:

1. the integral of the square of the first spatial derivative of the interface:

$$OF_1(T) = \frac{1}{L} \int_0^L \left[\frac{\partial h(z, T)}{\partial z} \right]^2 dz, \quad (6.1)$$

2. the integral of the square of the deviation of the interface from the unit value:

$$OF_2(T) = \frac{1}{L} \int_0^L [1 - h(z, T)]^2 dz. \quad (6.2)$$

It is evident that both functions vanish if the interface is perfectly plain ($h(z) \equiv 1$), are close to zero in the first stages of the process if the perturbation is little and, if the system is unstable, become larger when it evolves. Indeed, they are both related to the deformation of the system, but with a sort of ‘phase-shift’. The largest derivative of the interface will be where it exhibits the steepest slope, so approximately between a peak and a valley (where $h \simeq 1$), while its deviation from 1 will be maximum precisely in correspondence of peaks and valleys, where the derivative vanishes. If $h(z)$ is a sinusoid, then its spatial derivative and its deviation from the mean value are exactly the same function, shifted in space of a quarter of a period, so OF_1 and OF_2 have exactly the same value if the integration domain coincides with the period. Anyway, even if we set a sinusoidal initial condition, the interface, evolving, will deviate from the sinusoidal shape, so that OF_1 and OF_2 will provide respectively different information on the state of

the system. The functions OF_1 and OF_2 can be also defined substituting $F = h^2$ to h without any conceptual difference.

A preliminary test

In order to convince ourselves that OF_1 and OF_2 are actually ‘well-related’ with the break-up time, we display here some graphs that also allow us to make some considerations on these two functions. The idea is the same we used to compare pinch-off times to growth rates found via linear stability analysis in Subsection 4.3: we let the system evolve starting from sinusoidal initial conditions, varying the wavenumber k . The functions OF_1 and OF_2 , are evaluated at an intermediate time T , whose choice will be discussed briefly, and for every k their values are displayed along with the inverse of the pinch-off time $\frac{1}{t_{po}}$. This procedure is repeated for different Oh , adapting T to the specific case. We remark that the results coming from this test cannot be considered neither an outright proof nor a complete overview of the relationship between these functions and the time of rupture: indeed only sinusoidal initial conditions are taken into account, so that a priori it is impossible to predict what will happen in the most general case. Nonetheless, finding a relation between these functions and the pinch-off time would reasonably show that it is worth trying to optimize them in order to optimize break-up. The results are shown for F , but there would not be any difference if we displayed them for h : the trends are obviously the same. Figure 6.1-6.4 contain graphs in which on the x -axis there is the wavenumber k while on the y -axis there are OF_1 , OF_2 and $\frac{1}{t_{po}}$ normalized, so that their scale is such that they can be easily compared. In fact, the absolute value of these functions is not so important: what really matters is their trend. In the graphs of Figure 6.1-6.4 OF_1 is plotted in red, OF_2 in blue, $\frac{1}{t_{po}}$ in black and the maxima of all three are indicated on the respective lines by asterisks of the respective color. For $Oh = 0, 0.1, 1$ (Figure 6.1-6.3) it is evident that both OF_1 and OF_2 are quite good candidates as surrogate functions of pinch-off time, at least in the framework of sinusoidal initial conditions. In particular, the k that maximize OF_2 is always a little smaller and the k that maximize OF_1 is always a little larger than

the k that minimizes pinch-off time. However the deviation is quite small in both directions. In the case of $Oh = 10$, OF_2 behaves in the same way as in the other cases, while OF_1 shifts more toward larger wavenumbers. Nonetheless, the results of this preliminary test are positive and encouraging. It appears that one of the functions, or better still a combination of the two, should lead to good results in the optimization of break-up. In particular the idea of using as objective function a combination of OF_1 and OF_2 , with some weights to give more importance to one or the other, appears to be promising. Both functions seem to act quite coherently with pinch-off time, although with some slight differences between them. In fact, they deviate somehow in opposite ways, so that they could balance each other during the optimization.

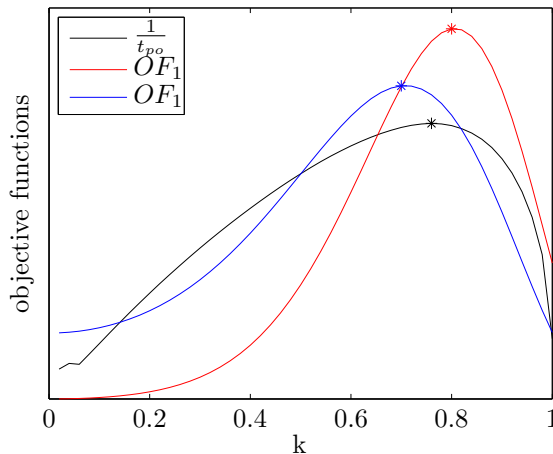


Figure 6.1: Test for objective functions: $Oh = 0$, $t_{po,min,lin} \simeq 9$, $T = 3$

In order to minimize t_{po} , OF_1 and OF_2 should be maximized. If minimizing is preferred, it is possible to take the inverse of the above-mentioned functions: $\frac{1}{OF_1}$ and $\frac{1}{OF_2}$. Since taking the inverse is a highly non-linear operation, we display the results of the preliminary test discussed above also for these new functions. Indeed, the maxima have to become minima, but

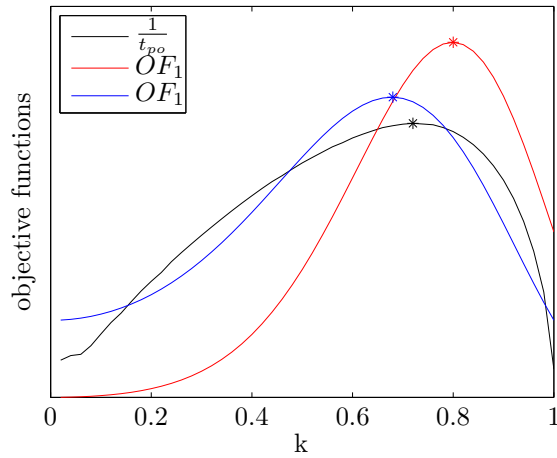


Figure 6.2: Test for objective functions: $Oh = 0.1$, $t_{po,min,lin} \simeq$, $T = 4$

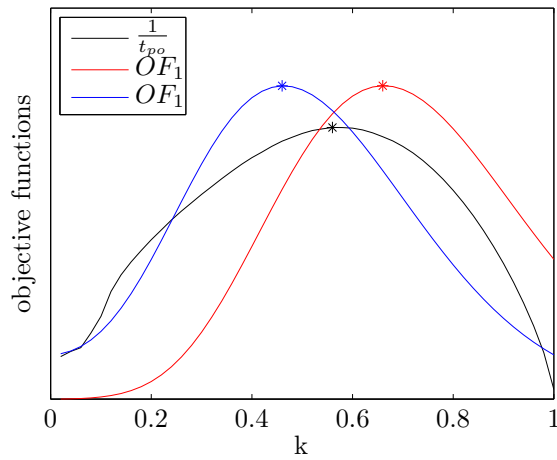


Figure 6.3: Test for objective functions: $Oh = 1$, $t_{po,min,lin} \simeq 30$, $T = 10$

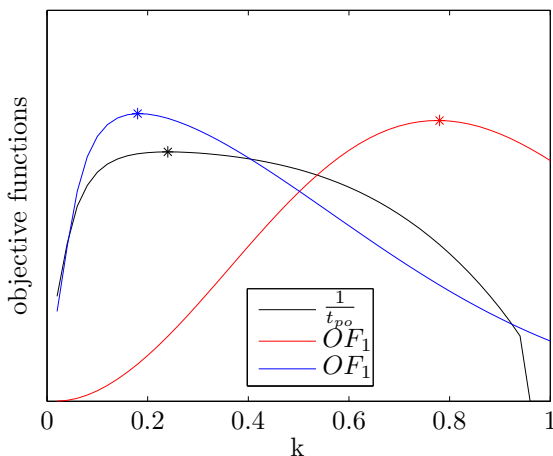


Figure 6.4: Test for objective functions: $Oh = 10$, $t_{po,min,lin} \simeq 234$, $T = 75$

the functions around optimal points can be much different. Since we use an iterative procedure, the shapes of the functions ‘near’ the optimal point is important in order to get good results. The trends of the inverses are shown through dotted lines, along with the ones obtained for the ‘original’ functions (continuous line); sets of values have been normalized again, in order to make the comparisons easier. Figure 6.5 shows that the inverse of OF_2 does not exhibit any problematic behavior: the valley appears to be a little ‘gentler’ than the corresponding peak, but the minimum is clearly visible and obviously located in correspondence of the same k . On the other hand Figure 6.6 shows that the inverse of OF_1 is very large (tends to infinity) for small wavenumbers, so that it appears almost flat elsewhere, and in particular in correspondence of the expected minimum. The problem is that OF_1 tends to zero for small wavenumbers, so that its inverse tends to infinity. Thus, in order to see what happens around the optimal point, we cannot consider all the range $k \in [0, 1]$. In Figure 6.7 OF_1 and its inverse are shown in the range $k \in [0.4, 0.9]$. Having restricted the range it is possible to remark that the trends ‘near’ to the optimal point are almost specular,

so that $\frac{1}{OF_1}$ also appears suitable as objective function in a minimization problem.

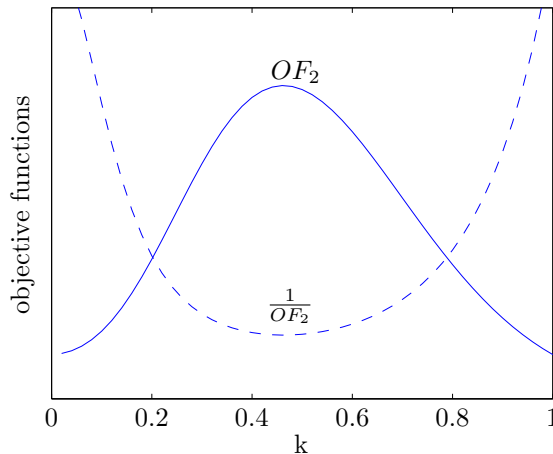


Figure 6.5: Test for OF_2 (continue line) and its inverse (dotted line): $Oh = 1$, $t_{po,min,lin} \simeq 30$, $T = 10$.

6.1.3 Choice of time domain

The time T at which we stop the integration of the system, evaluate the objective function and start the backward integration of the adjoint is an important parameter of the optimization. It cannot be too small, because the system has to evolve enough to provide significant information on the break-up (although it remains away from happening), but we want it to be the smallest possible in order to minimize computational effort. Again, we tested the influence of T on OF_1 and OF_2 letting the system evolve starting from sinusoidal initial conditions, varying their wavenumber and, this time, also the time span of integration $[0, T]$. We display the results in the case of $Oh = 0.1$, with $T = \{1, 2, 3, \dots, 11\}$ in Figure 6.8 and 6.9. Quite obviously OF_1 and OF_2 grow larger if T increases, but we reiterate that what it is

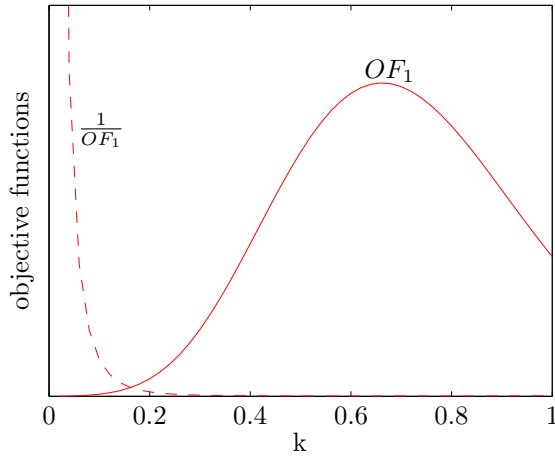


Figure 6.6: Test for OF_1 (continue line) and its inverse (dotted line): $Oh = 1$, $t_{po,min,lin} \simeq 30$, $T = 10$.

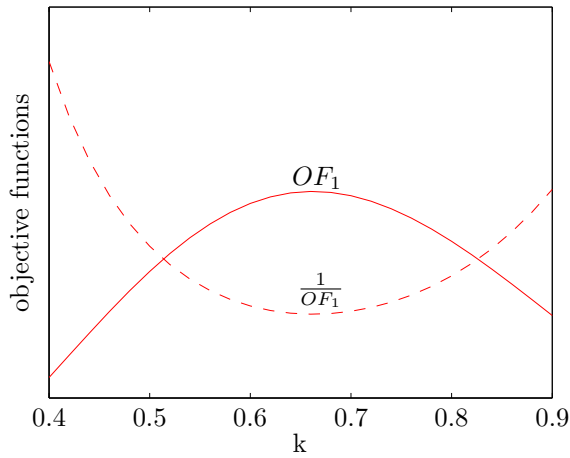


Figure 6.7: Test for OF_1 (continue line) and its inverse (dotted line), $k \in [0.4, 0.9]$: $Oh = 1$, $t_{po,min,lin} \simeq 30$, $T = 10$.

important are the location of the maxima, their adherence with pinch-off time and the shape of functions near them. The line of maxima, which is plotted in green, would be a straight vertical line if T had not any influence on the surrogate functions. Indeed, in both cases the green line becomes straight and vertical for large T . In particular from Figure 6.8 one can observe that the location of the maximum of OF_2 is never much affected by T , while a slightly stronger influence can be observed in Figure 6.9 on OF_1 for small T . In both cases, we can say that convergence is reached relatively ‘soon’ and one third/half of pinch-off time appears acceptable to be employed as T .

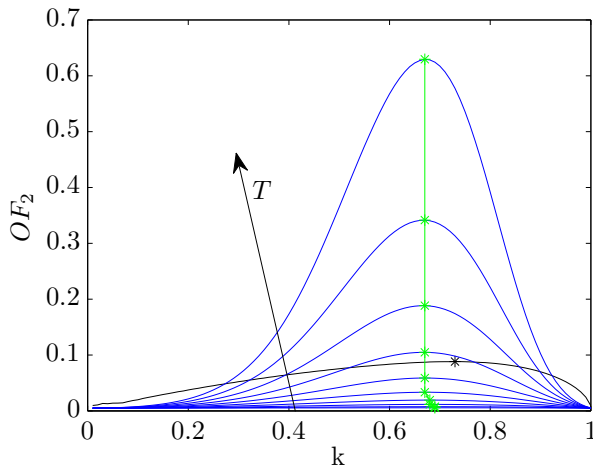


Figure 6.8: Test for OF_2 , $T = \{1, 2, 3, \dots, 11\}$, $Oh = 0.1$. Maxima are displayed in green, pinch-off time in black

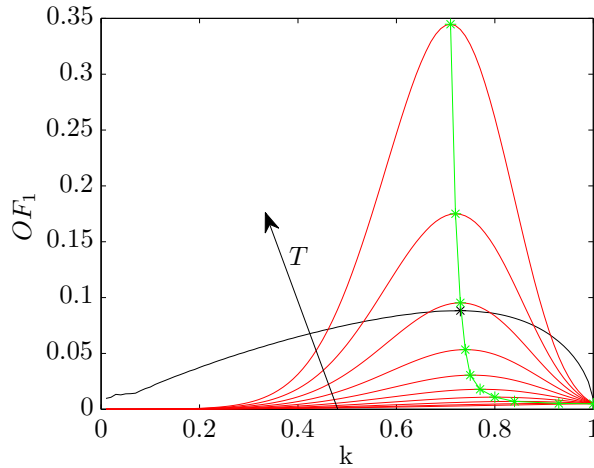


Figure 6.9: Test for OF_1 , $T = \{1, 2, 3, \dots, 11\}$, $Oh = 0.1$. Maxima are displayed in green, pinch-off time in black

6.1.4 Analytical expressions

In conclusion the objective function, or better its part directly related to pinch-off time, in case of minimization can be written as:

$$J_{po,min}(T) = \underbrace{\frac{\gamma_1}{\frac{1}{L} \int_0^L \left[\frac{\partial F(z,T)}{\partial z} \right]^2 dz}}_{J_1} + \underbrace{\frac{\gamma_2}{\frac{1}{L} \int_0^L [1 - F(z,T)]^2 dz}}_{J_2}. \quad (6.3)$$

Coefficients γ_1 and γ_2 are weights on which it is possible to act in order to give more relative importance to one term or the other. If one wants to use only one of the two terms, this is possible just setting the corresponding weight to zero.

6.2 Control

The control is the initial condition:

$$F(z, 0) = [h(z, 0)]^2 = g(z, 0), \quad (6.4)$$

expression which has to be introduced in the Lagrangian along with its Lagrange multiplier (or adjoint variable). For the Lagrangian to be complete, also a supplementary constraint on the control has to be specified. Deriving the adjoint equations, this will lead to find the *optimality condition*, a relation for updating the control during the iterative procedure. The constraint will have to somehow bind the initial condition on the interface. Indeed, it is intuitive that an earlier pinch-off could be trivially obtained just imposing a wider initial condition. Following this approach, at the limit, pinch-off time could easily tend to zero, if just somewhere the initial condition approaches the axis and $F(\bar{z}, 0) \simeq 0$. This is definitely not what we are looking for, since our goal is to find little but ‘well-shaped’ perturbations that, with minimal external effort, capitalize on the intrinsic instability features of the flow. The energy needed to attain break-up is provided by surface tension, and is ‘free’: we just have to trigger its release. Furthermore, claiming that a control is optimal we infer that it is ‘the best’ among controls with certain characteristics, so that it is important to define terms of comparison and to impose a condition which keeps the results of the optimization commensurate to one another.

6.2.1 Comparability criteria

The initial condition on the interface generally describes a perturbation of a cylinder of constant radius, and can always be written as $h(z, 0) = h_0 + h'(z)$. We already discussed the case in which $h'(z)$ is a sinusoidal function. Sinusoidal perturbations represent benchmarks for the optimal control we will find: indeed, our goal is to reduce the break-up time obtained letting the system evolve with the most unstable sinusoidal initial condition. We already pointed out that we want to do this without increasing the ‘amplitude’ of the control, but just acting on its shape. Now the

questions that arises is: how can the ‘amplitude’ of the control be defined? More generally, within which conditions can we consider two controls comparable? There are obviously many ways to approach this problem; we choose in particular two geometric criteria regarding the concept of amplitude (from a local and an average point of view) and a physical one involving the quantity of liquid.

- **Local amplitude**

A sinusoidally perturbed initial condition for the interface can be written as $h(z, 0) = h_0 + \epsilon \cos(kz)$, which implies that, $\forall z$:

$$h(z, 0) \in [h_0 - \epsilon, h_0 + \epsilon]. \quad (6.5)$$

The latter can be taken as a criterion for the generation of comparable controls. In other words for a general control to be comparable with its sinusoidal counterpart, it should not come out of the band in which the latter lies. It is a local criterion in the sense that it should be satisfied $\forall z$ or, in the numerical case, for every node. In an experimental framework it could represent the physical limits (established for convenience or necessity) in exceeding a certain value of the interface while imposing the initial condition. A weak enforcement of the criterion could be made considering acceptable controls in which the band is ‘passed’ only for a certain number of nodes, and not more than that. We can define two performance parameter; ω_{nodes} , which gives the percentage of nodes in which the criterion is not satisfied and ω_{max} , which compares the value of the maximum overrun to the band semi-width ϵ . As these two parameters increase, comparing pinch-off time originated by the control obtained through the optimization with that originated by the original sinusoidal condition becomes less acceptable, and eventually pointless.

- **Average amplitude**

A definition of average amplitude of the perturbation can be given

by:

$$\bar{A} = \frac{1}{L} \int_0^L [h(z, 0) - 1]^2 dz, \quad (6.6)$$

where, if \bar{A} is defined for the benchmark sinusoidal perturbation, the criterion will be satisfied if the average amplitude of the control does not exceed that value, or, in a weaker interpretation, the ratio $R_A = \frac{\bar{A}_{gen}}{\bar{A}_{ben}}$ of the generic control and its sinusoidal benchmark remains lower than a certain threshold. Physically, this means considering the perturbation as a whole, so that a larger peak is allowed if it is compensated by a ‘weaker’ zone somewhere else. The amplitude can be distributed in any way, so that the size of the spatial domain becomes also important in this this criterion. It is straightforward to substitute h with $h^2 = F$ without any conceptual difference: the physical meaning of \bar{A} changes, but it can be used in the same way as before to compare control laws.

- **Mass congruity**

When comparing two liquid threads breaking into drops, an important characteristic is their mass. Since the density ρ is constant, we can directly compute their volumes:

$$\mathcal{V} = \int_0^L \pi h(z, 0)^2 dz, \quad (6.7)$$

which is again an integral parameter. The mass of the optimal control should not be very different from the mass of the benchmark. In the following the parameter $\Delta_{mass} = 100 \frac{\mathcal{V}_{opt} - \mathcal{V}_{rif}}{\mathcal{V}_{rif}}$ will be used.

In order to materially keep the amplitude bound in one or more of the above-mentioned meanings during the optimization loop, suitable terms have to be added in the Lagrangian functional, as we are about to discuss. These criteria will be extensively used in the following part while evaluating effectiveness and performances of the optimization.

6.2.2 Implementation in the Lagrangian

There are two ways of applying limitations on the control in the formulation of the Lagrangian: addition of penalization terms in the objective function and direct enforcement of equality constraints (similarly to enforcement of initial and boundary conditions). These issues are discussed in the following paragraphs.

Penalization

Instead of optimizing an objective function $J(F)$ which is only dependent on the state, such as J_{po} described in (6.3), one can add to it terms containing also information on the size of the control, defining an overall functional $J_{overall}(F, g)$. In this manner the growth of the state at time $t = T$ and the amplitude of the control at time $t = 0$ are simultaneously optimized. The optimal control will be that which maximizes the growth of the system without being too far from the criteria above-discussed. Since every term is multiplied by a weight coefficient, it is possible to manipulate them with effects on the size of the control too. Obviously, the problem has changed, thus optimizers of $J_{overall}$ are not, in general, optimizers of J_{po} . We present now some penalization terms $J_{control}$ suitable for binding the amplitude of the control. From now on we consider $g(z) = F(z, 0)$.

- Deviation from the unit value:

$$J_{control} = \frac{1}{L} \int_0^L [g(z) - 1]^2 dz, \quad (6.8)$$

which is probably the most simplest way to limit the size of $g(z)$. This term grows larger the more $g(z)$ deviates from the unperturbed condition, increasing its size. If inserted into the objective function of a minimization problem it introduces a penalization for control laws that generate early pinch-offs just increasing their size. It is important to notice that in this case, if $J_{control} \rightarrow 0$ then $J_{po} \rightarrow \infty$, so that the overall minimum will be necessarily a compromise. As already pointed

out, it is possible to influence the quality of this compromise acting on the weights of the different terms of the objective function.

- Deviation from the unit value ‘with correction’:

$$J_{control} = \frac{1}{L} \int_0^L [(g(z) - 1)^2 - \bar{A}]^2 dz, \quad (6.9)$$

which is similar to the previous one, but pushes the control toward a sort of (non-zero) average deviation. It is convenient to take the average amplitude \bar{A} , defined in 6.6, as the average deviation, but it is neither obvious nor compulsory, since they are not the same thing.

Equality constraints

In this case the conditions have to be directly enforced in the Lagrangian functional with their own Lagrange multiplier. A plausible constraint is for example one related to the average amplitude:

$$\frac{1}{L} \int_0^L [g(z) - 1]^2 dz - \bar{A} = 0. \quad (6.10)$$

6.3 Equations and results

Against the above background, we can now assemble all the ingredients in several optimization ‘recipes’, discussing their effectiveness. What changes among the possible recipes is the way one chooses to limit the control, which determines the optimality condition. The different combinations are copious; our choice has been to display here a general form of the Lagrangian and a scheme of the equations.

The general Lagrangian reads:

$$\begin{aligned} \mathcal{L}(F(z, t), V(z, t), g(z), a_1(z, t), a_2(z, t), b_1(z), b_2(z), c) = \dots \\ \dots J(F(z, T), g(z)) - \int_0^T \int_0^L a_1(z, t) \cdot \left(\frac{dF(z, t)}{dt} + \dots \right) dz dt + \dots \end{aligned}$$

$$\begin{aligned} \dots - \int_0^T \int_0^L a_2(z, t) \cdot \left(\frac{dV(z, t)}{dt} + \dots \right) dz dt - \int_0^L b_1 \cdot (F(z, 0) - g(z)) dz \dots \\ \dots - \int_0^L b_2 \cdot (V(z, 0) - V_0) dz - c \cdot (\text{constraint}), \quad (6.11) \end{aligned}$$

where $J(F, g)$ and $c \cdot (\text{constraint})$ are made clear later for the respective cases.

The equations of the flow and the adjoint are respectively (3.31) and (5.32), along with the initial conditions:

$$\begin{cases} F(z, 0) = g(z), \\ V(z, 0) = V_0 \equiv 0, \\ a_1(z, T) = 2\gamma_1 L \frac{\frac{\partial^2 F(z, T)}{\partial z^2}}{\left[\int_0^L \left(\frac{\partial F(z, T)}{\partial z} \right)^2 dz \right]^2} + 2\gamma_2 L \frac{1 - F(z, T)}{\left[\int_0^L (1 - F(z, T))^2 dz \right]^2}, \\ a_2(z, T) \equiv 0, \end{cases} \quad (6.12)$$

where the initial conditions for the backward integration of the adjoint system are found collecting time boundary terms while setting to zero the variations of the Lagrangian with respect to variations of the state variables, considering the minimization case. Periodicity is imposed at space boundaries, implying that all the boundary terms that arise during the derivation of the adjoint vanish. Boundaries issues are not considered neither in the Lagrangian nor in the equations, as they are automatically treated within the discretization. The optimality condition on $g(z)$ has to be derived setting to zero the variations of the Lagrangian with respect to the variations of the control, which changes case by case. This relation and the results of the optimization are treated separately for every way of limiting the control, for each one exploring possible variations of the optimization and physical parameters. For every optimization three graphs are shown:

- comparison between optimal and benchmark controls, along with the initial guess used to initialize the iterative loop,

- comparison between the optimized flow at the moment of break-up and the benchmark flow at the same instant,
- trends of the objective function and its terms during the iteration loop.

In particular we will see that the choice of the initial guess $g_{in}(z)$ is very important for the final result. Indeed, the procedure drives towards a local optimum; the number of local optima is potentially large, so that the starting point becomes crucial in determining which one will be found. The benchmark is always the most unstable sinusoidal perturbation for the given Oh , normally with $\epsilon = 0.05$.

6.3.1 Penalization: first mode

In this case the objective function reads:

$$J(F(z, T), g(z)) = \underbrace{J_{po, min}}_{J_1+J_2} + \underbrace{\frac{\gamma_3}{L} \int_0^L [g(z) - 1]^2 dz}_{J_3}. \quad (6.13)$$

The optimality condition is given by:

$$g(z) = 1 - \frac{L}{2\gamma_3} a_1(z, 0) \quad (6.14)$$

The first results of the optimization we show are performed with $Oh = 10$ using the benchmark control itself as initial guess. Observing Figure 6.10 and the above-defined performance parameters we can remark that:

- break-up happens 0.23 times before than with the benchmark control, therefore the linear optimum does not correspond to a non-linear one,
- the average amplitude is almost half of the benchmark's, indeed the interface is very close to 1 for the main part of the axial length, except for two quite pronounced valleys that exhibit the same periodicity of the benchmark,

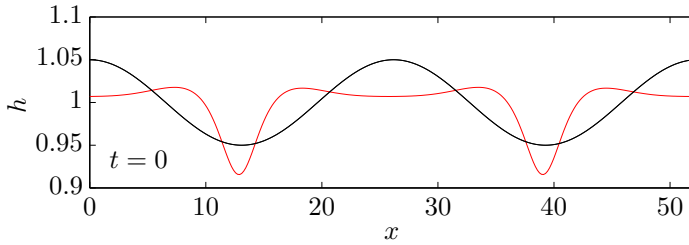
- although in a narrow space ($\omega_{nodes} = 10\%$), the interface goes out of the band, reaching in two points the value $\min(g) = 1 - 1.68\epsilon$,
- mass difference is negligible (it will not be discussed anymore if not substantial),
- J decreases during the iterative loop; so does J_3 , while J_2 increases and J_1 first increases and then decreases, eventually reaching a lower value than at the beginning. It is worth to notice that what is important is precisely that the overall objective function decreases, while the (limited) increase of one of its terms does not necessarily mean that pinch-off time becomes larger.

A very similar result would be attained changing just the amplitude ϵ of the initial guess, with the same wavelength.

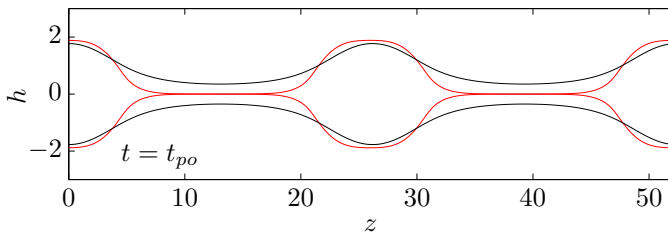
The case of a sinusoidal initial guess of lower wavelength, in particular with $k > 1$ (linearly stable), is presented in Figure 6.11, again with $Oh = 10$. In this case:

- break-up time decreases of a significant 45%.
- the average amplitude is again almost half of the benchmark's, indeed the interface is very close to 1 for the main part of the axial length, except for one deep valley (the optimal control does not maintain the same periodicity of the initial guess),
- in an even narrower space ($\omega_{nodes} = 5\%$), the interface goes well out of the band, reaching $\min(g) = 1 - 3.06\epsilon$,
- J decreases during the iterative loop along with all of its components.

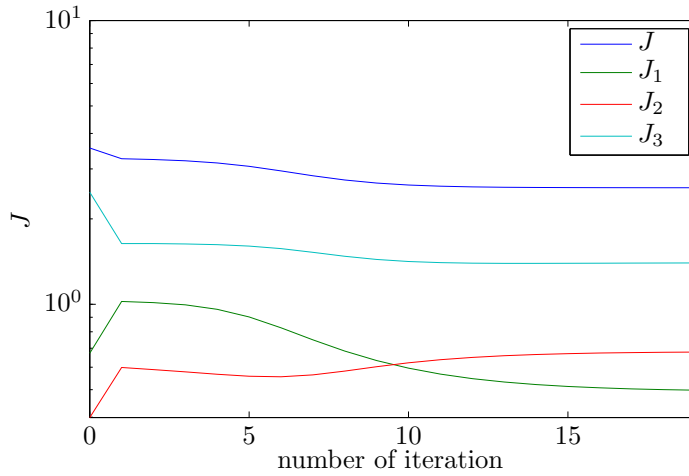
Thus, starting with this initial guess, we reach a local optimum that better minimizes break-up but, due to the definition of the objective function, quite heavily contradicts the local amplitude criterion. However, we found that a control made up of an almost constant part and a narrow and deep valley drives to quite early pinch-offs. Similar outcomes are also obtained when using random initial guesses, and setting $\gamma_2 = 0$ or $\gamma_3 = 0$ in the



(a) Benchmark/initial guess (black) and optimal control (red).



(b) Benchmark (black) and optimal (red) state at $t_{po,opt}$.



(c) Objective function (and its terms).

Figure 6.10: Results of the optimization with $g_{in}(z) = 1 + 0.05 \cos(k_{lin,opt}z)$, $Oh = 10$. $t_{po,bench} = 234$, $t_{po,opt} = 181$ (-23%), $R_A = 0.56$, $\omega_{nodes} = 10\%$, $\omega_{max} = 68\%$, $\Delta_{mass} = 0.36\%$

objective function does not change much. An example with random initial guess, $\gamma_2 = 0$ and $Oh = 10$ is shown in Figure (6.12).

So far, we tested only highly viscous flows ($Oh = 10$), thus we want to investigate what happens for lower Ohnesorge numbers. In general optimization of less viscous flows resulted more difficult than for the larger viscosity case, this for any choice on the objective function and the control. In Figure 6.13 is displayed an attempt of optimization in the case of $Oh = 1$, using as initial guess the most unstable sinusoidal perturbation. The solution to which the optimality procedure converges is very similar to the one used to initialize it, and so is the consequent pinch-off time.

Things change if we set a random initial guess for the control. In the case displayed in Figure 6.14, for example, the optimal control has a familiar shape, again given by a plainer part and a valley. Thus, this kind of control works also for low viscosity cases.

6.3.2 Penalization: second mode

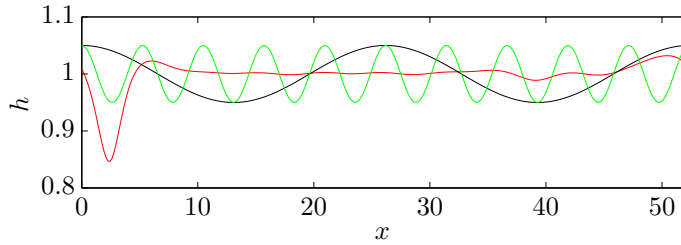
In this case the objective function reads:

$$J(F(z, T), g(z)) = \underbrace{J_{po, min}}_{J_1+J_2} + \underbrace{\frac{\gamma_3}{L} \int_0^L [(g(z) - 1)^2 - \bar{A}]^2 dz}_{J_3}. \quad (6.15)$$

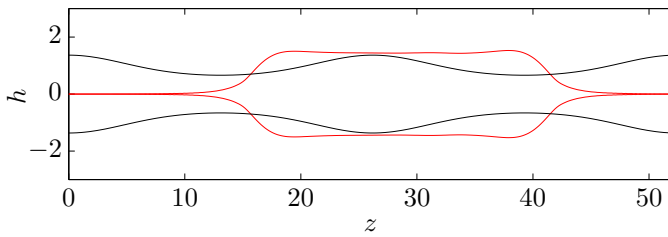
Deriving the optimality condition, we run into a polynomial equation. The polynomial is:

$$\mathcal{P}(g(z)) = g(z)^3 - 3g(z)^2 + (3 - \bar{A})g(z) + \bar{A} - 1 + \frac{L}{4\gamma_3} a_1(z, 0), \quad (6.16)$$

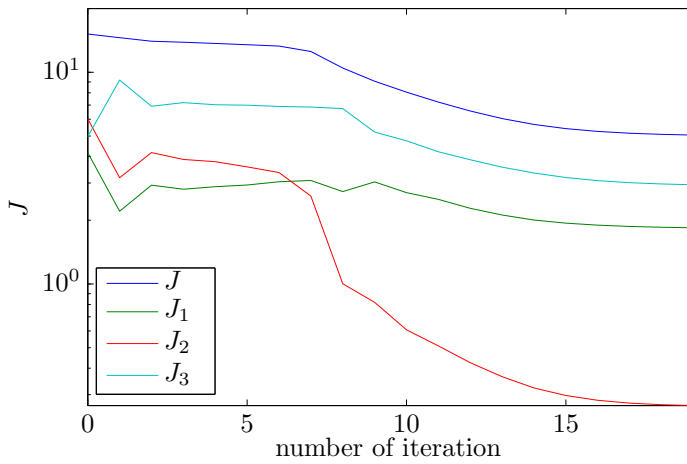
which, considering that $\bar{A} > 0$ by definition, has two complex and one real roots if $\bar{A} < 0.815$ or $\bar{A} \in (1.55, 3.56)$. Since \bar{A} is the average amplitude of a *small* perturbation, it will always be a number relatively close to zero, surely lower than 0.815, and so does any possible average deviation pertaining to the problem. Thus, the optimality condition can be enforced computing $g(z)$ as the only real root of $\mathcal{P}(g(z))$. In order to test the performances of the optimization with this configuration of the Lagrangian,



(a) Benchmark (black) and optimal (red) control. In green: initial guess.

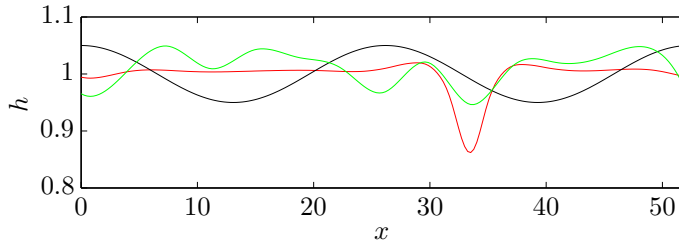


(b) Benchmark (black) and optimal (red) state at $t_{po,opt}$.

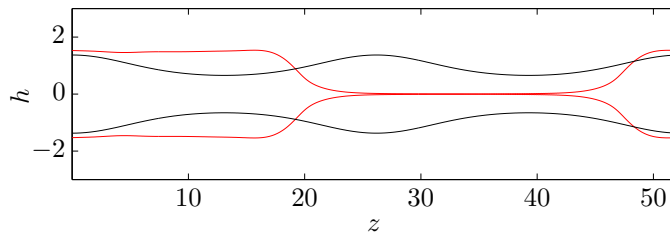
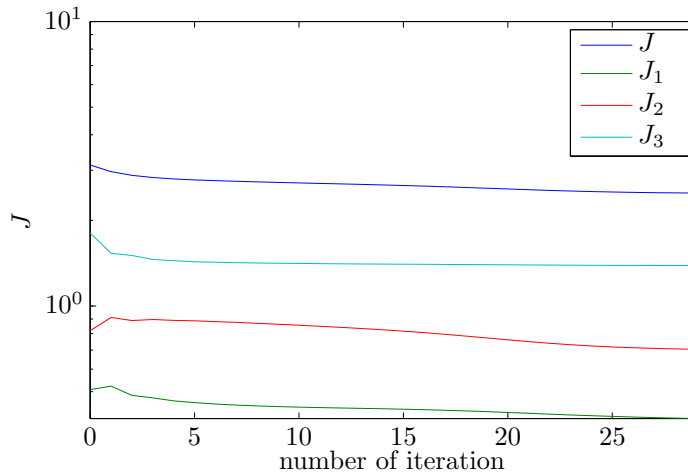


(c) Objective function (and its terms).

Figure 6.11: Results of the optimization with $g_{in}(z) = 1 + 0.05 \cos(5k_{lin,opt}z)$, $Oh = 10$. $t_{po,bench} = 234$, $t_{po,opt} = 127$ (-45%), $R_A = 0.59$, $\omega_{nodes} = 5\%$, $\omega_{max} = 206\%$, $\Delta_{mass} = 0.43\%$

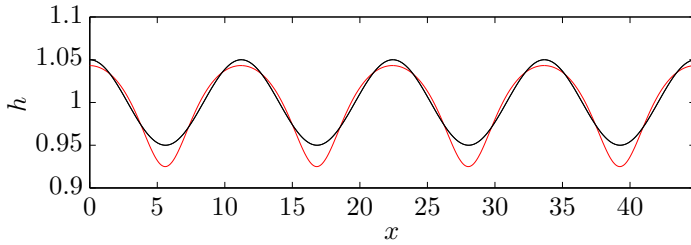


(a) Benchmark (black) and optimal (red) control. In green: initial guess.

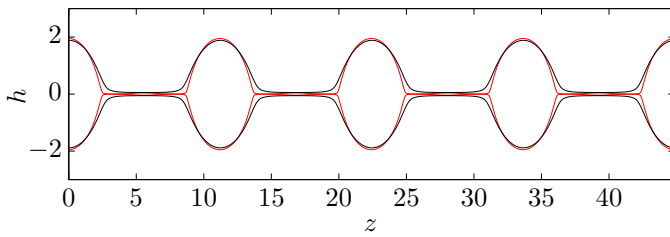
(b) Benchmark (black) and optimal (red) state at $t_{po,opt}$.

(c) Objective function (and its terms).

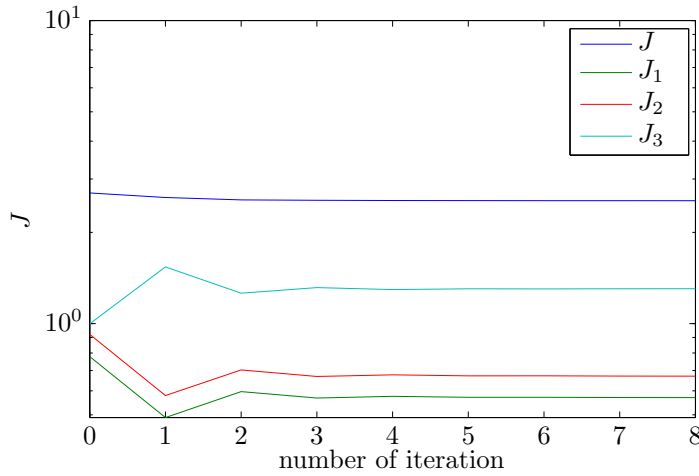
Figure 6.12: Results of the optimization with random $g_{in}(z)$, $Oh = 10$.
 $t_{po,bench} = 234$, $t_{po,opt} = 87$ (-63%), $R_A = 1.11$, $\omega_{nodes} = 5\%$, $\omega_{max} = 460\%$, $\Delta_{mass} = 0.83\%$



(a) Benchmark/initial guess (black) and optimal control (red).

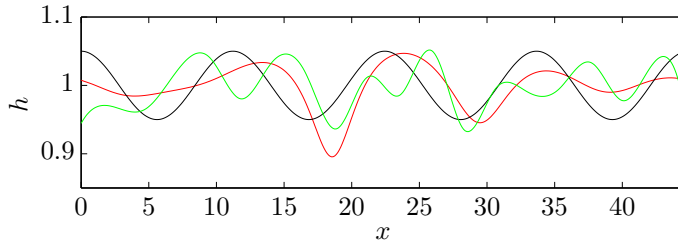


(b) Benchmark (black) and optimal (red) state at $t_{po,opt}$.

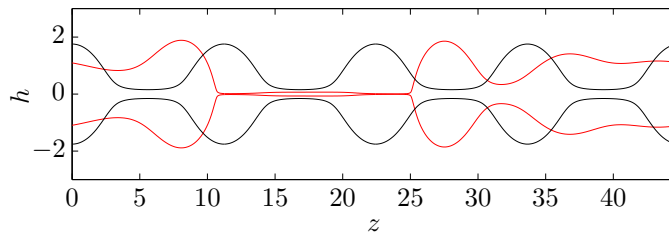
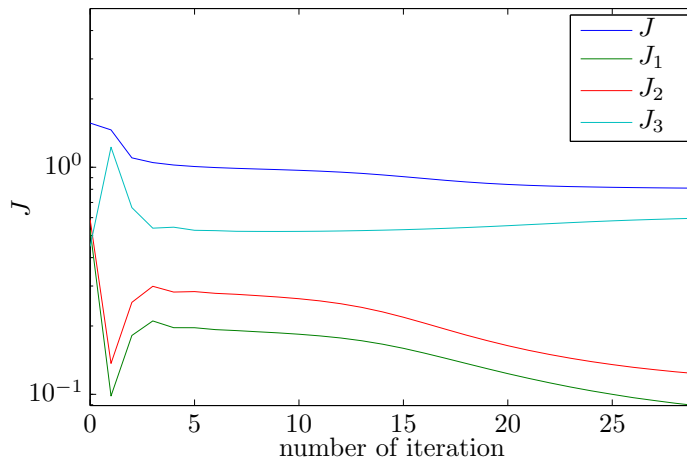


(c) Objective function (and its terms).

Figure 6.13: Results of the optimization with $g_{in}(z) = 1 + 0.05 \cos(k_{lin,opt}z)$, $Oh = 1$. $t_{po,bench} = 32$, $t_{po,opt} = 28.5$ (-11%), $R_A = 1.27$, $\omega_{nodes} = 20\%$, $\omega_{max} = 47\%$, $\Delta_{mass} = 0.70\%$



(a) Benchmark (black) and optimal (red) control. In green: initial guess.

(b) Benchmark (black) and optimal (red) state at $t_{po,opt}$.

(c) Objective function (and its terms).

Figure 6.14: Results of the optimization with random $g_{in}(z)$, $Oh = 1$. $t_{po,bench} = 32$, $t_{po,opt} = 26.4$ (-16%), $R_A = 0.73$, $\omega_{nodes} = 8.75\%$, $\omega_{max} = 108\%$, $\Delta_{mass} = 0.45\%$

we try different initial guesses at different Oh , similarly to what we have done in the previous Subsection.

Starting from the most unstable sinusoidal perturbation with $Oh = 10$, we obtain the results shown in Figure 6.15. We remark that the shape of the optimal control is approximately that of an asymmetric square wave, which will result to be characteristic of this configuration. Moreover:

- break-up happens 0.28 times before than with the benchmark control,
- the average amplitude has increased by 23%
- the local amplitude criterion is substantially respected: the control lies within the band $[1 + \epsilon, 1 - \epsilon]$ aside from negligible peaks in a small number of nodes.
- the mass of the flow in the domain has increased of almost 5% with respect to the benchmark case.

Considering a sinusoidal perturbation with a larger wavenumber and the same Oh , as in Figure 6.16, the result is even better. The average amplitude is lower, the local amplitude criterion is always respected and the pinch-off time has decreased. On the other hand, Δ_{mass} has increased.

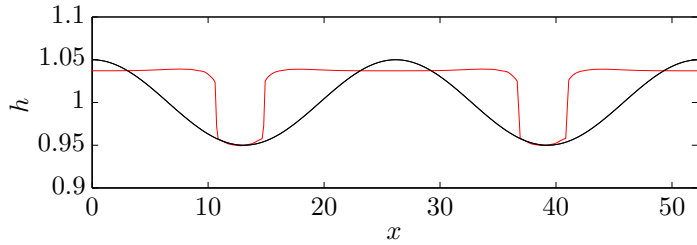
Initializing the optimization process with a random control, as in Figure 6.17, convergence is reached and an earlier pinch-off is found, even if, in this case, later than in the previous one. We recognize again the characteristic shape of this configuration.

The optimization with lower Oh has resulted impossible in this configuration. The loop does not converge and the square-like wave appears not to work with this Oh .

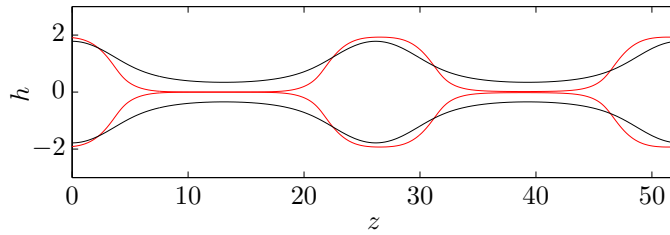
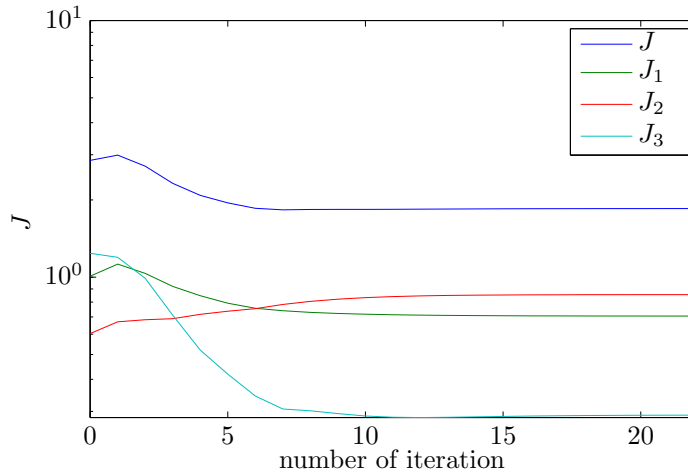
6.3.3 Enforcement of average amplitude

In this case the objective function is simply given by:

$$J\left(F(z, T), g(z)\right) = J_{po, min} \quad (6.17)$$

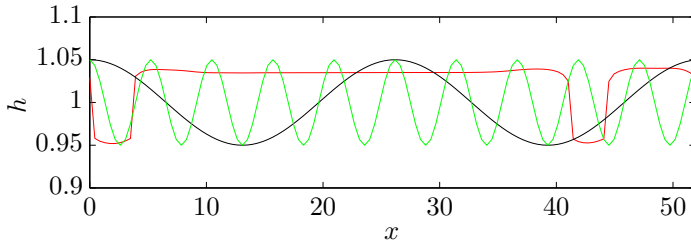


(a) Benchmark/initial guess (black) and optimal control (red).

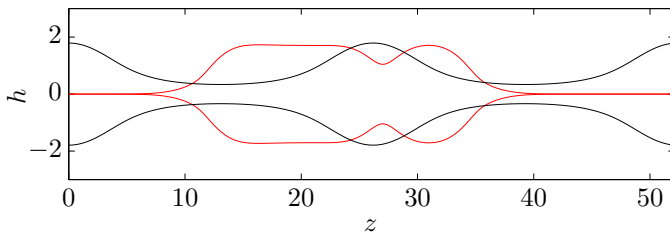
(b) Benchmark (black) and optimal (red) state at $t_{po,opt}$.

(c) Objective function (and its terms).

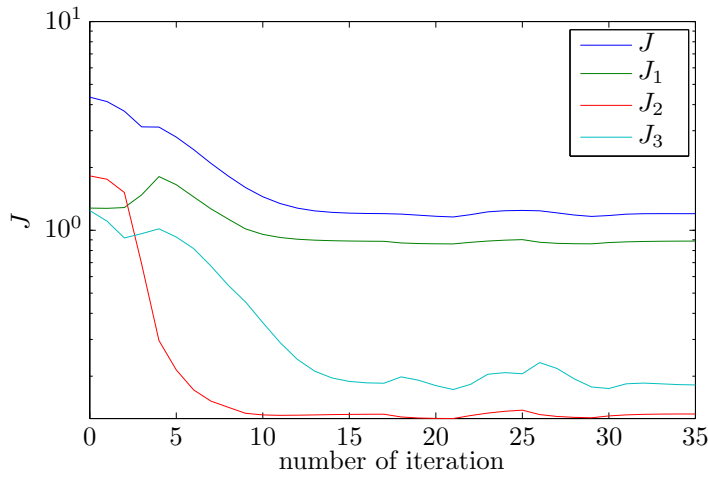
Figure 6.15: Results of the optimization with $g_{in}(z) = 1 + 0.05 \cos(k_{lin,opt}z)$, $Oh = 10$. $t_{po,bench} = 234$, $t_{po,opt} = 179$ (-24%), $R_A = 1.23$, $\omega_{nodes} = 2.7\%$, $\omega_{max} = 1.13\%$, $\Delta_{mass} = 4.78\%$



(a) Benchmark (black) and optimal (red) control. In green: initial guess.

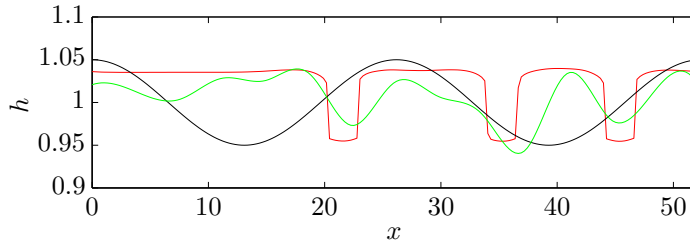


(b) Benchmark (black) and optimal (red) state at $t_{po,opt}$.

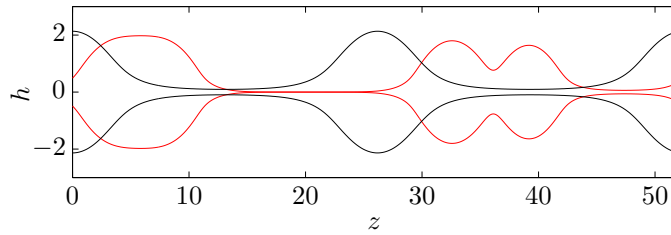
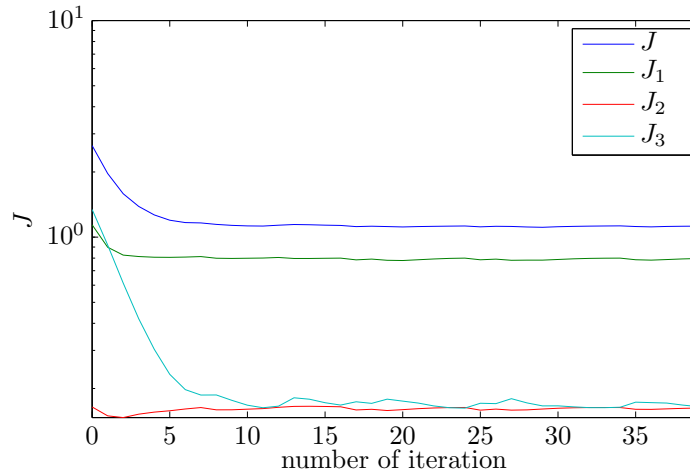


(c) Objective function (and its terms).

Figure 6.16: Results of the optimization with $g_{in}(z) = 1 + 0.05 \cos(5k_{lin,opt}z)$, $Oh = 10$. $t_{po,bench} = 234$, $t_{po,opt} = 174$ (-26%), $R_A = 1.15$, $\omega_{nodes} = 0\%$, $\omega_{max} = 0\%$, $\Delta_{mass} = 5.21\%$



(a) Benchmark (black) and optimal (red) control. In green: initial guess.

(b) Benchmark (black) and optimal (red) state at $t_{po,opt}$.

(c) Objective function (and its terms).

Figure 6.17: Results of the optimization with random $g_{in}(z)$, $Oh = 10$.
 $t_{po,bench} = 234$, $t_{po,opt} = 216$ (-8%), $R_A = 1.13$, $\omega_{nodes} = 0\%$, $\omega_{max} = 0\%$,
 $\Delta_{mass} = 4.81\%$

As far as the constraint on the control is concerned, we can make 6.12 more explicit, writing:

$$(\text{constraint}) = \frac{1}{L} \int_0^L [g(z) - 1]^2 dz - \bar{A}. \quad (6.18)$$

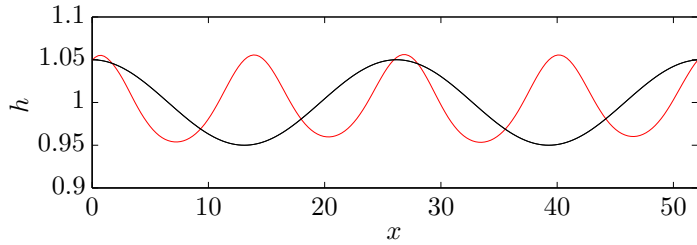
The optimality condition is then given by:

$$\begin{cases} g(z) = 1 + \frac{L}{2c} a(z, 0), \\ c = \sqrt{\frac{L}{2A} \int_0^L (a_1(z, 0))^2 dx}, \end{cases} \quad (6.19)$$

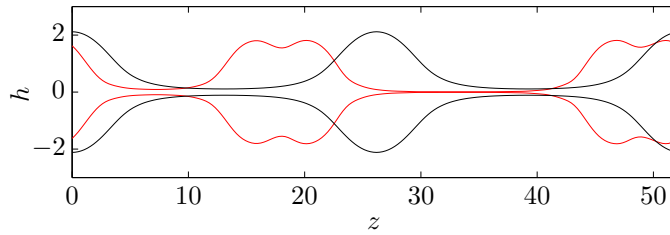
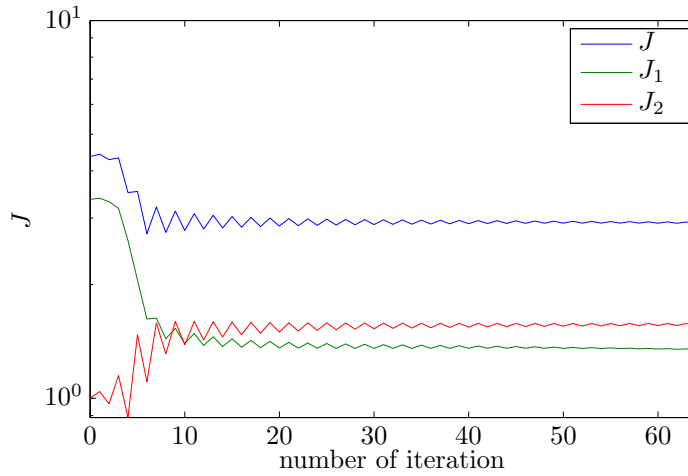
Employing the most unstable sinusoidal perturbation as initial guess with $Oh = 10$, we obtain the results shown in Figure 6.18. We can remark that

- the optimal control exhibits a periodicity characterized by a wavelength which is half of the benchmark's;
- break-up decreases only of 0.07% with respect to the benchmark control;
- the average amplitude is directly enforced, and so it is strictly satisfied (this aspect will not be discussed anymore);
- the optimal interface is not far from respecting the local amplitude criteria, given the low values of ω_{nodes} and ω_{max} ;
- the loop converges oscillating, fact that can be explained with the non-linearity of the system and the re-scaling operated at every iteration while enforcing the condition on average amplitude.

Using a sinusoidal perturbation with a lower wavelength as initial guess, with $Oh = 10$, we obtain better results, as shown in Figure 6.19. The optimal control is quite wavy but tends to form a single big drop if it is allowed to evolve. The local amplitude criteria is broken in greater measure

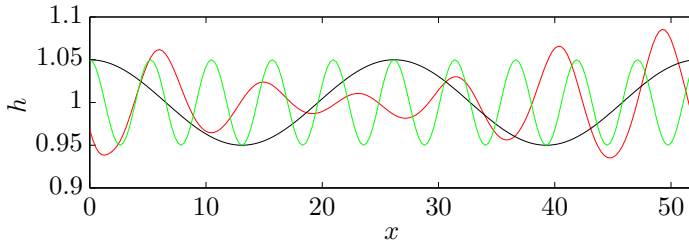


(a) Benchmark/initial guess (black) and optimal (red) control.

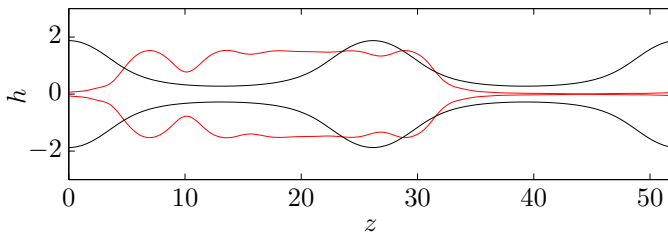
(b) Benchmark (black) and optimal (red) state at $t_{po,bench}$.

(c) Objective function (and its terms).

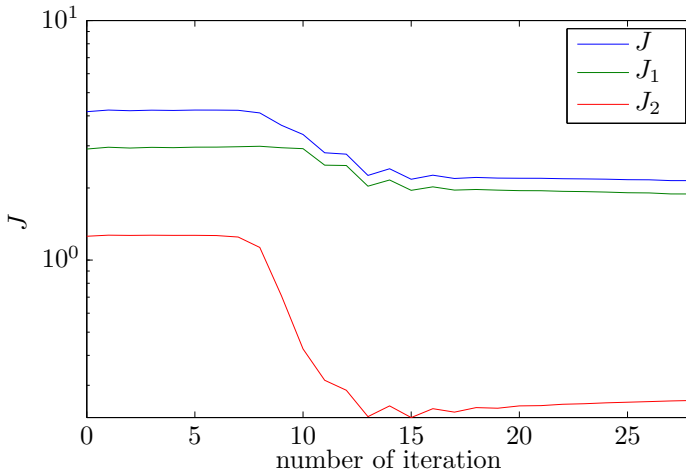
Figure 6.18: Results of the optimization with $g_{in}(z) = 1 + 0.05 \cos(k_{lin,opt}z)$, $Oh = 10$. $t_{po,bench} = 234$, $t_{po,opt} = 217$ (-7%), $R_A = 1$, $\omega_{nodes} = 11.5\%$, $\omega_{max} = 12\%$, $\Delta_{mass} = 0.21\%$



(a) Benchmark (black) and optimal (red) control. In green: initial guess.



(b) Benchmark (black) and optimal (red) state at $t_{po,bench}$.



(c) Objective function (and its terms).

Figure 6.19: Results of the optimization with $g_{in}(z) = 1 + 0.05 \cos(5k_{lin,opt}z)$, $Oh = 10$. $t_{po,bench} = 234$, $t_{po,opt} = 193$ (-18%), $R_A = 1$, $\omega_{nodes} = 20.5\%$, $\omega_{max} = 71\%$, $\Delta_{mass} = 0.23\%$

than in the previous case, and the reduction of the break-up time is larger.

Using a random initial guess, with $Oh = 10$, we obtain a similar result, as shown in Figure 6.20.

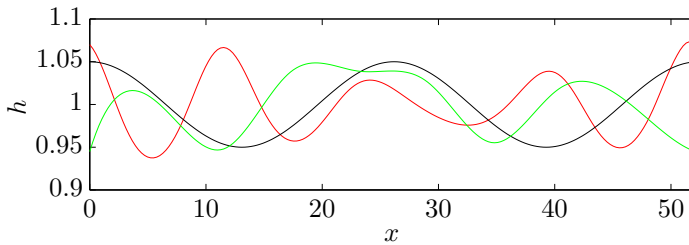
When considering flows with lower Oh the optimization is ineffective if starting with a sinusoidal initial guess. Better results are obtained using a random initial guess, as displayed in Figure 6.21.

6.3.4 Conclusions

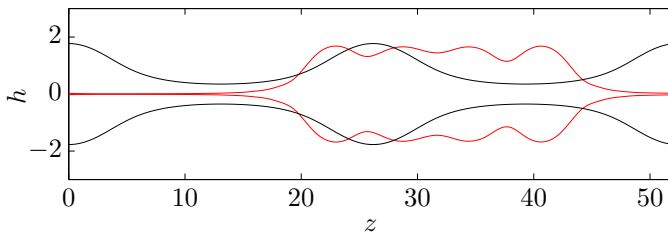
Summarizing, we can state that:

- the first mode of penalization produces controls which are equal to 1 everywhere but a narrow deep valley, with a very little average amplitude but breaking macroscopically the local amplitude criterion;
- the second mode of penalization produces square wave-like controls, which fit very well within the band $[1 + \epsilon, 1 - \epsilon]$ respecting local amplitude criterion even if exhibiting a larger average amplitude than the benchmark's;
- enforcing the average amplitude leads to wavy and rounded controls, with some peaks and valleys well outside of the band $[1 + \epsilon, 1 - \epsilon]$.

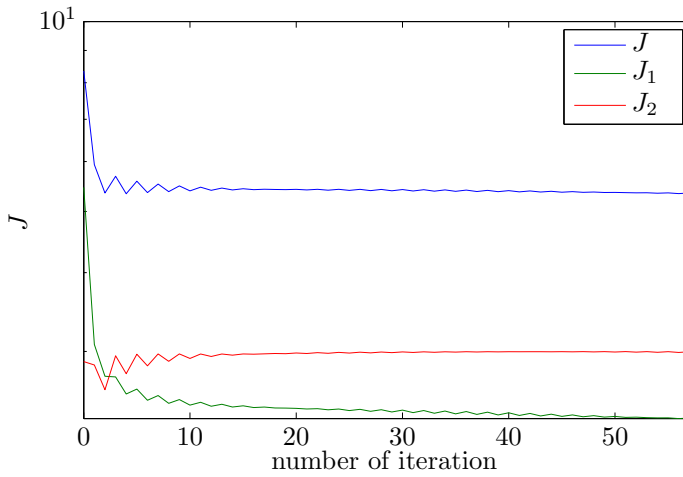
Optimization has been possible in all three the configurations for $Oh = 10$, but only in two of them for the lower viscosity fluid. In general, it appears that less viscous flows are more complicated to optimise, and the linear optimum found via linear stability analysis is 'hard to beat'.



(a) Benchmark (black) and optimal (red) control. In green: initial guess.

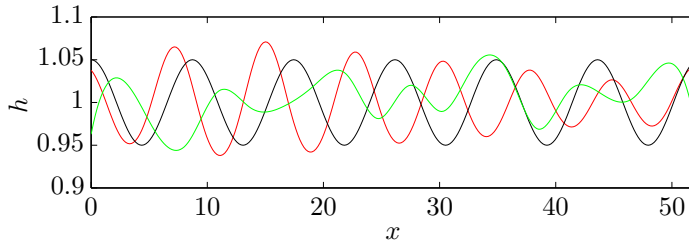


(b) Benchmark (black) and optimal (red) state at $t_{po,bench}$.

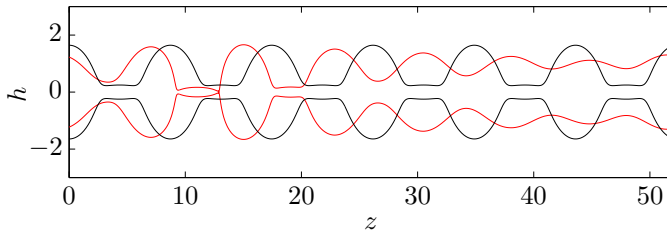
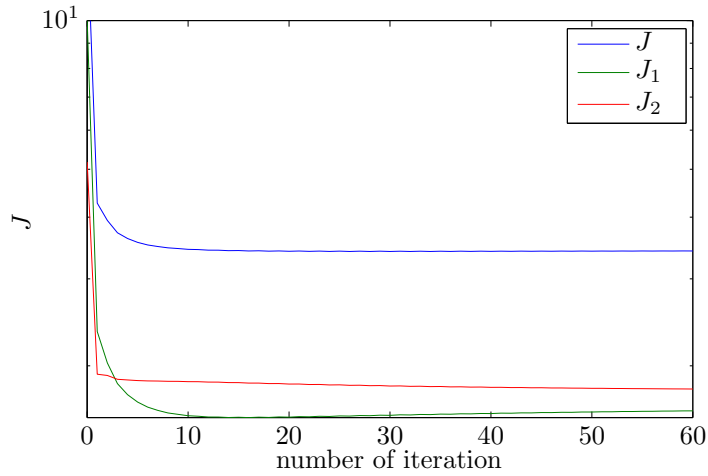


(c) Objective function (and its terms).

Figure 6.20: Results of the optimization with a random g_{in} , $Oh = 10$. $t_{po,bench} = 234$, $t_{po,opt} = 182$ (-23%), $R_A = 1$, $\omega_{nodes} = 18\%$, $\omega_{max} = 47\%$, $\Delta_{mass} = 0.07\%$



(a) Benchmark (black) and optimal (red) control. In green: initial guess.

(b) Benchmark (black) and optimal (red) state at $t_{po,bench}$.

(c) Objective function (and its terms).

Figure 6.21: Results of the optimization with a random g_{in} , $Oh = 0.1$.
 $t_{po,bench} = 11.3$, $t_{po,opt} = 10.2$ (-8%), $R_A = 1$, $\omega_{nodes} = 18\%$, $\omega_{max} = 41\%$,
 $\Delta_{mass} = 0.18\%$

Chapter 7

Attempts at an experimental verification

While running the simulations object of the previous Chapter, a natural desire to experimentally check the results arose. The problem is definitely not trivial and accomplishing an experimental validation could take years of research. Experimental studies on breaking filaments are not rare, but most of them consider the response to perturbations at a precise wavelength. Few studies look at white-noise perturbations or turbulence, and we did not find any considering precise interface laws to be enforced in the flow. Hence, the question we asked ourselves is: how could one shape a liquid thread interface in the ways indicated in the previous Chapter, and then let the flow evolve until break-up?

Everybody has experienced the explosion of a water balloon, when thrown against an obstacle or punched with a sharp object. What has this disorderly phenomenon to do with the careful shaping of a fluid? The answer can be found observing it with the aid of technology. High-speed cinematography has made great progress in the last decades, and cameras capable of taking videos at thousands of frames per second, even if still expensive for the single consumer, are nowadays affordable for research purposes even without the availability of astonishing budgets. This enables

us to observe reality at an incredible level of definition in time, so that otherwise epistemologically unreachable phenomena are now at close hand. In particular, what is surprising about a water balloon explosion when looking at it in slow-motion, is how rapidly the plastic shrinks with respect to other effects, because of its high elasticity. Thus the idea is to take advantage of this feature, giving the shape to the balloon and then making it explode. The wish is that the shrinking of the balloon is fast enough and it leaves the contents ‘free’ with their shape substantially unaffected. If this is true, then the flow will hopefully evolve as predicted by the numerical model. A preliminary (and inevitably not exhaustive) investigation aiming to check this wish is carried out in this Chapter, with the support of some tests we had the chance to run in EPFL laboratories in Lausanne (CH), using a high speed camera.

We employed a Phantom MiRo M 310, which is based on a 1 Mpx, 1280x800, custom-designed CMOS sensor from Vision Research. It exhibits 3.2 Gpx/s throughput and over 3200 fps at full resolution. A 20 μm pixel size and 12-bit depth guarantee high-light sensitivity and good dynamic range. Maximum frame rate at reduced resolution is 650000 fps. The balloons used in the experiments have been bought in a common toy shop, and the liquids in a supermarket. This experimental verification has been conducted thanks to the aid of Pierre-Thomas Brun, post-doctoral fellow at LFMI, EPFL.

7.1 Balloons explosion

The idea is to observe the explosion of balloons immersed in air and water and filled with different liquids, with a particular focus on the behaviour of the interface’s shape. The balloons, under the scrutiny of the high-speed camera, are put in position and then punched with a needle. For every experiment we display a picture per millisecond for approximately a dozen milliseconds.

7.1.1 **Bursting in air**

The first experiment, shown in Figure 7.1, has been carried out with a balloon filled with water and suspended in air, hung by hand at its extremities. The fastest phenomena is without any doubt the shrinking of the balloon. After 2 ms from the punching it has been pulled back by elastic forces for more than half of its initial position. At 6 ms it is no more enveloping any part of the liquid cylinder, and what remains of it gathers approximately around the point opposite to the punching one. The rapid retraction of the membrane creates a small-scale shear instability on the air/water interface, which, due to high density difference, leads to a fast radial spreading of very tiny droplets [25]. This occurs far before any other physical phenomenon: gravity is so slow that it is impossible to notice the cylinder of water falling in this small period of time. If we look at the upper part of the interface, it is surprising how the shape of the cylinder holds after the explosion. the spreading of droplets is not so important, so that the two sharp bends observable in the first picture are still recognizable in the last one, in which, for several milliseconds, the balloon does not even exist anymore. Nonetheless, the effects of the instability are preponderant on the lower part of the cylinder, where the water spreading is such that it is difficult to individuate a tidy line of interface. This appears to be connected to the way in which the balloon retracts. Starting from the punching point, which lies behind the human hand visible on the upper left of the frames in Figure 7.1, the balloon breaks up on a line which extends across the upper part of the cylinder. Then the plastic is pulled back by the portion of the balloon which is further from the rupture point. So, the lower part of the interface, as it is clear from figures displaying the space of time 2 ms - 6 ms, undergoes an extended sliding of the plastic on it. Because of this, a considerable amount of water pulls away.

A further proof that the way in which the balloons retracts affects quantity and direction of spreading droplets is given by Figure 7.2. In this case, similar to the previous one, the balloon is not simply held at its far ends: a torque is applied, creating a sort of knot in the middle. Due to this extra tension, the balloon breaks and then it twists while returning in a relaxed

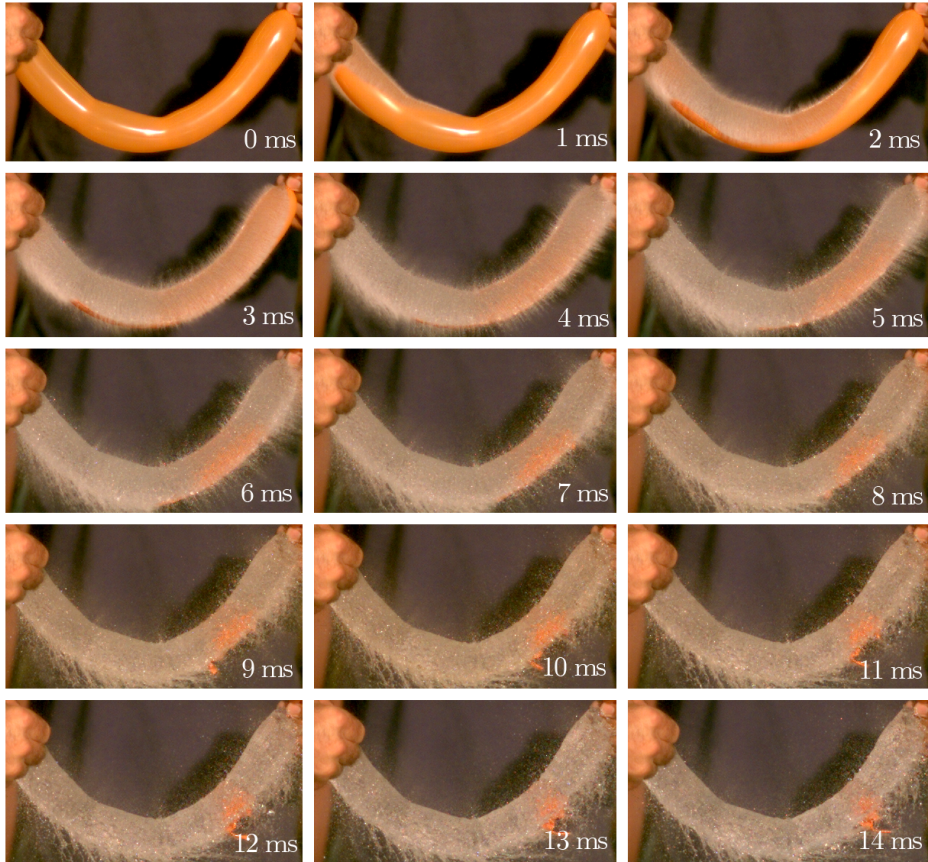


Figure 7.1: Explosion of a cylindrical balloon filled with water and suspended in air, hung by hand at its extremities.

configuration. The shear instability that follows is affected by this twisting, and the water spreads in the direction given by the retracting plastic. In particular the part of the cylinder to the left of the knot, less chaotic because closer to the punching point, maintains its shape in the upper part and undergoes a wide spreading in the lower one, while in the right part the reverse happens. Again, the retracting balloon influences very much the spreading of droplets from the surface, so that, in this configuration, we cannot say that the shape remains unaffected by the explosion.

In Figure 7.3 another similar experiment is displayed, this time with a horseshoe initial shape. Here the balloon breaks quite symmetrically, so that the droplets are spreading in all direction more or less in the same manner. What is interesting is the formation, visible in the last pictures, of a larger scale instability. Indeed, some waves are visible on the surface, particularly in the left ‘internal’ part of the horseshoe contour. This is a manifestation of the Richtmyer-Meshkov instability, which occurs when an interface between fluids of differing density is impulsively accelerated. It can be seen as the impulsive acceleration limit of the Rayleigh–Taylor instability.

7.1.2 **Bursting in water**

It appears that a water balloon bursting in air, although being a very interesting physical phenomenon, does not represent a good way to enforce a precise shape on a liquid. Nonetheless, we demonstrated that the balloon effectively retracts very fast, so that we are encouraged to keep investigating. The next step is to observe the explosion of balloons submerged in water, so that the density difference vanishes (or is less significant if we do not use water to fill the balloons). This should reduce some of the undesired effects of the previous configurations. Moreover, if the density of the liquid inside the balloon is the same (or almost the same) of the external one, gravity has effectively a negligible role. The balloons are submerged in water inside a fish tank, and anchored to the bottom using a weight and a girdle. The balloon should not contain air, a requirement not so easy to satisfy. However, this appears to be a problem surmountable just by

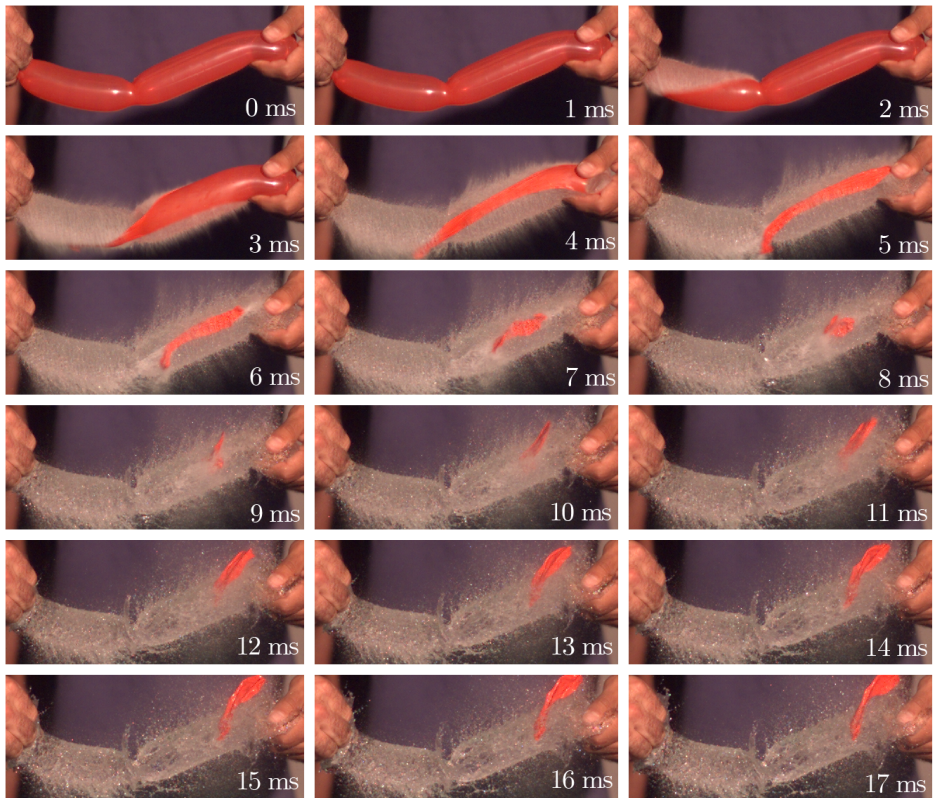


Figure 7.2: Explosion of a cylindrical balloon filled with water and suspended in air, hung and twisted by hand at its extremities.

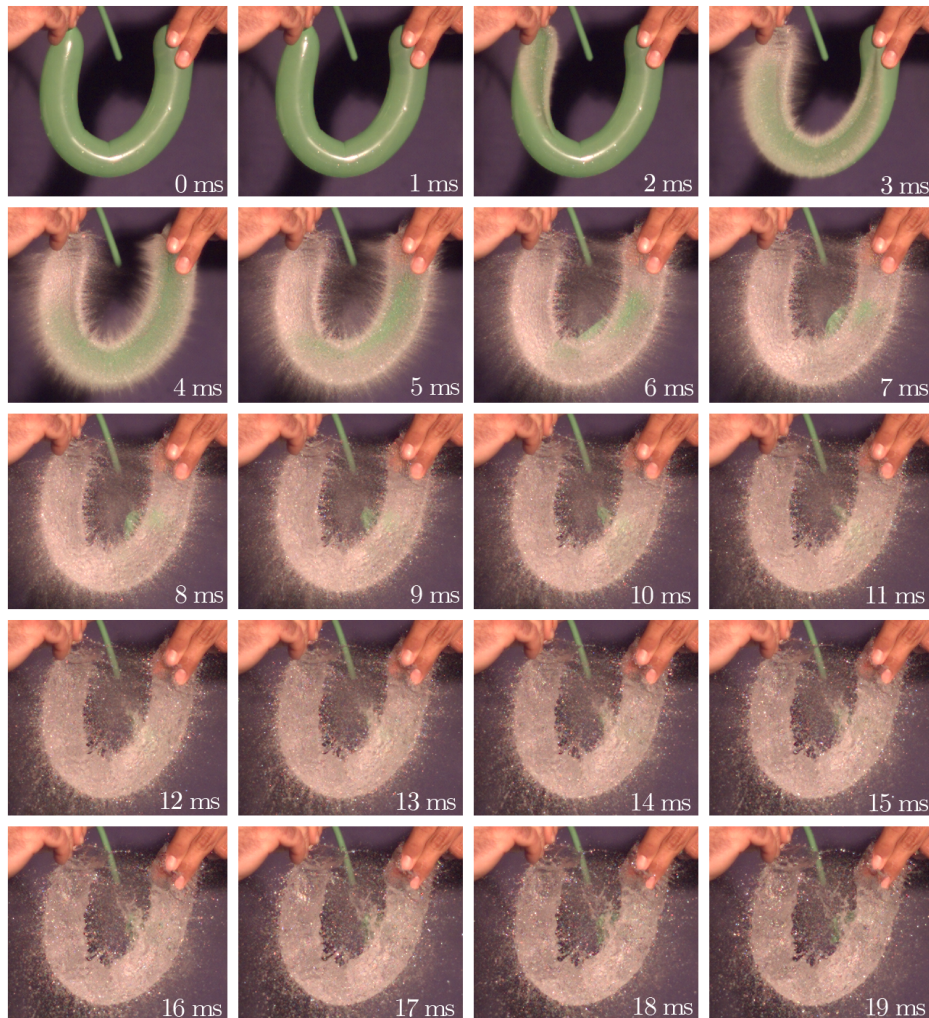


Figure 7.3: Explosion of a cylindrical balloon filled with water and suspended in air, hung by hand at its extremities.

improving the technique used to fill the balloons.

A test with a balloon filled with colored water is displayed in Figure 7.4. The balloon retracts very fast, even if a little more slowly than it would do in air. Since it is tied to the bottom of the tank, its lower part remains ‘in position’ for a longer period. Some air is present in the upper part of the balloon, introducing an undesired third phase. During the retracting phase, the plastic shows some wrinkles, which however do not have a big effect on the liquid. The absence of density difference between inside and outside thwarts the spreading of droplets and the interface remains amazingly still while the plastic slides on it, freeing the surface. Since the liquids are water and colored water, there is no surface tension between them, circumstance that definitely supports the stability of the surface itself. Anyway, the results of this attempt are distinctly positive: the shaping of a liquid using the idea of a bursting balloon appears practicable, or at least it is worth to be further examined.

Two more experiments are displayed in Figure 7.5 and 7.6, in which the balloons have been filled, respectively, with a mixture water/milk powder and with oil seed. The first case is not much different from the colored water one. The liquid appears a little bit more chaotic and ‘disposed’ to turbulence, disposition that is verified in the reality if looking at the evolution at larger times. The second case is interesting because it displays what happens with two immiscible liquids. Surface tension is not zero, but there is a non-negligible density difference (gravity eventually holds an important role). In this case, some undesired waves appear. When looking for larger times, we can observe the dissipation of these waves, but the presence of air and the density difference inevitably move the liquid and deform its shape.

7.2 Actual feasibility

The preliminary tests in these pages show some interesting characteristics of bursting water balloons, and encourage us to explore the possibility of using them to give shapes to liquids. Nonetheless, a few issues must be



Figure 7.4: Underwater explosion of a balloon filled with a mixture of water and green colorant. The balloon is anchored at the bottom of the tank in which it is immersed.



Figure 7.5: Underwater explosion of a balloon filled with water mixed with milk powder. The balloon is anchored at the bottom of the tank in which it is immersed

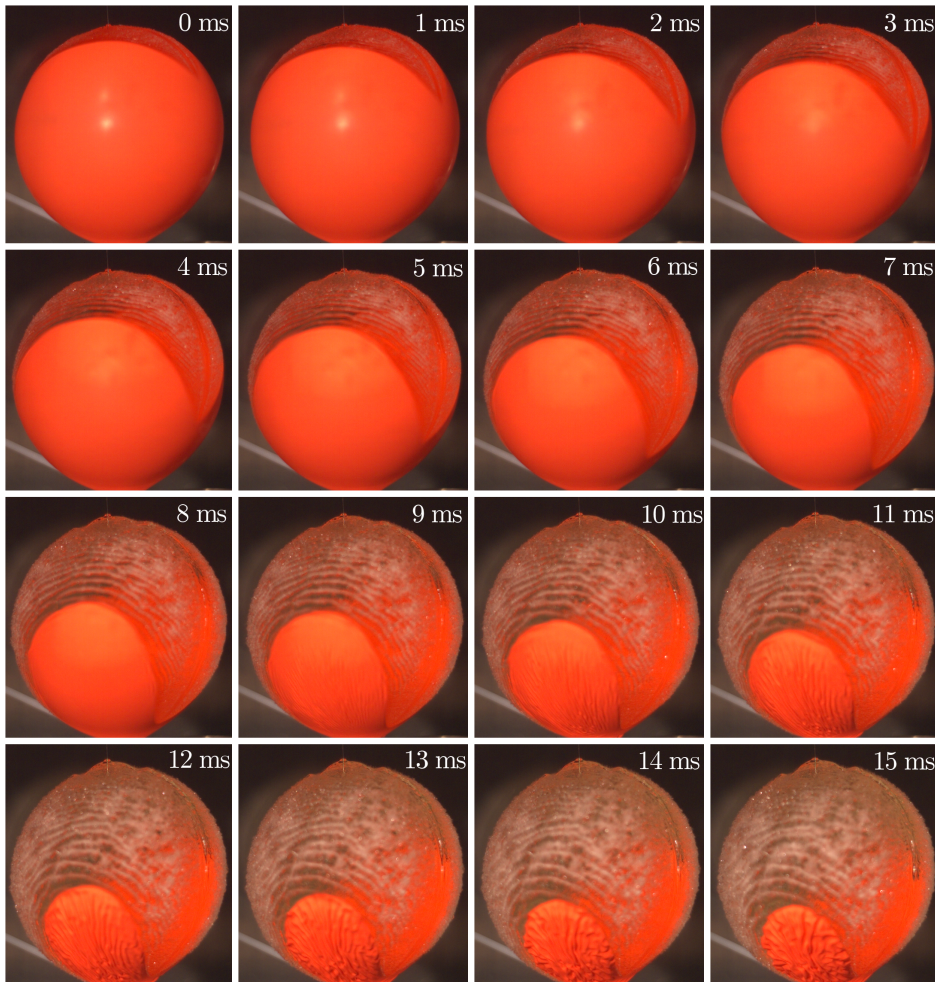


Figure 7.6: Underwater explosion of a balloon filled with oilseed. The balloon is anchored at the bottom of the tank in which it is immersed

faced:

- Small-scale shear instability. We have seen that this instability is particularly detrimental in the case of air/water interface, since it is responsible of the spreading of plenty of tiny droplets. It is not visible in the case of a submerged balloon.
- Richtmyer-Meshkov instability. The manifestation of this phenomenon is due to density differences at the interface, and it can be avoided submerging the balloons.
- Effects of the retraction of the balloon. The presence of undesired waves on the interface after the retraction of the balloon is a potential obstacle to the shaping, but not crucial if they are decaying in time.
- Presence of a dense outer medium. We saw how submerging the balloons in water improves the performances of the shaping attempts. Nonetheless, in this case we should be careful to model the physics using Eggers and Dupont equations without any modification. Indeed, in Equation (3.5) we neglected the interaction between the thread and the outer fluid. In reality, when the viscosity of the outer fluid is no more negligible the dynamics is influenced by visco-capillary stresses and this approximation could become unacceptable [26].
- Infinite thread approximation. In the previous Chapter we made the assumption of infinity in the axial direction, which is difficult to be applied to the liquid contained in a balloon. An idea could be using a torus-shaped balloon with a large enough radius, but the best thing would be dropping the infinity hypothesis and re-writing the code for a finite thread, so as to have a better comparison between experiments and numerical results. This is not immediate and surely requires some work, but should not be unfeasible.

Chapter 8

Conclusions and future work

The main objective of this thesis was to develop an optimization tool capable of minimising the break-up time of liquid threads under the effect of surface tension. This has been accomplished through the following steps:

1. study of Rayleigh-Plateau capillary instability, both from the physical point of view and from the analytical one;
2. employment of Eggers and Dupont one-dimensional model, comparison with Rayleigh-Plateau's and further analysis (transient growth);
3. development of a method for the numerical solution of the flow and implementation in a MATLAB code, taking advantage of Ansaldi's previous work [20];
4. study of the adjoint method applied to constrained optimization in a non-linear, space and time dependent framework;
5. elaboration of the Lagrangian functional and the optimality system for different cases, changing definitions and limits on objective function and control;
6. development of a numerical method for the solution of the adjoint equations and integration in a MATLAB script containing a loop for the minimisation of break-up time.

The methods that have been chosen to carry out the investigation and perform the optimization have demonstrated to be appropriate and effective, allowing us to find optimal controls for the minimisation of break-up time in many configurations and for different levels of viscosity. Acting on the definition of the Lagrangian and on the parameters of the optimization, the shape and the characteristics of the optimal control can be modified, attaining different results in term of average and local amplitude, mass congruity and speed of rupture. The results of the optimization are particularly interesting due to the non-linearity and the space and time dependence of the problem. Moreover, to the best of the author's knowledge, there is no study in the literature performing optimization on a similar flow using the adjoint method.

In addition, some preliminary experiments have been conducted, in order to test whether plastic balloon explosion can be employed for the shaping of liquid interfaces. A conclusive answer to the question has not been obtained, due to the lack of time and to the complicated nature of the observed phenomena. Nonetheless, some significant remarks have been made.

As for the future, there are various developments of this work that are worth to be carried out. Among them, one can mention:

- further examination of the infinite thread, testing the effects of different objective functions and constraints on the control;
- optimization on more complex thread configurations, such as a finite thread or a free jet;
- experimental campaign for the verification of the results taking advantage of the considerations about bursting balloons, or using other methods.

With regard to the free jet configuration, in particular, some work that has not been shown in this thesis has already been done in parallel to the infinite thread, leading for the moment to non-conclusive results. Nonetheless, this appears a promising subject to be examined in more depth, also considering the possible applications.

Appendix

Given the terms:

$$T_1 = -\frac{3}{4} \frac{\frac{\partial^3 F}{\partial z^3} F - \frac{\partial^2 F}{\partial z^2} \frac{\partial F}{\partial z} - 2 \frac{\partial F}{\partial z}}{\left(\frac{1}{4} \left(\frac{\partial F}{\partial z}\right)^2 + F\right)^{\frac{5}{2}}},$$

$$T_2 = \frac{\frac{1}{2}}{\left(\frac{1}{4} \left(\frac{\partial F}{\partial z}\right)^2 + F\right)^{\frac{3}{2}}},$$

$$T_3 = -\frac{15}{8} \frac{\frac{1}{2} \left(\frac{\partial F}{\partial z}\right)^3 \frac{\partial^2 F}{\partial z^2} + \left(\frac{\partial F}{\partial z}\right)^3 - \frac{1}{2} \left(\frac{\partial^2 F}{\partial z^2}\right)^2 \frac{\partial F}{\partial z} F + 2 \frac{\partial F}{\partial z} F}{\left(\frac{1}{4} \left(\frac{\partial F}{\partial z}\right)^2 + F\right)^{\frac{7}{2}}},$$

$$T_4 = \frac{\frac{3}{4}}{\left(\frac{1}{4} \left(\frac{\partial F}{\partial z}\right)^2 + F\right)^{\frac{5}{2}}},$$

$$T_5 = \frac{3Oh}{F^2};$$

the terms A_i and B_i read:

$$A_1 = \frac{\partial F}{\partial z}, \quad A_2 = F, \quad A_3 = \frac{\partial V}{\partial z}, \quad A_4 = V,$$

$$B_1 = \frac{\partial V}{\partial z}, \quad B_2 = V - T_5 \frac{\partial F}{\partial z} F, \quad B_3 = -3Oh,$$

$$B_4 = -T_1 - T_2 \frac{\partial^3 F}{\partial z^3} - T_3 + T_4 \left(\frac{1}{2} \left(\frac{\partial^2 F}{\partial z^2} \right)^2 \frac{\partial F}{\partial z} - 2 \frac{\partial F}{\partial z} \right) + T_5 \frac{\partial F}{\partial z} \frac{\partial V}{\partial z},$$

$$B_5 = -T_1 \frac{1}{2} \frac{\partial F}{\partial z} + T_2 \left(\frac{\partial^2 F}{\partial z^2} + 2 \right) - T_3 \frac{1}{2} \frac{\partial F}{\partial z} + \dots$$

$$\dots - T_4 \left(\frac{3}{2} \frac{\partial^2 F}{\partial z^2} \left(\frac{\partial F}{\partial z} \right)^2 + 3 \left(\frac{\partial F}{\partial z} \right)^2 - \frac{1}{2} \left(\frac{\partial^2 F}{\partial z^2} \right)^2 F + 2F \right),$$

$$B_6 = T_2 \frac{\partial F}{\partial z} - T_4 \left(\frac{1}{2} \left(\frac{\partial F}{\partial z} \right)^3 - \frac{\partial^2 F}{\partial z^2} \frac{\partial F}{\partial z} F \right),$$

$$B_7 = T_2 F.$$

Acknowledgements / Ringraziamenti

Firstly I would like to thank Prof. Alessandro Bottaro and Prof. François Gallaire for having proposed to me this interesting and prolific topic, and for the opportunity to work on it at EPFL in Lausanne. I am grateful to Prof. Gallaire for the way he welcomed me in his group, for the time he dedicated to me and for his always enlightening advice, which has guided me through this research. I profoundly acknowledge Prof. Bottaro for his dedicated support, his careful oversight, his patience and especially for his trust.

I also want to express my gratitude to all the LFMI staff. I thank Cristobal and Edouard for their knowledge of adjoint-based optimization, Marc-Antoine for his expertise in numerical methods, for his friendship and for the weekends spent skiing together, Andrea and Francesco for their continuous help and for the volleyball and beach-volley matches, Laura for her availability and willingness, Pierre-Thomas for his confidence in my research skills and for his dexterity with high-speed cinematography, Vlado for his enthusiasm, Mathias for his competence about microfluidics, Yoan for his kindness. Each of you has given a fundamental professional and personal contribution to this work and to my stay in Lausanne.

I take this opportunity to also thank all the people that have been close to me in the last five years, of which this thesis and my graduation are somehow a conclusion. I hope nobody will feel offended if I switch from

english to italian to do that.

Vorrei ringraziare innanzitutto coloro i quali hanno condiviso con me questi anni di corsi ed esami. Albi e Zac per aver sempre salutato in casa, e perché so che non scorderanno mai di farlo, Edi e Ale per essere diventati così grossi, Fabione per le gioie del turco, Andre per ogni singola maneggia, la Pola per aver sopportato tutto questo. E poi Volpa, Alca, Franco, Jacopo, Gandalf, Marci e tutti gli altri.

Ringrazio profondamente i miei amici di sempre: Lorenzo, che sarà uno sbirro fantastico, Rocco, sperando che prima o poi riesca a capire cosa diavolo ci frulla in testa, Emmanuele, che è destinato a curare le varie legnate che prenderemo, e tutti gli altri e le altre che non ho lo spazio per citare uno ad uno, ma sanno di meritare un grazie gigante.

Ringrazio mia madre, mio padre e mio fratello, perché se ho qualche pregio e dei motivi per sentirmi ricco è principalmente grazie a loro.

Infine ringrazio Camilla, certo anche per la sua perizia nell'uso di Photoshop, ma soprattutto perché illumina col suo sorriso tutti i miei giorni, e non potrebbe esserci regalo più bello.

Bibliography

- [1] Eggers J & Villermaux E, (2008). Physics of liquid jets. *Reports on Progress in Physics*, 71(3), 1-3.
- [2] Young T, (1805). An essay on the cohesion of fluids. *Philosophical Transactions of the London Royal Society*, 95, 65–87.
- [3] Navier CL, (1827). Memoire sur les lois du mouvement des fluides. *Royale Academie des Sciences*, 6, 389–440.
- [4] Stokes GG, (1845). On the theories of internal friction of fluids in motion, and of the equilibrium and motion of elastic solids. *Transactions of the Cambridge Philosophical Society*, 8, 287.
- [5] Savart F, (1833). Memoire sur le constitution des veines liquides lancees par des orifices circulaires en mince paroi. *Annales de chimie et de physique*, 53, 337-398.
- [6] Plateau JAF, (1849). Memoire sur les phenomenes que presente une masse liquide et soustraite a l'action de la pesanteur. *Nouveaux memoires de l'Academie Royale des Sciences et Belle-Lettres de Bruxelles*, 23, 5.
- [7] Rayleigh Lord, (1879). On the Instability of Jets. *Proceedings of the Royal Society of London*, 10, 4-13.
- [8] Rayleigh Lord, (1892). On the instability of a cylinder of viscous liquid under capillary force. *Philosophical Magazine*, 34, 145–154.

- [9] Grubelnik V & Marhl M, (2005). Drop formation in a falling stream. *American Journal of Physics*, 73(5), 415.
- [10] Gallaire F, (2013). Unpublished lecture notes. *Classes of Instability and Turbulence*, EPFL.
- [11] Attane P, (2006). Breakup length of forced liquid jets. *Physics of Fluids*, 15(9), 2469.
- [12] Chaudhary KC & Maxworthy T, (1980). The nonlinear capillary instability of a liquid jet; Part 2: Experiments on jet behavior before droplet formation. *Journal of Fluid Mechanics*, 96, 275-286.
- [13] Chaudhary KC & Redekopp LG, (1980). The nonlinear instability of a liquid jet; Part 1: Theory. *Journal of Fluid Mechanics*, 96, 257-274.
- [14] Eggers J & Dupont TF, (1994). Drop formation in a one-dimensional approximation of the Navier-Stokes equations. *Journal of Fluid Mechanics*. 262, 205-221.
- [15] do Carmo MP. Differential geometry of curves and surfaces. Prentice-Hall, Englewood Cliffs. New Jersey, 1976.
- [16] Bale R & Govindarajan R, (2010). Transient growth and why we should care about it. *Resonance*, 15(5), 441-457.
- [17] Cantwell CD. Transient growth of separated flows. PhD thesis, University of Warwick, 2009.
- [18] Selimefendigila F, Sujithb RI & Polifkea W, (2011). Identification of heat transfer dynamics for non-modal analysis of thermoacoustics. *Applied Mathematics and Computation*, 217(11), 5134-5150.
- [19] Trefethen LN & Bau D. Numerical Linear Algebra. Society for Industrial & Applied Mathematics. New York, 1997.
- [20] Ansaldi T. Droplet formation in a free stream jet using a reduced model. Master thesis, University of Genova, 2013.

- [21] Hamdi S, Schiesser WE & Griffiths GW. (2007). Method of lines. *Scholarpedia*, 2(7), 2859.
- [22] Canuto C, Hussaini M, Quarteroni A & Zang T. Spectral methods. Fundamentals in single domain. Springer-Verlag, 2006.
- [23] Cossu C, (2013). A rough introduction to constrained optimization flow. Unpublished lecture notes, Nordita Summer School, Stockholm.
- [24] Pralits OJ, (2012). Unpublished lecture notes of *Advanced fluid dynamics*, University of Genova.
- [25] Lund HM & Dalziel SB, (2011). Bursting water balloons. arXiv:1110.3320.
- [26] Petit J, Riviere D, Kellay H & Delville JP, (2012). Break-up dynamics of fluctuating liquid threads. *Proceedings of the National Academy of Science, USA*, 109(45), 18327-18331.

Contents

1	Introduction	1
I	Stability and solution of the flow	5
2	Plateau-Rayleigh instability	7
2.1	Some History	7
2.2	A semi-quantitative approach	9
2.2.1	Drop formation	10
2.3	Rayleigh linear stability analysis	14
3	Equations of motion	23
3.1	Eggers and Dupont (1D) model	24
3.2	Non-dimensional equations	29
3.2.1	Equations in $F = h^2$	30
3.3	Linear stability analysis	31
3.4	Transient growth analysis	35
3.4.1	Mathematical description	37
3.4.2	Results	39
4	Flow configuration and numerical solution	45
4.1	Physical configuration	45
4.2	Numerical method	46
4.2.1	Discretization	48

4.3	Stability analysis and pinch-off time	49
4.4	Examples	50
II	Optimization and control of droplet formation time	57
5	Method and equations	59
5.1	Preliminaries and some notation	59
5.2	Optimization methods	60
5.2.1	Gradient method with finite difference approximation	61
5.2.2	The adjoint method	61
5.3	Adjoint equations of E-D model	67
5.3.1	A formal synopsis	68
5.3.2	Linearized equations	69
5.3.3	Adjoint equations	71
6	Break-up time minimisation	73
6.1	Objective function	74
6.1.1	A problem of definition	74
6.1.2	Choice of surrogate function	75
6.1.3	Choice of time domain	81
6.1.4	Analytical expressions	84
6.2	Control	85
6.2.1	Comparability criteria	85
6.2.2	Implementation in the Lagrangian	88
6.3	Equations and results	89
6.3.1	Penalization: first mode	91
6.3.2	Penalization: second mode	94
6.3.3	Enforcement of average amplitude	99
6.3.4	Conclusions	106
7	Attempts at an experimental verification	109
7.1	Balloons explosion	110
7.1.1	Bursting in air	111

<i>Contents</i>	133
7.1.2 Bursting in water	113
7.2 Actual feasibility	116
8 Conclusions and future work	121
Appendix	123
Acknowledgements / Ringraziamenti	125

